

A MODEL FOR FIRING PATTERNS OF AUDITORY NERVE FIBERS

by

THOMAS FISCHER WEISS

B.E.E., The City College of New York
(1956)

M.S., Massachusetts Institute of Technology
(1959)

SUBMITTED IN PARTIAL FULFILLMENT OF THE
REQUIREMENTS FOR THE DEGREE OF
DOCTOR OF PHILOSOPHY

at the

MASSACHUSETTS INSTITUTE OF TECHNOLOGY
June, 1963

Signature of Author _____
Department of Electrical Engineering, May 24, 1963

Certified by _____ Thesis Supervisor

Accepted by _____
Chairman, Departmental Committee on Graduate Students

✓

A MODEL FOR FIRING PATTERNS OF AUDITORY NERVE FIBERS

by

THOMAS FISCHER WEISS

Submitted to the Department of Electrical Engineering

on May 24, 1963

in Partial Fulfillment of the Requirements for the Degree of

Doctor of Philosophy

ABSTRACT

Recent electrophysiological data obtained from auditory nerve fibers of cats have made possible the formulation of a model of the peripheral auditory system. This model relates the all-or-none activity of these fibers to acoustic stimuli. The constituents of the model are intended to represent the major functional constituents of the peripheral system. These constituents are: (1) a linear mechanical system intended to represent the outer, middle, and the mechanical part of the inner ear; (2) a transducer intended to represent the action of the sensory cells; and (3) a model neuron intended to represent the nerve excitation process. A general purpose digital computer has been used to determine the response of the model to a variety of acoustic stimuli. These results have been compared to data obtained from auditory nerve fibers.

Thesis Supervisor: Moise H. Goldstein, Jr.

Title: Associate Professor of Electrical Engineering

ACKNOWLEDGEMENT

It is a pleasure to acknowledge the guidance and assistance of a few of the many people who have contributed to the completion of this work. I am most indebted to Dr. N. Y-S. Kiang for suggesting the topic of this thesis and for his constant counsel. The data he has been able to obtain have made possible the formulation of models and theories. Professor M.H. Goldstein, who supervised this thesis, Professor W.M. Siebert, Professor W.T. Peake, Dr. G.L. Gerstein and Mr. J.L. Hall were very generous with their time and provided critical appraisal of the work when this was needed. The members of the Communications Biophysics Laboratory provided a stimulating intellectual environment in which to work. This atmosphere of freedom of inquiry is a consequence of the leadership of Professor W.A. Rosenblith. We wish to acknowledge the opportunity to work and to learn in this environment.

The TX-2 computer has been generously made available by the Lincoln Laboratory, M.I.T. In particular, we wish to thank Mr. W.A. Clark for his efforts in our behalf. The friendship and assistance of Lt. C.E. Molnar is also acknowledged.

Several people aided in the preparation of the manuscript. Mr. P. Karas provided the photography despite considerable harassment from the author. Miss L. Clark and Miss M. French were invaluable in their help with the figures. Miss B. Morneault, Mrs. K. Jordan and Mrs. E. Imbornone helped in many ways to make the completion of the manuscript possible.

Finally, I wish to thank my family. My son, Max, suffered a few delayed feedings during the preparation of the manuscript. My wife, Aurice, prepared the final manuscript and was the source of much-needed encouragement throughout this thesis.

TABLE OF CONTENTS

Title Page 1

Abstract 2

Acknowledgement 3

Table of Contents 4

List of Figures 6

Chapter I: Introduction11

Chapter II: Anatomy of the Peripheral Auditory
System14

Chapter III: Systems Physiology of the Peripheral
Auditory System20

 A. Dynamics of the Outer and Middle
 Ear20

 B. Dynamics of the Cochlea32

 C. Brief Electrophysiology of the
 Cochlea51

 D. Patterns of Action Potentials in the
 Afferent Fibers of the VIIIth Nerve .53

Chapter IV: A Model of the Peripheral Auditory
System63

 A. Assumptions of the Model66

 B. Discussion of Assumptions68

Chapter V: Results of Testing the Model77

 A. Response of the Model Neuron to
 "Short" Pulses79

	B. Spontaneous Activity of the Model.	89
	C. Response of the Model to Sinusoidal Stimuli.107
	D. Acoustic Click Response of the Model.136
Chapter VI:	Concluding Remarks161
	A. Comparison of the Data Generated by the Model with Data Obtained from VIIIth Nerve Fibers161
	B. Appraisal of the Model and Suggestions for Further Study.164
	C. A Note on Models and Digital Computer Simulations.167
Appendix A:	A Discussion of the Distribution of Spontaneous Events169
Appendix B:	Derivation of Statistics of D_n^2172
Appendix C:	A Description of the Computer Programs176
	Bibliography.186
	Errata.193
	Biographical Note194

LIST OF FIGURES

Figure 1. Block diagram representation of a model of the peripheral auditory system 15

Figure 2. Ratio of amplitude of pressure at the tympanum to amplitude of sinusoidal pressure at the entrance of the meatus 22

Figure 3. Circuit representation of the middle ear . 25

Figure 4. Open circuit pressure ratio from the entrance of the meatus and tympanum to the stapes . 27

Figure 5. Amplitude and phase of the volume displacement of the round window for a sinusoidal pressure variation at the tympanum 29

Figure 6. Elasticity of the cochlear partition as a function of distance from the stapes 33

Figure 7. Position of the maximum displacement of the cochlear partition as a function of the frequency of sinusoidal stapes displacement . 36

Figure 8. Amplitude and phase of the displacement of the cochlear partition as a function of frequency for several different positions along the cochlear partition 39

Figure 9. Volume displacement of stapes divided by maximum amplitude of the displacement of the cochlear partition as a function of the frequency of stapes displacements 41

Figure 10.	Impulse responses of models of the displacement of the cochlear partition (after Flanagan) .	46
Figure 11.	Impulse response of models of the displacement of the cochlear partition (after Siebert) .	49
Figure 12.	Interval histogram of the spontaneous firings of a fiber in the auditory nerve (of a cat) plotted in semi-logarithmic co-ordinates . .	55
Figure 13.	Tuning curves for several fibers in the auditory nerve (cat)	57
Figure 14.	Post-stimulus time histograms of the click responses of several auditory nerve fibers (cat)	59
Figure 15.	Block diagram of a model relating the firing patterns of fibers in the auditory nerve to acoustic stimuli	64
Figure 16.	Diagrammatic representation of membrane potential, threshold potential and spike activity of the model	67
Figure 17.	Number of responses of the model to a train of short pulses as a function of the amplitude of the pulses	82
Figure 18.	Histogram of intervals of time between responses of the model to a periodic train of short pulses	84
Figure 19.	Histograms of intervals of time between responses of the model to periodic trains of short pulses as a function of pulse amplitude . .	87

Figure 20.	Membrane potential and threshold potential of the model	90
Figure 21.	Conditional average interspike intervals of the spontaneous activity generated by the model as a function of noise spectrum	94
Figure 22.	Interval histograms of the spontaneous activity generated by the model as a function of noise spectrum	97
Figure 23.	Interval histograms of the spontaneous activity generated by the model as a function of noise spectrum (plotted in semi-logarithmic co-ordinates)	99
Figure 24.	Spontaneous rate of firing of the model versus the high frequency limit of the noise . . .	101
Figure 25.	Interval histograms of the spontaneous activity generated by the model versus the standard deviation of the noise	103
Figure 26.	Spontaneous rate of firing of the model versus the ratio of the standard deviation of the noise to the resting threshold (σ/R_R).	105
Figure 27.	Threshold of firing of VIII th nerve fibers to tone bursts (delivered at the CF) as a function of CF	113
Figure 28.	Response of the model to sinusoidal stimulation as a function of intensity.	116

Figure 29. Rate of firing of the model versus amplitude of sinusoidal stimulation 119

Figure 30. D_n versus amplitude of sinusoidal stimulation of the model 121

Figure 31. "Threshold" of firing of the model versus frequency of sinusoidal stimulation 124

Figure 32. Rate of firing of the model versus amplitude of sinusoidal stimulation for different spontaneous rates of firing 127

Figure 33. Mechanical and neural tuning curves 131

Figure 34. Mechanical tuning curves 134

Figure 35. Response of the cochlear partition and model for two different polarities of acoustic clicks 137

Figure 36. Response of an VIIIth nerve fiber to condensation and rarefaction clicks as a function of intensity 140

Figure 37. Times of occurrence of peaks in the PST histogram of the response of an VIIIth nerve fiber to condensation and rarefaction clicks as a function of intensity 142

Figure 38. Acoustic click response of the model for a linear and non-linear transducer function as a function of intensity 144

Figure 39. Response of the model to positive and negative clicks as a function of the intensity of click stimulation 148

Figure 40. Times of occurrence of peaks in the PST histograms of the response of the model to acoustic clicks 150

Figure 41.	Acoustic click response of the model for different values of CF	152
Figure 42.	Acoustic click response of the model as a function of intensity	154
Figure 43.	Acoustic click response of the model as a function of intensity	156
Figure 44.	Schematic representation of computer programs	178
Figure 45.	High-speed printer display of the results of a typical computation	183

CHAPTER I: Introduction

The passing of a century of research in audition has produced gross changes of attitude on the part of the physiologist. The speculative views of antiquity were followed by the empiricism of the late nineteenth and the twentieth century. We quote from M.J.P. Flourens (1794-1867):*

"Almost every physiologist will admit that we are in complete ignorance as to the usage of the various parts of the ear. Those who do not hold this view are hard pressed to disguise their ignorance by suppositions, conjectures or by some of those words which are used everywhere but which, according to Fontenelle, have no other merit than that of having been considered as real things for a long time. Reasoning alone serves poorly if the question to decide is a question of fact. Everywhere people have started by theorizing instead of doing the necessary experiments. Even in physiology the time has come to proceed in the opposite direction, and to multiply, to repeat, to accumulate experiments in order to end up some day with theories . . ."

While it is probably true that physiology is still in a developmental stage where the careful gathering of relevant data is pre-eminent, we feel that it is never too early to organize empirical data along formal and conceptual lines. It is the bias of the writer that such organization of empirical evidence leads both to deeper insights into the phenomena under investigation and to the suggestion

*Von Bekesy, G. and Rosenblith, W.A. "The early history of hearing--observations and theories". J. Acoust. Soc. Am., 20, 1948: 728.

of new and hopefully critical experiments. In a sense Flourens' advice has been heeded and it is now time to produce the theories which were premature in his day.

We feel that the primary requisite of a model or theory is precision. The model may be a crude representation of the system (or phenomenon) under investigation, but it must itself be precise in order for it to be verifiable. It must be possible to test the model in at least a "gedanken" experiment sense. There are other desirable features of models, beyond their precision, but we shall not belabor the point.

Data obtained recently from single nerve fibers in the auditory nerve (of cats) have made possible the formulation of a model of the peripheral auditory system. This model relates the all-or-none potentials of these fibers to acoustic stimuli. Since the initial encoding of acoustic signals into the times of occurrence of spike potentials is accomplished in the peripheral auditory system, an understanding of this encoding is essential to the understanding of the performance of higher centers in the auditory system.

The discussion of the formulation and testing of the model is organized into six chapters. Chapter II contains a brief discussion of the anatomy of the peripheral auditory system and is intended to introduce some of the terminology associated with the peripheral system. Chapter III contains a discussion of the physiology of the peripheral auditory system. The physiological bases for the model described

in Chapter IV are contained in Chapter III. A discussion of the results of testing the model is contained in Chapter V and concluding remarks are included in Chapter VI.

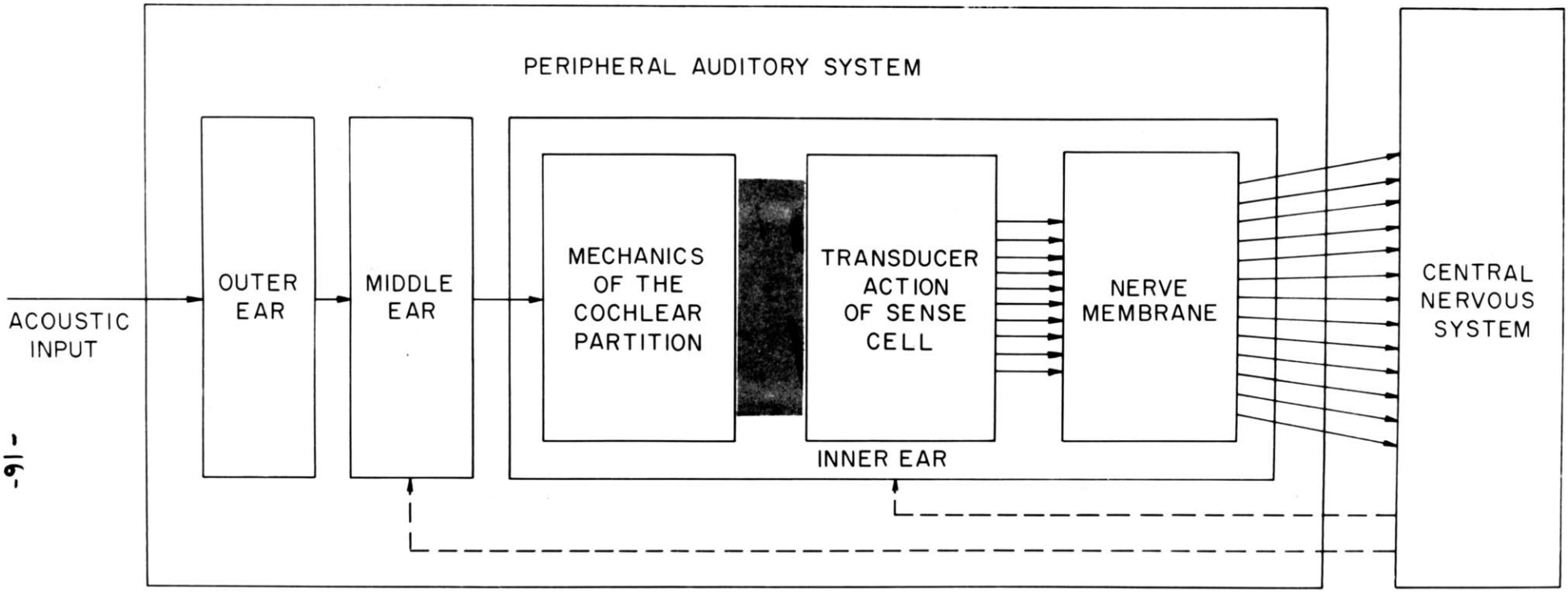
CHAPTER II: Anatomy of the Peripheral Auditory System

The gross anatomy of the peripheral auditory system of man (and other higher species) is relatively well known (see, for instance Polyak⁽¹⁾) and only the briefest description need be given here. For our purposes we can divide the auditory system into four parts (as shown in Figure 1.) --the outer, middle, and inner ear, constituting the peripheral auditory system, and the central nervous system.

Air-borne sound enters the outer ear past the auricle (the externally visible ear lobe structure) via the external auditory meatus (a canal that is 2.5 cm long in man) and impinges on the tympanic membrane. The sound waves set the tympanic membrane in motion. This motion is transmitted to the middle ear, which contains a set of three tiny bones, the ossicles. The three-ossicle chain, malleus to incus to stapes, transmits the motion of the tympanic membrane to another membrane, the "oval window", which is the mechanical input to the inner ear. The auditory part of the inner ear is comprised of the cochlea, a functionally and morphologically complex system that converts the mechanical motion of the stapes into spike potentials. The 3×10^4 nerve fibers⁽²⁾ emerging from the cochlea go directly into the central nervous system as a part of the VIIIth Cranial nerve at the level of the medulla oblongata.

The detailed anatomy of the cochlea is the most complex part of the peripheral system. It is in the cochlea

Figure 1. Block diagram representation of a model of the peripheral auditory system.



BLOCK DIAGRAM REPRESENTATION OF A MODEL OF THE PERIPHERAL AUDITORY SYSTEM

that the mechanical motions are converted into neural signals. The cochlea is in the form of a spiral tube, i.e., a tube wound on a cone such that the axis of the tube is helical. The interior of this helix is called the modiolus and contains the nerve fibers as they emerge from the tube, or cochlear canal. The number of revolutions of the canal differs in different species: 2 3/4 cochlear turns in man, 3 in cat, and 4 1/2 in guinea pig. The lengths of the axes of the canal are 35 mm, 23 mm, and 18 mm, respectively. The canal diameter decreases from the basal end of the cochlea (near the base of the cone) to the apical end. In man this variation is from 2.5 mm to 1.2 mm.

The cross-section of the cochlear canal is divided by a multi-membraneous "cochlear partition". This partition separates the cochlear canal into two canals filled with fluid, the perilymph. These two canals, the scala vestibuli and scala tympani, are connected through a hole (0.15 mm^2) in the apex of the cochlear partition, called the helicotrema. Perilymph can thus flow from scala vestibuli to scala tympani, and vice versa, through the helicotrema. At the basal end of the cochlea the two scalae are each sealed by a membrane. The oval window seals the scala vestibuli and the round window seals the scala tympani. It is the oval window that is displaced by motions of the footplate of the stapes.

The cochlear partition is bounded by and includes Reissner's membrane and the basilar membrane. The partition

consists of the ductus cochlearis--a space filled with the endolymph fluid, the Organ of Corti--containing the auditory receptor cells and their innervation, and certain structural and trophic parts (such as the spiral ligament, stria vascularis, etc.). There are at least two types of auditory receptor cells: a single row of inner hair cells (approximately 3.5×10^3 cells in man) and three or four rows of outer hair cells (approximately 20×10^3 cells in man).⁽³⁾ These cells are supported on the basilar membrane and give off hairs at their apices that extend through the reticular lamina and into the tectorial membrane. The innervation of these hair cells is not entirely known. The inner hair cells appear to be innervated locally and preponderantly by the radial fibers,⁽⁴⁾ one radial fiber innervating perhaps one or two inner hair cells and a hair cell being innervated by one or two radial fibers. The outer hair cells seem to be innervated primarily by the spiral fibers which enter radially, and after making a right angle turn, travel toward the round window along the base of the outer hair cells for as much as a half turn of the cochlea.⁽⁵⁾ There is some evidence in the literature that these cells innervate several outer hair cells along their path.⁽⁶⁾ In addition to these two groups of fibers, there are a smaller number of fibers that innervate both inner and outer hair cells.⁽⁷⁾

The nerve fibers that innervate the hair cells have their cell bodies in the spiral ganglion and send

their other processes through the modiolus to the cochlear nucleus in the medulla oblongata (a distance of about 5 mm). The cells (27×10^3 in man) of the spiral ganglion are bipolar cells and no synaptic connections have been seen in the ganglion.⁽⁸⁾ Histology of a gross-section of the VIIIth nerve reveals a remarkable uniformity of fiber diameters--between 3 and 5 μ . (9, 10)

The VIIIth nerve exhibits another regularity worth mentioning: as the fibers exit the modiolus, the fibers originating in the apex of the cochlea tend to be in the center of the fiber bundle and the more basal fibers wind around them. Thus, the VIIIth nerve presents a fairly regular array of apical fibers in the center of the bundle with the more basal fibers progressively farther from the center.

There is evidence in the literature for several efferent neural pathways to the peripheral auditory system. First, there is the innervation of the hithertofore unmentioned middle ear muscles. The stapedius muscle, connected to the stapes, is innervated by the facial (VIIth Cranial) nerve and the tensor tympani, which exerts tension on the manubrium of the malleus, is innervated by the mandibular division of the trigeminal (Vth Cranial) nerve. In addition, there is the efferent olivary-cochlear bundle of Rasmussen⁽¹¹⁾--a set of fibers that originate in the medulla and terminate in the vicinity of the hair cells.

CHAPTER III: Systems Physiology* of the Peripheral
Auditory System

A. Dynamics of the Outer and Middle Ear

The detailed physiology of the middle and outer ear is well documented (see for instance Wever and Lawrence¹²) and thus we shall concentrate in our description on a systems approach. The role of these two structures is now quite clear. The specific acoustic impedance of air is 41.5 ohms/cm^2 (at 20° C.) and the specific acoustic impedance for a fluid like the perilymph has been estimated to be approximately $16 \times 10^3 \text{ ohms/cm}^2$. Thus, an impedance matching device is needed in order to make the transmission loss of sound waves going from air to perilymph (the site of the receptor cells) tolerable. The middle ear provides this mechanism for transforming the relatively large displacements and small pressures in air into relatively small displacements and large pressures in the perilymph. Essentially, the transformer ratio is achieved by the difference in effective cross-sectional areas of the tympanic membrane and oval window (approximately 21 in man), but the ossicular chain provides an additional mechanical advantage (estimated to be 1.3 in man). (13)

*We are primarily interested in the relation between the firing patterns of single fibers in the VIIIth nerve and acoustic stimuli delivered to the ear. Our approach takes into account the input-output relations of the major components of the peripheral system, rather than the detailed structure and function of each part.

While these principles are quite simple, the realization of the transformation and detailed motion of the middle ear structures are quite complex. For instance, the tympanic membrane does not have a simple drum-like motion,⁽¹⁴⁾ nor is its characteristic motion the same for all frequencies of sinusoidal pressure stimulation.⁽¹⁵⁾ Similarly, the oval window seems to change its mode of vibration as a function of intensity.⁽¹⁶⁾ In addition, the incudostapedial joint is loose and lowers the efficiency of sound transmission to the cochlea at high intensities.⁽¹⁷⁾ For high intensities of prolonged sound stimulation, a middle ear muscle contraction reflex is actuated that effectively decreases the efficiency of transmission through the middle ear.⁽¹⁸⁾

Despite this complexity, there is a wide range of intensity of stimulation over which the operation of the mechanical part of the peripheral auditory system can be considered as linear. The transfer characteristic of the mechanical part of the system has been determined, albeit in an approximate way and over a limited range of frequencies.

Since none of the studies to which we will make reference use free field stimulation, we can ignore the effects of the auricle on sound transmission to the ear. The external meatus is a bony tube terminated by the tympanic membrane. Wiener and Ross⁽¹⁹⁾ measured the pressure transformation from the outside of the ear to the tympanum in human subjects. Figure 2 shows their results. The

Figure 2. Ratio of amplitude of pressure at tympanum to amplitude of sinusoidal pressure (at entrance to the meatus (measured in man)). (19)

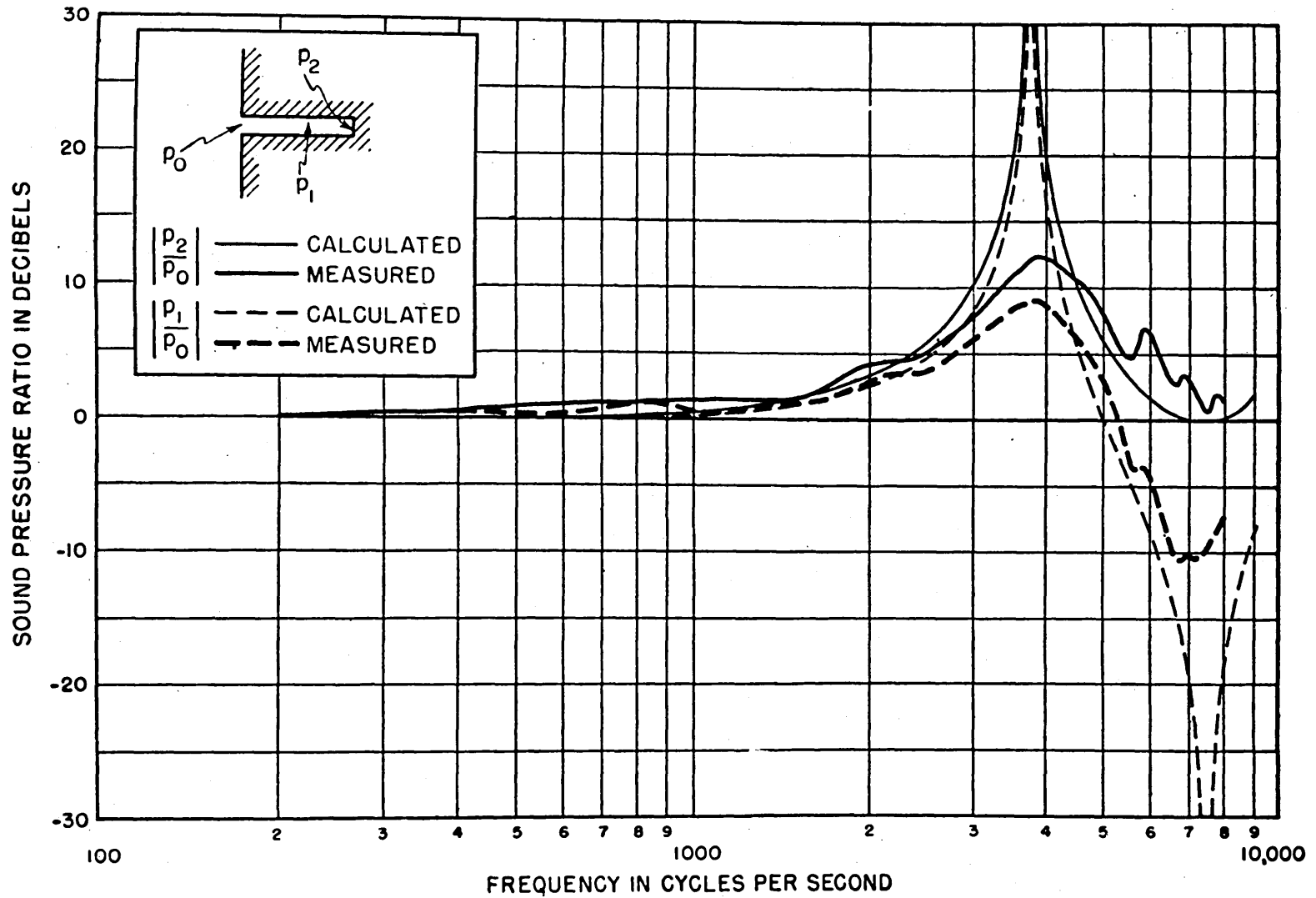


FIG. 12. Showing a comparison between the pressure ratios calculated for an auditory canal with rigid walls and rigid termination, and the pressure ratios obtained from measurements on real ears.

relatively flat peak of the response occurs at the resonance frequency (3.8 Kc) that one would predict for a closed tube approximately 2.5 cm long. Since the termination of the tube is a flexible membrane, the resonance is relatively flat. Note that the transfer function varies less than 10 db over the 8 Kc range of the measurements.

Von Békésy has made a number of measurements that aid in revealing the transfer characteristic of the middle ear. By transfer characteristic we mean the ratio of the amplitude of the displacement of the stapes to the amplitude of a sinusoidal pressure variation at the tympanum. The utility of such a function depends strictly on the linearity of the system. Von Békésy has reported that the middle ear is essentially linear up to the threshold of feeling.⁽²⁰⁾

In discussing the data on the middle ear it is useful to think of its circuit representation. In Figure 3, P_d is the pressure at the ear drum, v_d is the velocity of displacement of the ear drum, p_o is the pressure at the oval window, v_o is the velocity of the displacement of the oval window (or stapes) and z_o is the mechanical input impedance of the cochlea as seen from the oval window. z_{11} , z_{12} , z_{22} are the mechanical impedances that characterize the middle ear.

Von Békésy⁽²⁰⁾ has measured the pressure ratio (for human cadavers) from both the entrance of the meatus and the tympanum to the stapes by balancing the pressure at the stapes from inside the cochlea until the stapes was motionless. This corresponds in our framework to a measurement of the open

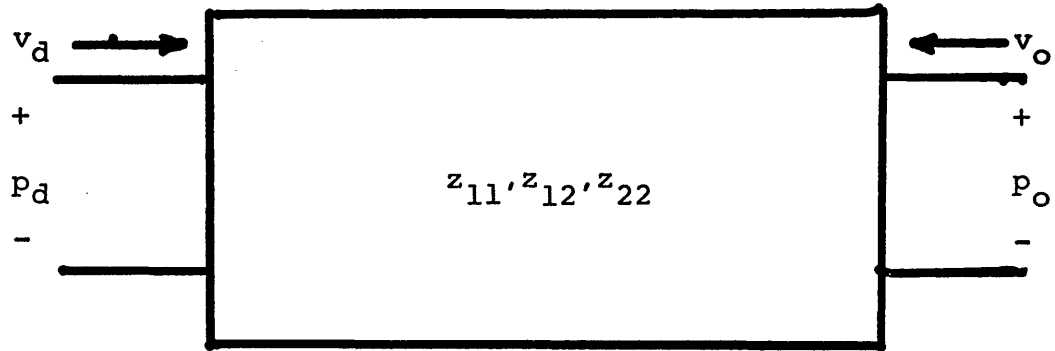


Figure 3. Circuit representation of the middle ear.

$$p_d = z_{11}v_d + z_{12}v_o$$

$$p_o = z_{12}v_d + z_{22}v_o$$

circuit pressure ratio, $(p_o/p_d)_{v_o=0} = z_{12}/z_{11}$. Figure 4 shows these data. Note once again that the variation over a 2 Kc range is not greater than 10 db. Von Békésy⁽²¹⁾ has also measured the volume displacement of the round window to a known pressure at the ear drum as a function of frequency. Von Békésy's measurement corresponds to measuring $(q_o/p_d) = -(k/j\omega)(z_{12}/z_{11})(z_o+z_{22} - (z_{12}^2/z_{11}))^{-1}$, where q_o is the displacement of the oval window, under the assumption that the displacement of the oval window is proportional to the displacement of the round window. Von Békésy's data are shown in Figure 5. Once again the amplitude variation as a function of frequency is under 10 db. The impedances of the cochlea, as measured at the oval and round windows, are probably not very different since the cochlea appears quite symmetrical (in a dynamic sense) when viewed from these two membranes. Wever and Lawrence⁽²²⁾ present data (in cat) on direct acoustic driving of the oval and round windows, with the middle ear mechanisms removed, for a frequency range of 100 cps to 10 Kc. These data* support the above assumption that the oval and round window displacements are equal.

Further data on the dynamics of the middle ear have

*The data are based on observations of the cochlea microphonics.

Figure 4. Open circuit pressure ratio from the entrance to the meatus (hash) and the tympanum (solid) to the stapes. (20)

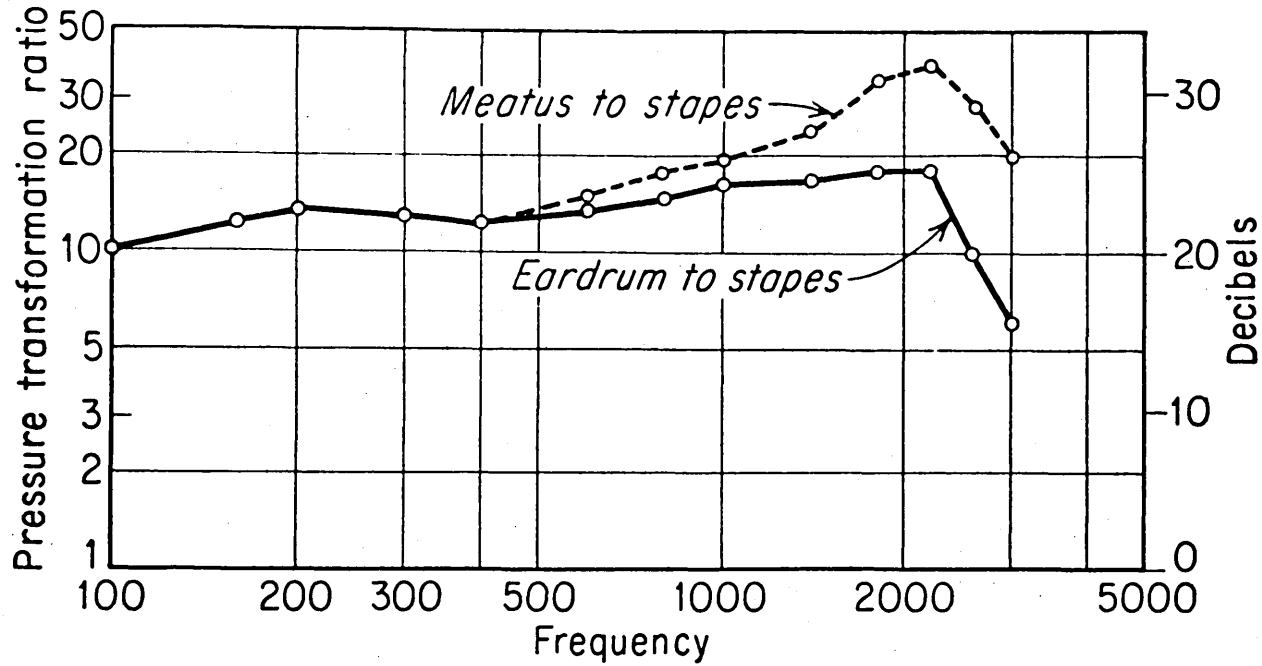


FIG. 5-4. The pressure-transformation ratio between the meatus or the eardrum and the footplate of the stapes.

Figure 5. Amplitude and phase of the volume displacement of the round window for a sinusoidal pressure variation at the tympanum. (21)

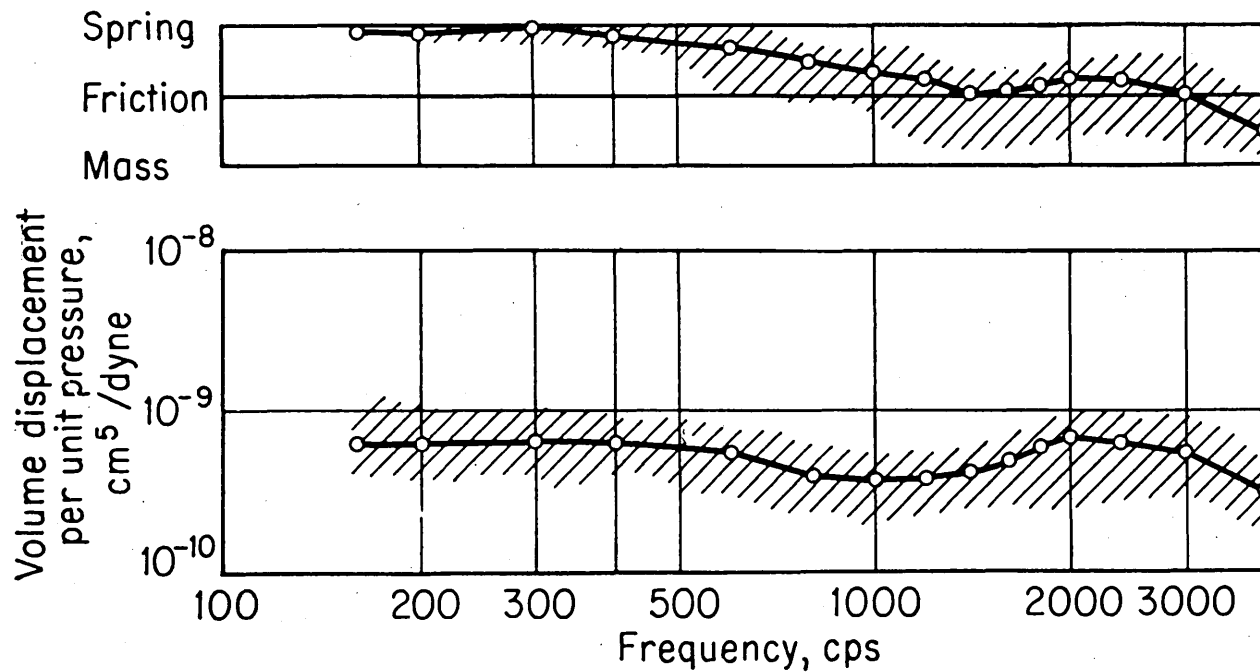


FIG. 11-31. The responses of the round-window membrane to sound. The upper curve shows the phase angle and the lower curve the volume displacement per unit of pressure.

been obtained from measurements of the input impedance of the ear in human subjects. In our terminology, $z_{in} = (p_d/v_d) = (z_{11}/z_{22} + z_o)(z_{22} + z_o - (z_{12}^2/11))$. On the basis of their measurements of the input impedance of the ear, both Møller^(23,24) and Zwislocki⁽²⁵⁾ have constructed equivalent electric circuits of the middle ear.

Transfer characteristics plotted from Møller's data, are relatively flat in the region of 100 cps to 1 Kc. A similar computation performed by Flanagan⁽²⁶⁾ on Zwislocki's data yields results, that, while they are not the same in detail as our results that are calculated from Møller's model, they again indicate a flat amplitude response up to about 1 Kc.

We have tried to summarize a wide variety of data concerning the mechanical transmission of displacements to the stapes.* To our knowledge, no reliable data for frequencies above 2 Kc exist** and we can conclude from available data that the frequency response of the outer and middle ear is flat within 10 db for frequencies below 2 Kc.*** Above 2 Kc inertial effects probably begin to have an effect and the transfer function exhibits a roll-off.

*A recent paper⁽¹¹¹⁾ indicated that gross post-mortem changes occur in the acoustic impedance of the ear.

**The measurements on acoustic transmission and impedance of the ear show great variability for frequencies above 2 Kc. At high frequencies the motion of the various middle ear structures becomes quite complicated and this has complicated the measurement problem.

***This is probably true for the cat as well as for man. (27)

B. Dynamics of the Cochlea

The direct observations and measurements of the dynamics of the cochlea are due entirely to von Békésy. In this section we shall consider von Békésy's measurements of various physical properties (such as viscosity, density, elasticity, etc.) of the cochlea. We shall then discuss his observations of the motion of the cochlear partition (in physiological preparations as well as in mechanical models) as a function of the displacement of the stapes.

The most important physical parameters that von Békésy measured were the properties of the cochlear partition. He⁽²⁸⁾ showed that the cochlear partition was not in tension and could not, therefore, be considered as a stretched membrane. Von Békésy⁽²⁹⁾ discovered that the elasticity of the cochlear partition varies from the basal to the apical end of the cochlea. Figure 6 shows a curve of the variation of the elasticity of the cochlear partition for human cadavers. Notice that at the basal end the partition is relatively stiff, while at the apical end it becomes relatively flacid. Von Békésy⁽³⁰⁾ was further able to show that it is the elasticity distribution of the basilar membrane that dominates this pattern. The elasticity of the other structures in the cochlear partition (tectorial membrane, Reissner's membrane and reticular lamina) are relatively constant over the length of the cochlea. Needless to say, the elastic characteristics of the partition are much more complex than depicted here. For instance, it is clear that the elastic

Figure 6. Elasticity of the cochlear partition as a function of distance from the stapes. (29)

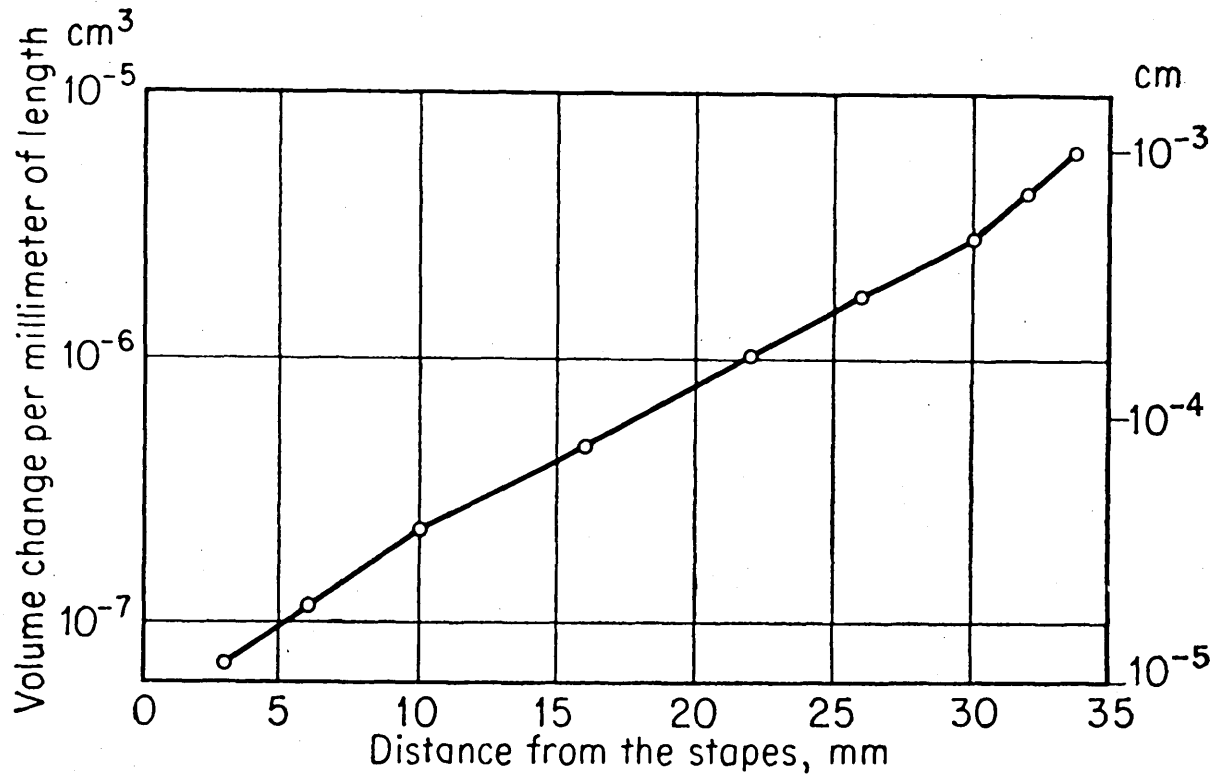


FIG. 11-73. Volume displacement per millimeter of the cochlear duct (left-hand ordinate) and maximum displacement of the cochlear partition (right-hand ordinate) for a pressure of 1 cm of water.

properties must vary in the cross-section since the basilar membrane is supported on one side by bone while the other side is supported by ligament. Nevertheless, it is the 100:1 variation in elasticity of the basilar membrane in its longitudinal direction that gives the cochlear partition its chief dynamic properties.

Von Békésy has also estimated the density and viscosity of the perilymph⁽³¹⁾ and shown that the mass loading of this fluid⁽³²⁾ on the cochlear partition was an important factor in the dynamics of the cochlea. In addition, von Békésy⁽³³⁾ has estimated the damping of the cochlear partition.

Observations on the motion of the cochlear partition in human cadavers were achieved by cutting away various portions of the cochlea and/or replacing these portions with transparent surfaces. The cochlea was stimulated mechanically through an artificial stapes usually located at the round window. Even for the relatively large stapedial displacements he used, von Békésy found that the relation of the displacement of the cochlear partition to a stapes displacement was linear.⁽³⁴⁾ For a sinusoidal stimulus, the displacement of the cochlear partition was sinusoidal in time, and the envelope of the displacement exhibited a spatial pattern whose maximum moved as a function of frequency.⁽³⁵⁾ Figure 7 is such a "cochlear map"⁽³⁶⁾ obtained by measuring the position of the maximum displacement of the cochlear partition as a function of frequency.

Figure 7. Position of the maximum displacement of the cochlear partition as a function of the frequency of sinusoidal stapes displacements. (51)

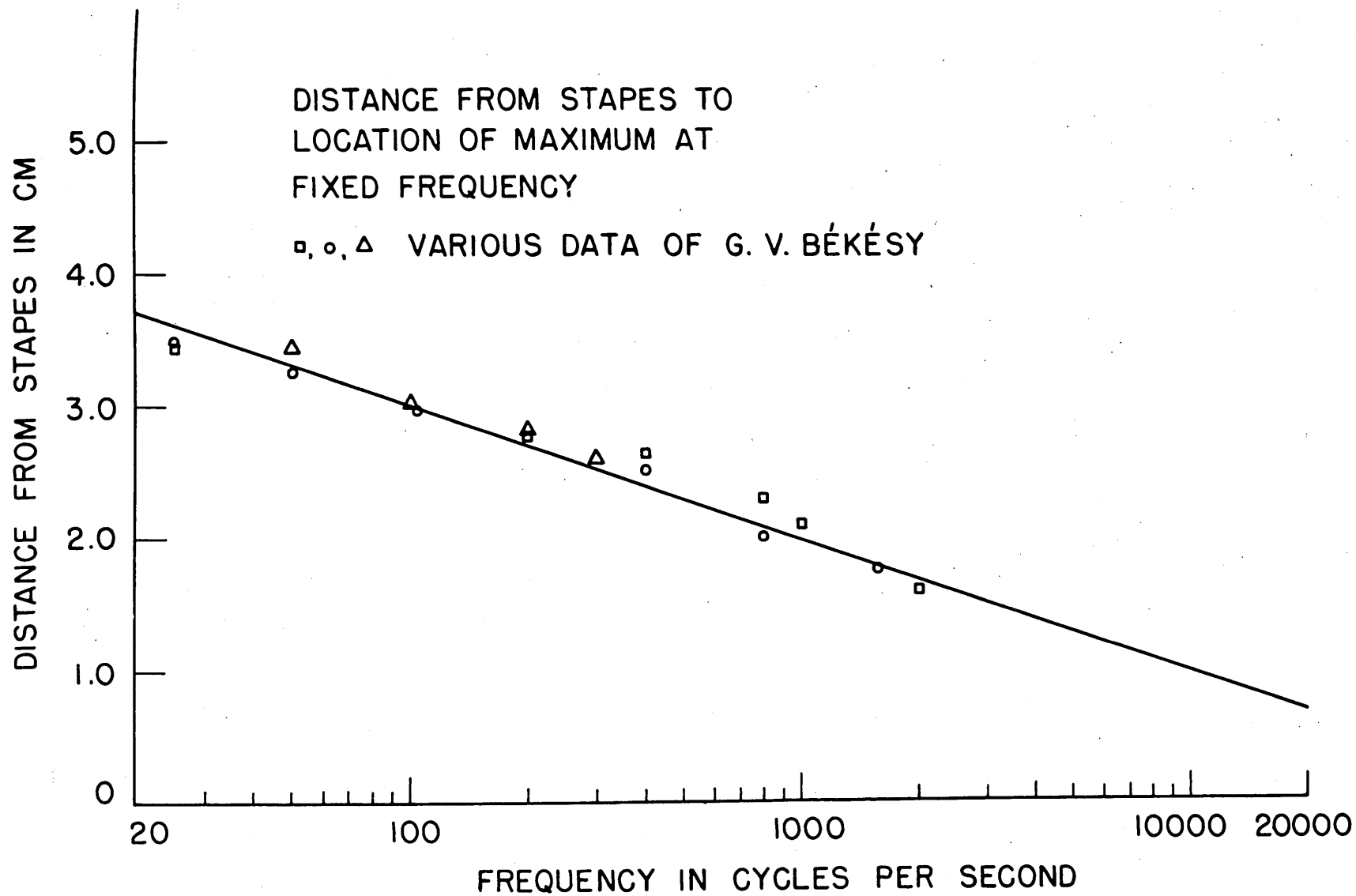


Fig. XXVI-3. A "cochlear map" - plot of $x_{\max}(f)$.

Von Békésy has stated that these measurements show "great stability" for different cochleas.

Figure 8 shows the amplitude of displacement at a point on the membrane as a function of frequency for several different points plotted on a normalized scale.⁽³⁷⁾ Note that the curves all have the same general shape when plotted in logarithmic coordinates. If the frequencies of their maxima are brought into coincidence on a logarithmic frequency scale, the curves are almost identical. These curves show a relatively broad resonance with a figure of merit, $Q = 1.6$ (when Q is defined as the ratio of the resonant frequency to the bandwidth measured at -3 db with respect to the maximum). Figure 9 shows values of the displacement at the maxima as a function of frequency.⁽³⁸⁾

Von Békésy has also obtained curves of the displacement pattern of the cochlear partition as a function of position for various frequencies of stapes displacement.⁽³⁹⁾ He describes the motion of the cochlear partition⁽⁴⁰⁾ as that of a traveling wave whose envelope has a maximum at some position (determined by the frequency of the stapes displacement) and whose wavelength decreases as a function of distance from the stapes.

This entire response pattern is reported to be independent of the point of excitation. That is, when the fluid displacements are introduced into the apical end of the cochlea via an artificial opening, the same pattern of traveling waves is seen from the base to the apex.^(41, 42)

Figure 8. Amplitude and phase of the displacement of the cochlear partition as a function of frequency for several positions along the cochlear partition. $H_x(f)$ is the transfer function of the cochlear partition for a sinusoidal displacement of the stapes. The scales of the amplitude and phase responses are the same. Solid curves, von Békésy (1943) (37); dashed curves, von Békésy (1947) (40). The figure is reproduced from Siebert (51).

-07-

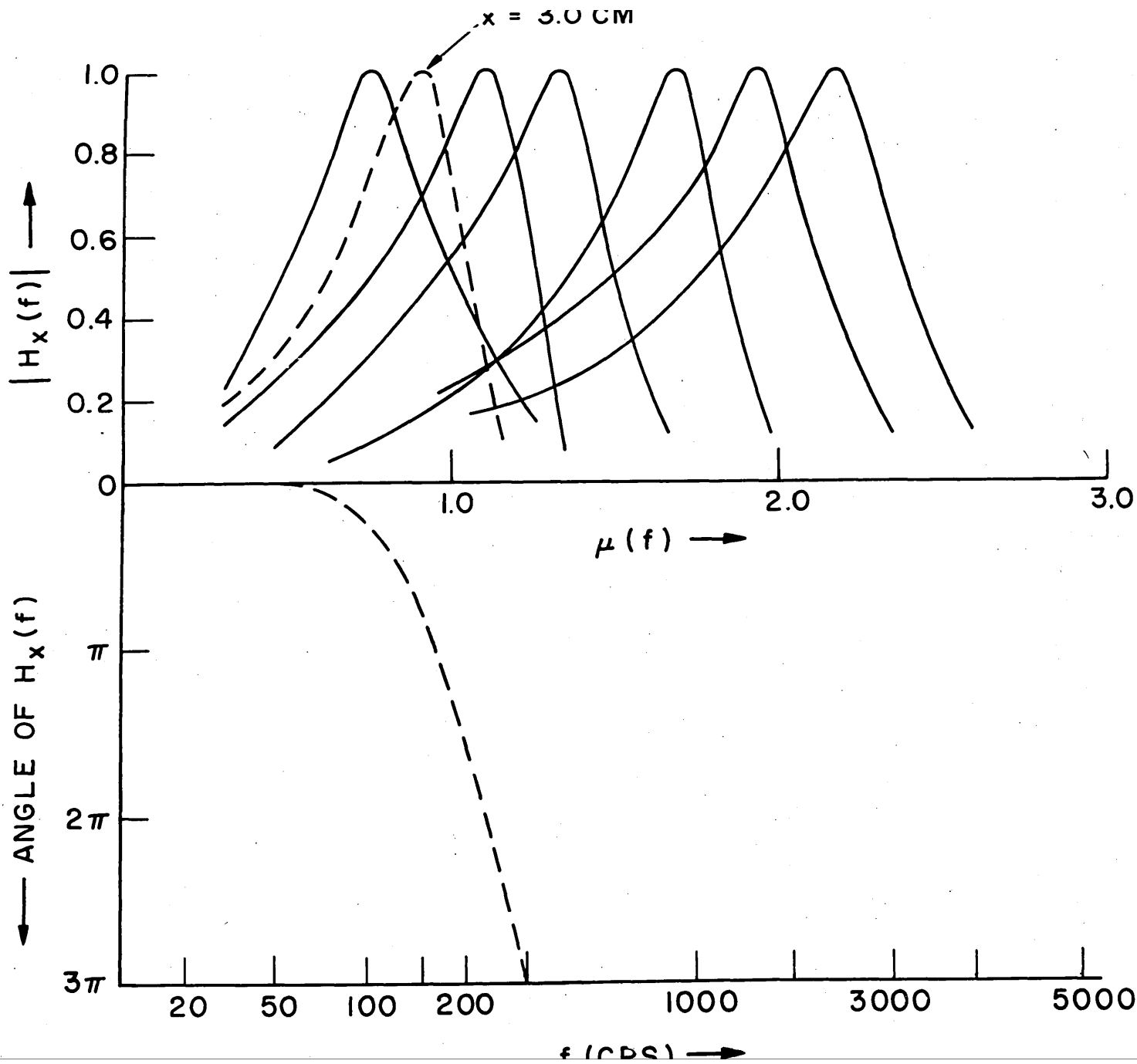
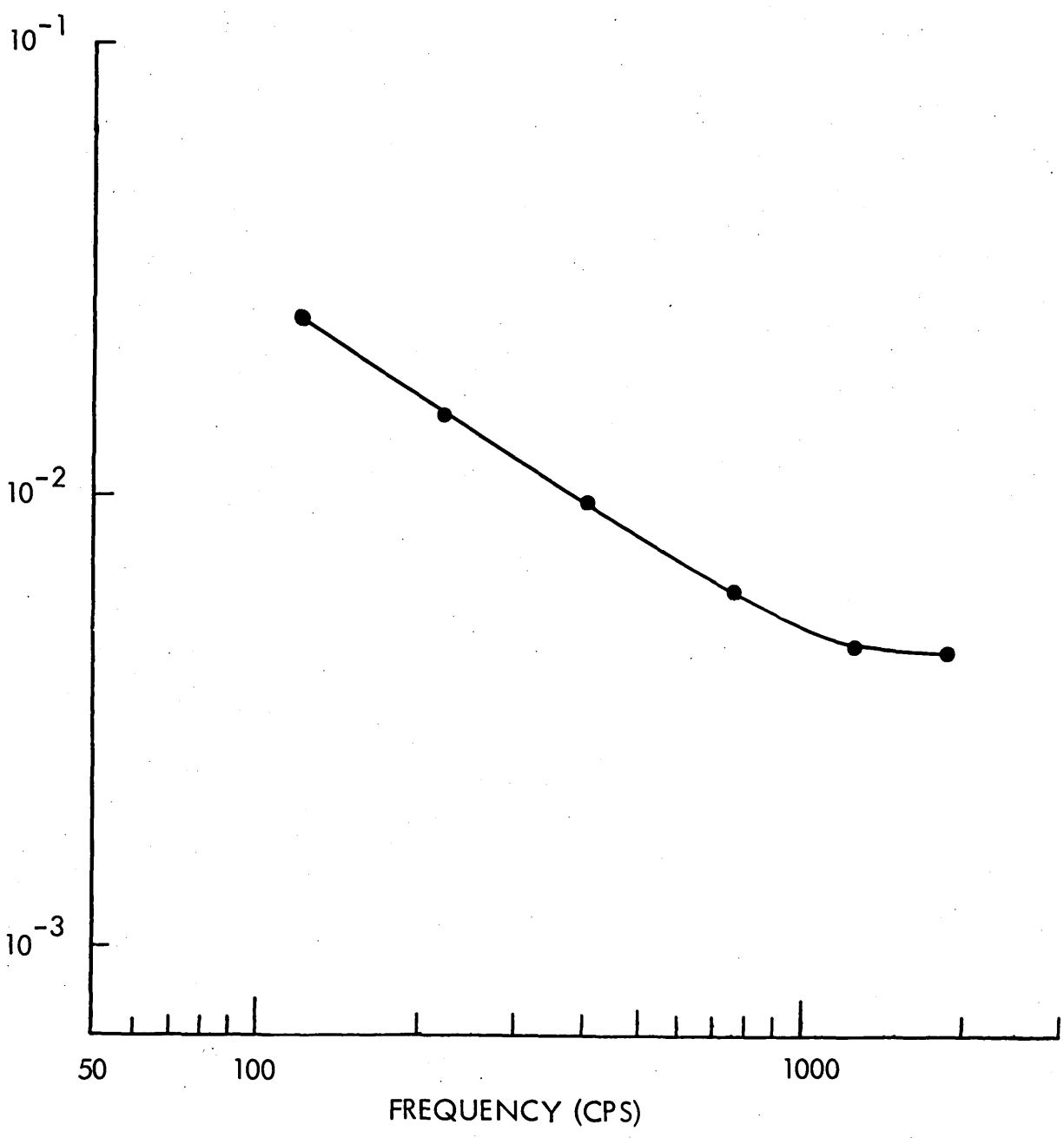


Figure 9. Volume displacement at stapes divided by maximum amplitude at cochlear partition as a function of frequency. (38)

VOLUME DISPLACEMENT AT STAPES DIVIDED BY MAXIMUM
AMPLITUDE AT COCHLEAR PARTITION (cc/cm)



This phenomenon was named the "paradoxical direction of propagation" by von Békésy.

The dynamics of the cochlea can now be understood, at least in a qualitative way. First, consider the propagation velocity of a compression or sound wave in a medium such as perilymph. Since the density of perilymph is approximately the same as that of water, we can assume that the velocity of sound in water is a reasonable estimate of the velocity of sound in perilymph. This velocity is 1.4×10^3 mm/msec. The cochlea of man is about 35 mm long; thus the propagation time of sound from one end of the cochlea to the other is about 25 μ sec. This is about two orders of magnitude smaller than the propagation time of the traveling waves that von Békésy observed at the apical end of the cochlea. Therefore, the pressure wave generated by stapes displacements, (or stimulation at any other point in the cochlea) can be assumed to reach the apical end of the cochlea almost instantaneously.

The response of a point on the cochlear partition to this pressure change depends upon the physical parameters of the membranes and fluids. The frequency of stimulation giving maximal response for that point, f_0 , is determined largely by 1) the elasticity of the cochlear partition at that point and 2) the mass loading of the fluid in the neighborhood of that point, in addition to 3) friction, viscosity, and membrane coupling effects. Since the elasticity increases continuously as a function of distance from the

stapes, we would intuitively expect that f_0 will decrease. Furthermore, as the elasticity increases, the response time or lag time of a point on the cochlear partition also increases. Since the parameters of the cochlear partition vary continuously, this response time varies continuously and thus the response of this membrane to a sudden displacement of the stapes appears as a progressive set of displacements or as a wave that travels down the cochlea. This pattern is not a traveling wave in the ordinary sense, since all of the energy is not transferred from one element of the membrane to another. Von Békésy, using scaled models of the cochlea, has demonstrated that, most likely, the energy for the motion of the membrane is transmitted to the membrane from the fluid. Thus, it is the change in elasticity of the basilar membrane as a function of distance that gives the cochlea its particular response characteristics. Unfortunately, the equations of motion of such a system are complicated by both the geometry and the interaction terms. That is, one can probably not reduce the mechanics of the cochlea to a simple lumped parameter system that includes mass, elasticity, and damping. The cochlea can best be regarded as a distributed parameter system whose parameters vary grossly with distance from the stapes.

Several workers have attempted to derive the equations of motion of the cochlear partition, (43, 44, 45, 46, 47, 48) with varying degrees of success. Most of the analytic approaches that yield solutions ultimately arrive at a

one-dimensional representation of the cochlea. The relevant equations that have been used are 1) the continuity equation for an incompressible fluid, 2) the Navier-Stokes equation of motion for an incompressible fluid with irrotational, infinitesimal motion, and 3) the beam equation, including elasticity, mass, and damping. Various authors have made various further assumptions as to which terms in the equations dominate and therein lie the differences in the approaches.

One of the earlier and more interesting analytic approaches to the problem is that of Zwislocki, who derived a closed form expression (under a multitude of assumptions) for the displacement of the cochlear partition for a sinusoidal displacement of the stapes. The results he plots seem to fit the von Békésy frequency response curves rather well.

In the past few years, with the participation of communications engineers in studies of the auditory system, interest has been aroused in the impulse response of the cochlear partition. At least two such studies have been undertaken. In the first of these studies, Flanagan^(49, 50) has approximated the frequency response data of von Békésy, by using rational functions of frequency. Flanagan has also derived impulse responses of the cochlear partition (shown in Figure 10) that can be realized with lumped parameter electric circuit components. Siebert⁽⁵¹⁾ also

Figure 10. Impulse responses of several models of the displacement of the cochlear partition. (After Flanagan(50)).

$$f_3(t) = \frac{c_3 \beta^{1+r}}{6} [\beta(t-T)]^2 e^{-\beta(t-T)/1.7} \sin \beta(t-T) \quad \text{for } t \geq T$$

$$= 0 \quad \text{for } t < T$$

$$\beta T = 3\pi/4$$

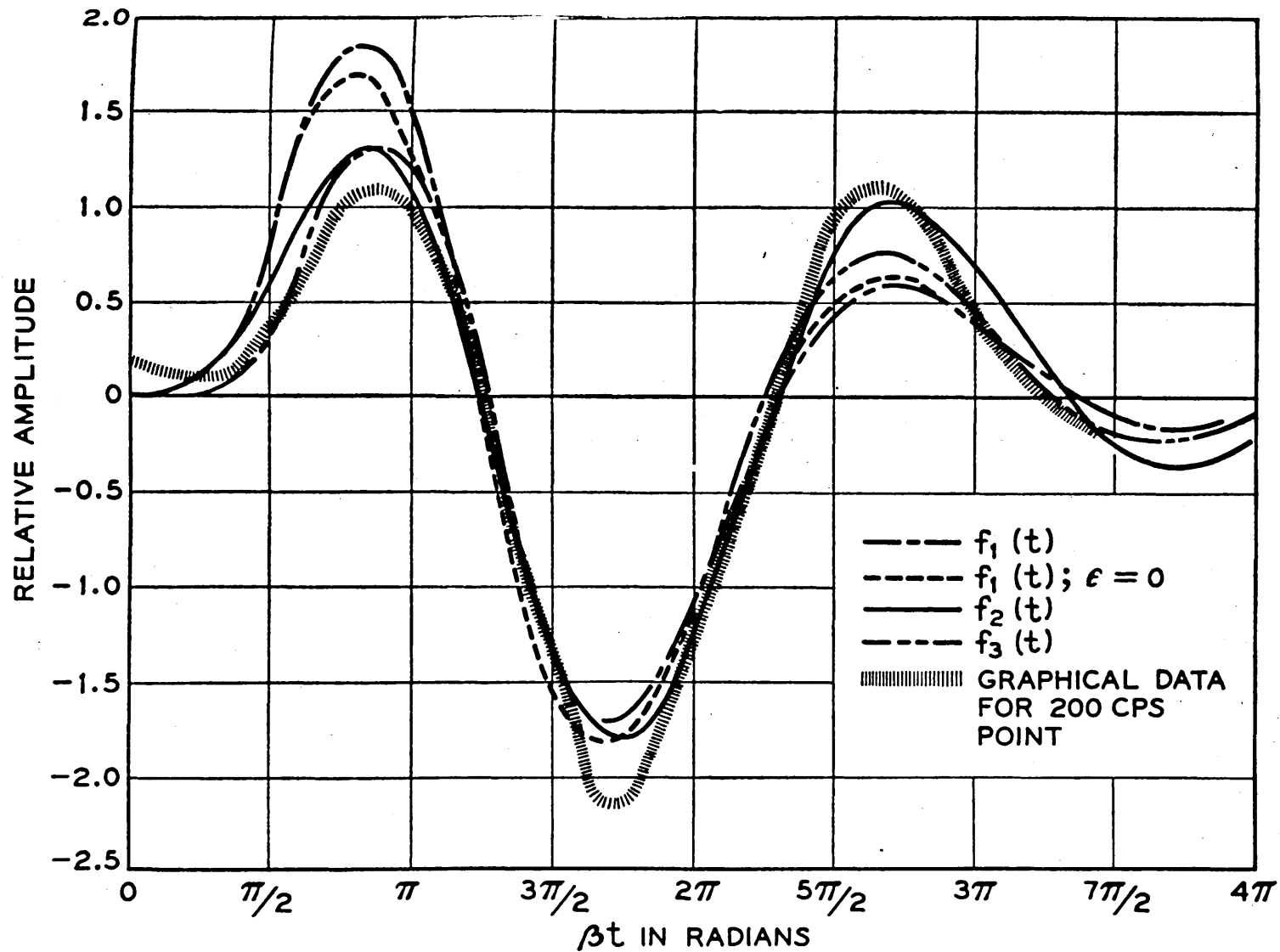


Fig. 12 — Impulse responses of the models. These displacement functions are the inverse transforms of the frequency-domain data in Figs. 10 and 11. Time delay has been equalized to compare waveforms. Locations of absolute origins are given in the text.

has empirically determined analytic expressions that approximate the frequency response data. Siebert's functions are not rational functions and are not unlike Zwislocki's formulas, derived from fundamental considerations. Siebert's transfer functions yield the impulse response seen in Figure 11. Neither of these empirically derived impulse responses can be entirely accurate. All of the impulse responses derived by Flanagan are based on lumped parameter models. Real delays are included to aid in the approximation of the phase data. The impulse response derived by Siebert is unrealizable and, therefore, can not be entirely correct. These discrepancies may, however, be inconsequential in the study of the activity of VIIIth nerve fibers resulting from displacements of the cochlear partition.

These impulse responses are plotted on normalized time scales. For a point at the basal end (a point tuned to relatively high frequencies) the impulse response is a relatively fast transient with an oscillation whose frequency is approximately the tuning frequency of that point on the basilar membrane. For an apical or low frequency location the impulse response is a slow transient with correspondingly slow oscillations. It is well to point out that these impulse responses are all based upon the data of von Békésy. These data extend over a range of frequencies up to about 2 Kc. Strictly speaking, the impulse responses can be considered valid only over this range of frequencies.

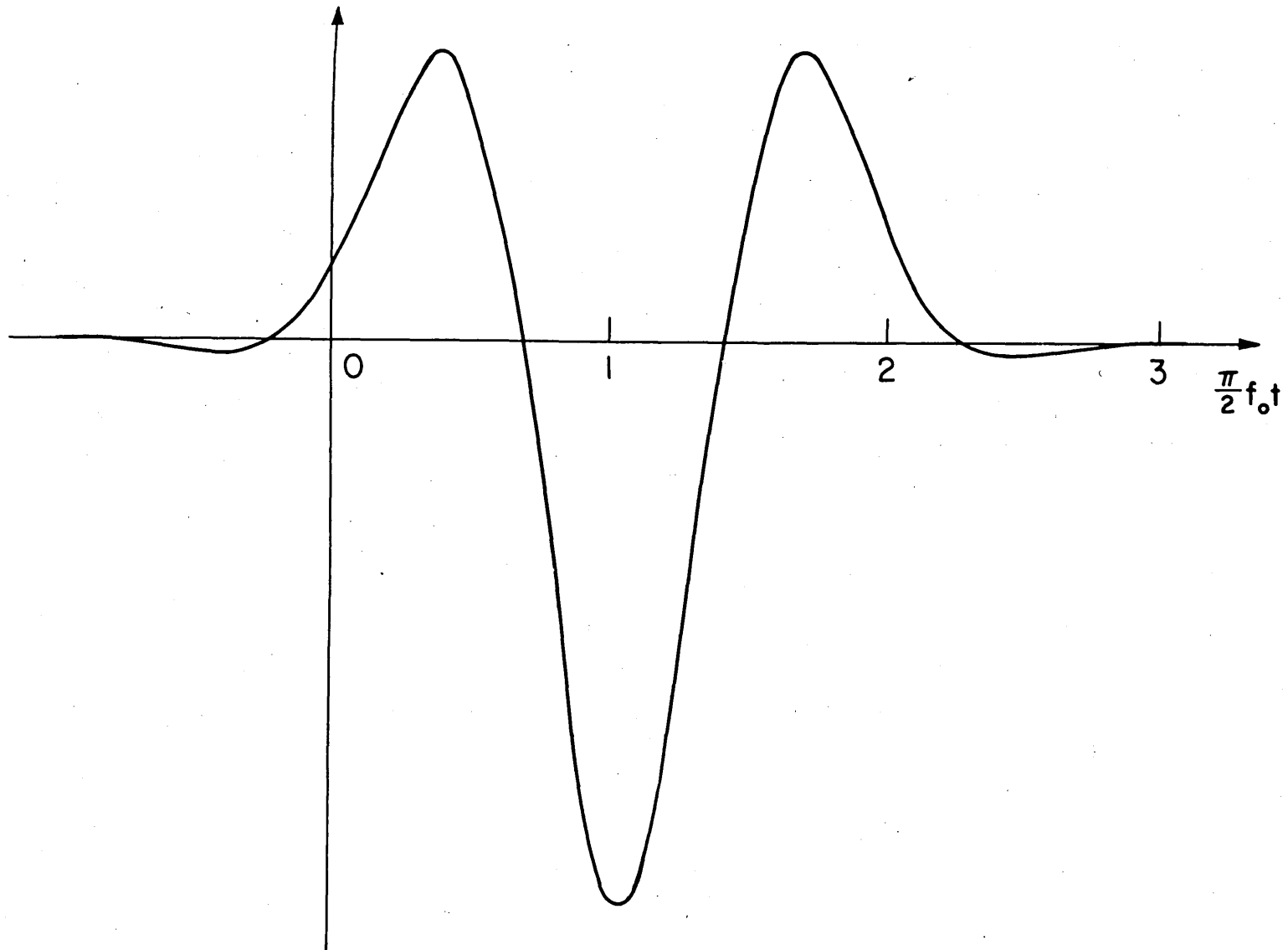
Figure 11. Impulse response of a model of the displacement of the cochlear partition. (After Siebert⁽⁵¹⁾).

$$h(x,t) = 2.03f_{\max}(x)e^{-2v^2} (3/4\cos 3v - v\sin 3v)$$

where $h(x,t)$ is the impulse response

and $f_{\max}(x) = 10^{5-x}$

$$v = \pi(1/3 - (1/2)f_{\max}(x)t)$$



-50-

Fig. XXVI-11. Impulse response at point on cochlear partition which responds maximally to frequency f_0 . (From Model, normalized.)

C. Brief Electrophysiology of the Cochlea

Measurements of the electrical activity recorded with electrodes placed on the round window or in the cochlea scalae indicate the presence of several distinguishable electrical potentials. In the absence of stimulation the endolymph in scala media is at a potential of +50 millivolts (a potential referred to as the EP or endocochlear potential) with respect to the perilymph.⁽⁵²⁾ If the ear is stimulated with sound, several other potentials may be observed at the same time. These are the cochlear microphonic potential (CM), the summing potential (SP) and the gross action potential (N_1). Stevens and Davis,⁽⁵³⁾ among others,^(54, 55, 56) have shown that CM is linearly related to the acoustic signal over a range of at least 60 db SPL. Von Békésy⁽⁵⁷⁾ has further shown that CM is proportional to the displacement of the cochlear partition, rather than to the time derivative of the displacement. Davis^(58, 59, 60) has constructed a consistent set of hypotheses concerning the function and origination of CM. In this scheme, the bending of the outer hair cells, which results from a displacement of the basilar membrane, changes the electrical milieu in the Organ of Corti. The electric currents that result from this change flow through and depolarize the nerve endings near the hair cells and thus set up action potentials in the nerve fibers. Therefore, CM is viewed as a mechanism for the initiation of electrical activity in the VIIIth nerve. Local recordings of CM at

the hair cells are, however, difficult to obtain. CM has been recorded intracochlearly (between scala vestibuli and scala tympani), (61, 62) and the results indicate that the time course of CM as a function of distance along the cochlea is similar in some qualitative respects to von Békésy's observations on the motion of the basilar membrane. These results are difficult to interpret however, since one cannot be certain that the recordings are sufficiently local in origin. Nevertheless, it is quite certain that CM is involved in the process of initiation of action potentials in the VIIIth nerve. The extent of this participation, and the dynamic range of stimuli over which it is the principal mode of excitation is not known.

The SP^(63, 64) (there is an SP+ and an SP-) is similarly felt to be involved in the process of neural activation. It is also a cochlear potential, probably generated in some way by forces on or by movements of the hair cells. The SP is not linearly related to the acoustic stimulus, but is thought to represent the root-mean-square of the stimulus.

Finally, N₁^(65, 66, 67) is thought to represent a spatio-temporal summation of electrical activity in the fibers of the VIIIth nerve, and it can be recorded from a variety of locations, such as in, on, or outside the cochlea and in the VIIIth nerve. At this point, we shall not discuss the voluminous literature on N₁ since we are more concerned here with the all-or-none events in the nerve at the single fiber level.

D. Patterns of Action Potentials in the Afferent Fibers of the VIIIth Nerve

Although the recording of spike potentials in the VIIIth nerve has been reported previously in the literature* (68, 69) the recent work of Kiang et al⁽⁷⁰⁾ gives by far the most complete picture of unit fiber activity in the VIIIth nerve. Most of this work is as yet unpublished and since it is germane to our problem, we shall briefly discuss some of the major results.

All of the data were obtained by means of micro-electrodes from cats anaesthetized with Dial and urethane. These electrodes were placed in the VIIIth nerve peripheral to its entry into the cochlear nucleus. From the wave shape of the spike potentials, location of the electrodes, absence of injury discharges and other indications, it appears that all of these data were obtained from fibers of the VIIIth nerve.

The fibers exhibit a number of interesting properties. First, all the fibers studied to date exhibit spontaneous firings, i.e., action potentials can be observed to occur in the absence of acoustic stimulation. The average rate of firing varies from fiber to fiber, but generally lies in the range of a few spikes per second to as many as 150

*Only reports in which the locations of the electrode have been verified to be in the VIIIth nerve are considered here.

spikes per second. Figure 12 shows a representative histogram of time between the occurrence of spikes for a typical fiber (plotted on semi-logarithmic coordinates). The distribution of intervals can adequately be described as exponential except for very short intervals. Presumably, this is the range where the refractoriness of the fiber affects the firing pattern.

Figure 13 shows tuning* curves for several fibers observed in one cat. Note that different cells seem to tune (that is, are maximally sensitive) at different frequencies. The cells that tune to higher frequencies are found farther from the center of the VIIIth nerve than the cells that tune to low frequencies.

From further data of this kind, it can be seen that the relative width of tuning, Q , of these curves does not vary with frequency up to about 1 Kc. Above 1 Kc the Q increases markedly as a function of frequency, i.e., the tuning curves get narrower at high frequency. When wide-band noise is added to the sinusoidal stimulation, the overall sensitivity decreases but the general shape of these tuning curves remains the same.

Figure 14 shows the response to acoustic clicks (100 μ sec electrical pulses applied to a condenser earphone)

*Tuning curves are graphs of the threshold of synchronous firing of a unit as a function of the frequency of sinusoidal sound stimulation. The threshold can be determined very accurately within 1 or 2 db of intensity. Chapter V contains a further discussion of these tuning curves.

Figure 12. Interval histogram of the spontaneous firings of a fiber in the auditory nerve (in cat) plotted in semi-logarithmic coordinates. (70)

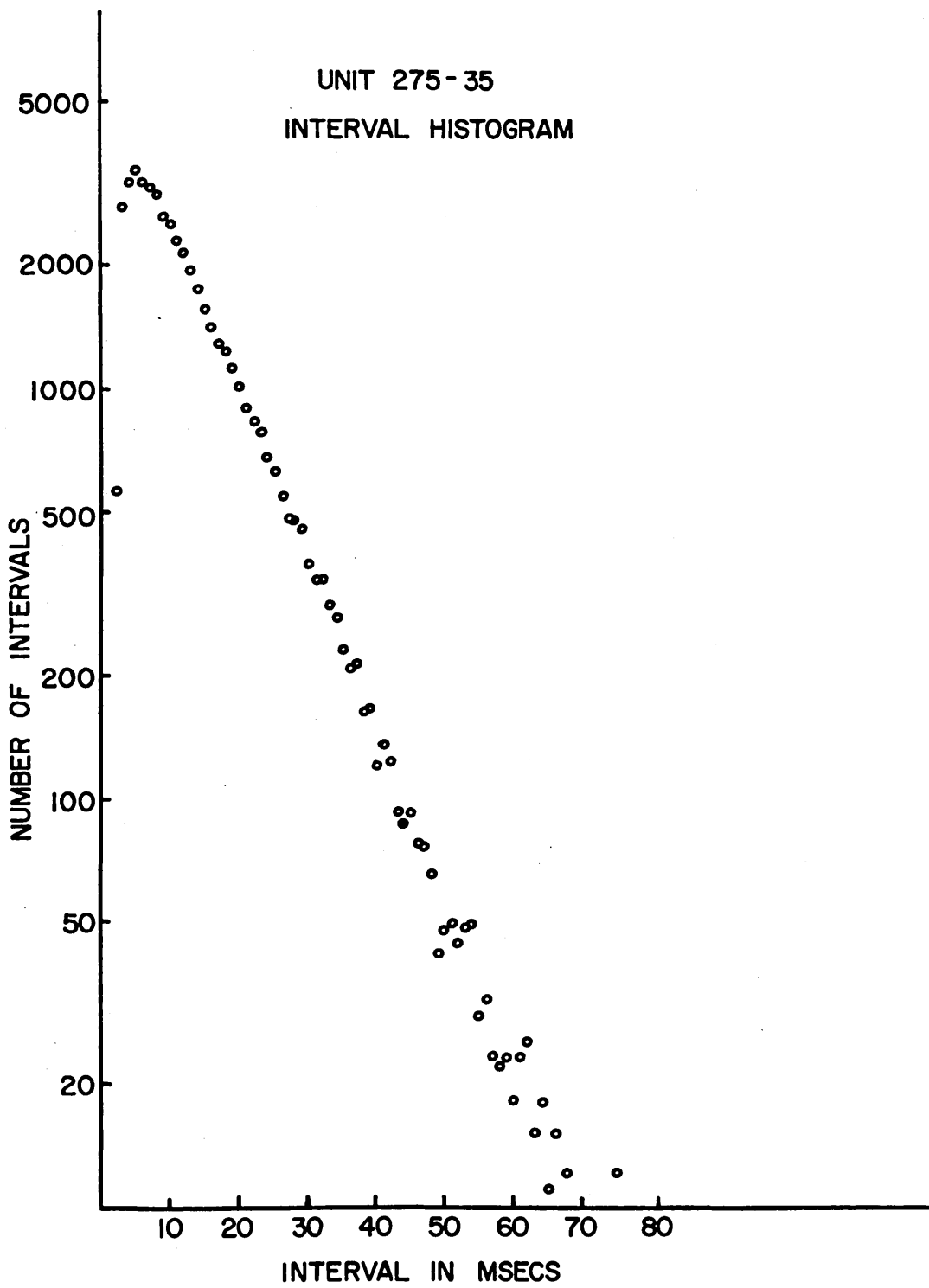


Figure 13. Tuning curves for several fibers in the auditory nerve (cat). (70)

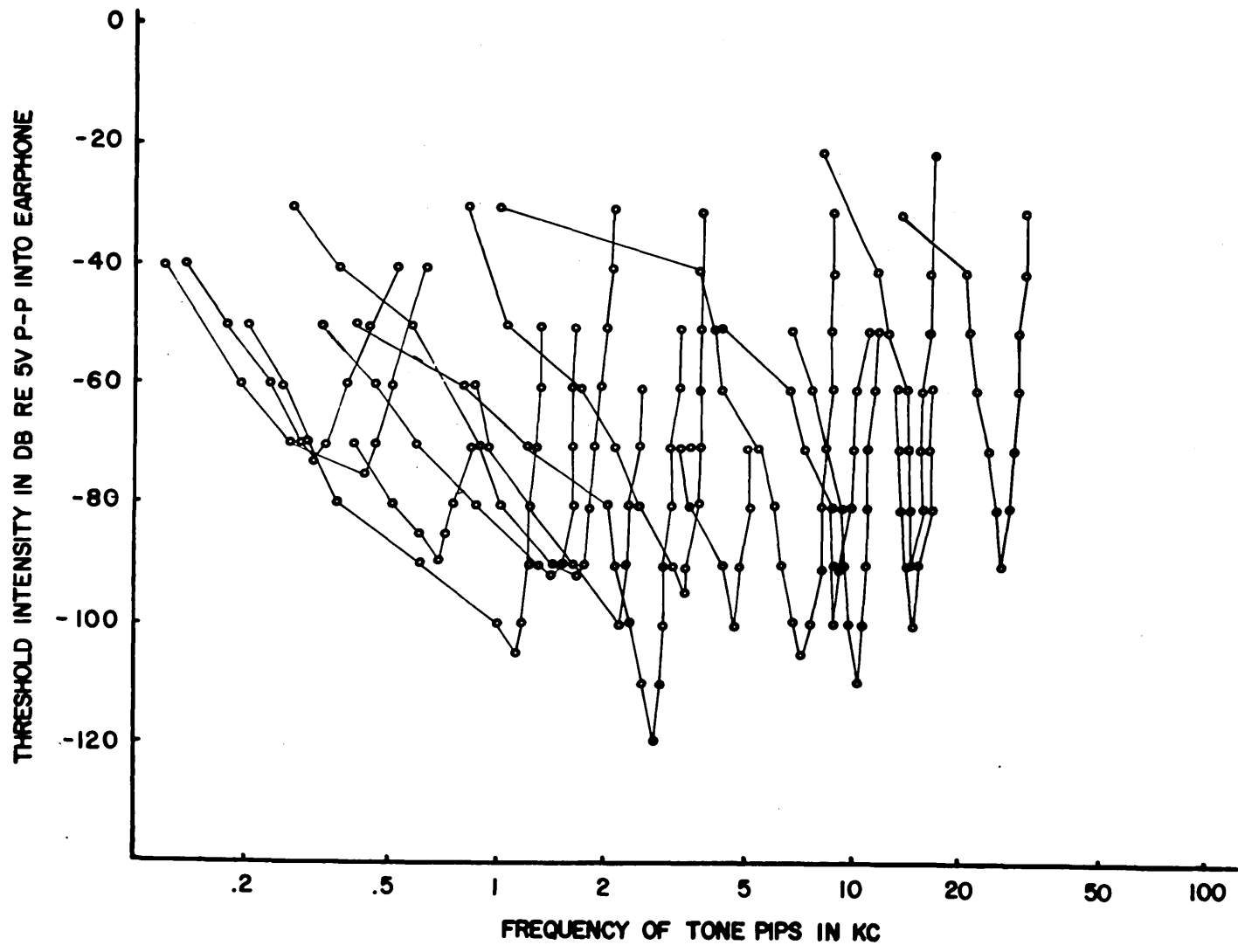
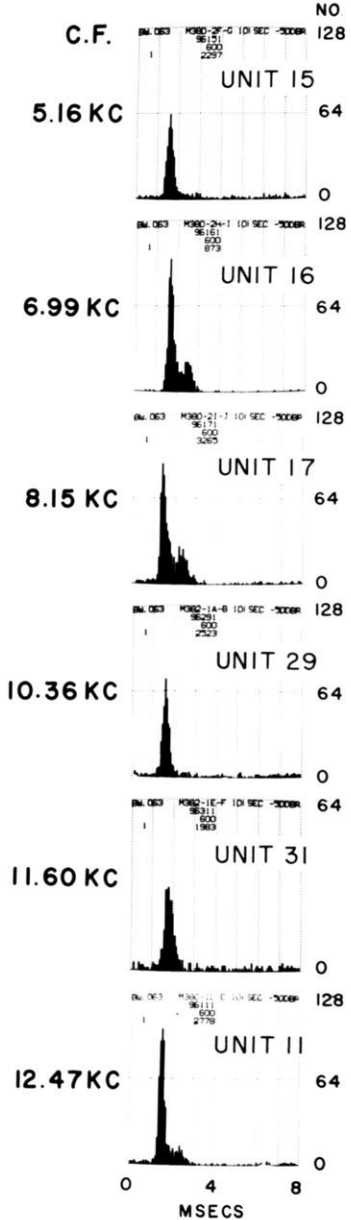
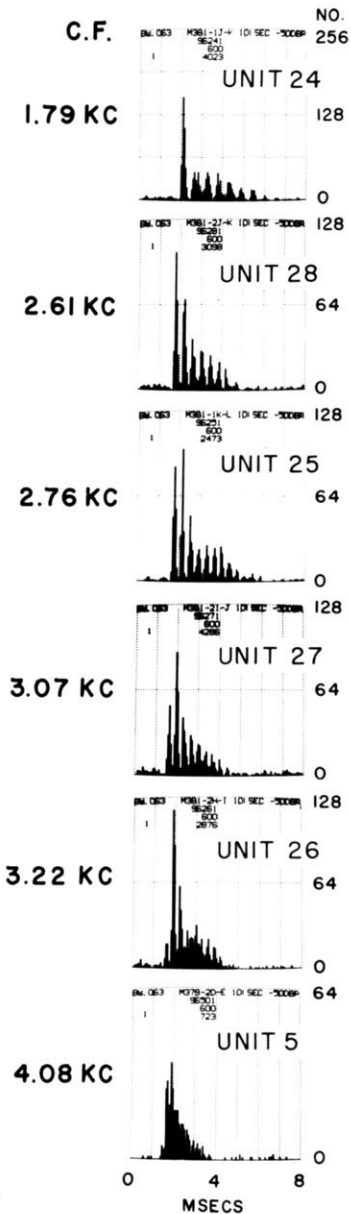
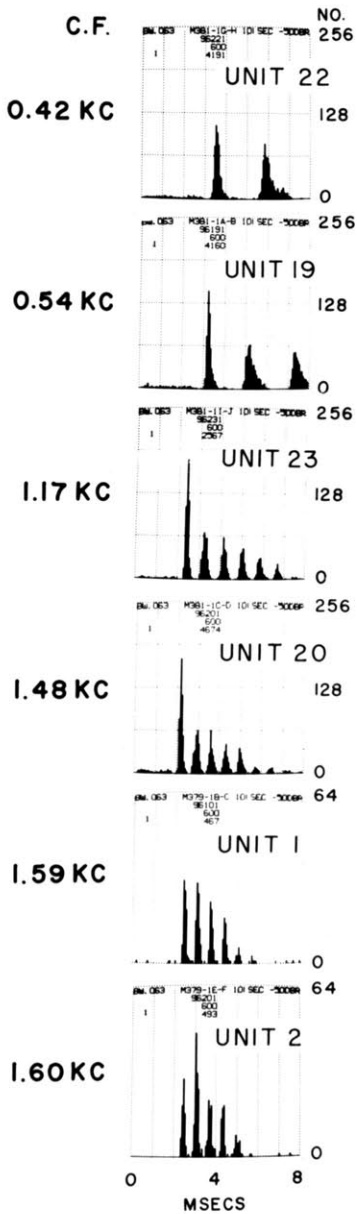


Figure 14. Post stimulus time histograms for fibers in the auditory nerve (cat) to click stimulation. Click intensity is +30 db (VDL) at a rate of 10/sec. CF is the frequency for which the lowest intensity of sinusoidal acoustic stimulation is required in order to elicit synchronized firings in the fiber. (70)

K-296
PST HISTOGRAMS



CLICK RATE: 10/SEC

of units tuned to different characteristic frequencies f_0 (frequency of lowest threshold of firing). The figure consists of post-stimulus-time (PST) histograms⁽⁷¹⁾ (histograms of the times of occurrence of spike potentials measured from the onset of the last stimulus). Note that the time of occurrence of the first peak is later for low frequency tuning units than for high frequency tuning units. Note also that the time between maxima in the PST histograms is inversely related to the tuning frequency (in fact this time can be shown to be $1/f_0$ within statistical variations).

Further data obtained by Kiang et al indicate that the time of occurrence of the first peak in the PST histogram of a unit does not vary much (less than $\frac{1}{4}f_0$) with changes in intensity of stimulation. At high intensities an additional peak may appear preceding the first peak. These peaks appear at times corresponding to integral multiples of $1/f_0$ with respect to the original first peak.

The responses to clicks of different polarity (condensation clicks and rarefaction clicks) show differences in the times of occurrence of maxima in the PST histogram that correspond to $\frac{1}{2}f_0$. At high intensities, the first peak in the PST histogram in response to a rarefaction click leads the first peak in the PST histogram for the response to a condensation click.

For f_0 greater than approximately 4 Kc, the PST histograms exhibit no such multiple peaks. This may be

due to (1) the resolution limiting the measurements,
(2) the inability of the fiber to resolve these peaks, or
(3) the mechanism of excitation may be different for
frequencies above 4 Kc.

CHAPTER IV: A Model of the Peripheral Auditory System

This chapter contains a discussion of a model of the peripheral auditory system that relates the spike activity of fibers in the VIIIth nerve of cats (as reported by Kiang, et al.) to acoustic stimuli. An attempt has been made to include the principle functional constituents of the peripheral system in the model. Figure 15 shows this model. The "Mechanical System" represents the functional relation between an acoustic pressure input to the ear and a displacement of the cochlear partition at a point x centimeters from the stapes. The excitatory process is interposed between the displacement of the cochlear partition and the firing of an VIIIth nerve fiber. This process is not well understood, but it undoubtedly involves the action of the hair cells. In the model the "Transducer" is intended to represent the action of these hair cells. The final block shows a "Model Neuron"--a formal and simplified model of excitable nerve membrane. The output of the transducer serves as the input to the "Model Neuron" and is filtered and then added to noise. Noise is included in order to account for both the spontaneous activity and the probabilistic response behavior characteristic of VIIIth nerve fibers. The noisy membrane potential is next compared to a threshold in the box labelled "C". If the threshold is exceeded then a spike is defined to occur and the threshold is

Figure 15. A model relating the firing patterns of fibers in the auditory nerve to acoustic stimuli.

$p(t)$ is the pressure at the ear

$y(t,x)$ is the displacement of the cochlear partition

$z(t,x)$ is the output of a sensory cell

$f(t,x)$ is the sequence of spikes generated in an VIIIth nerve fiber

$r(t,x)$ is the threshold potential

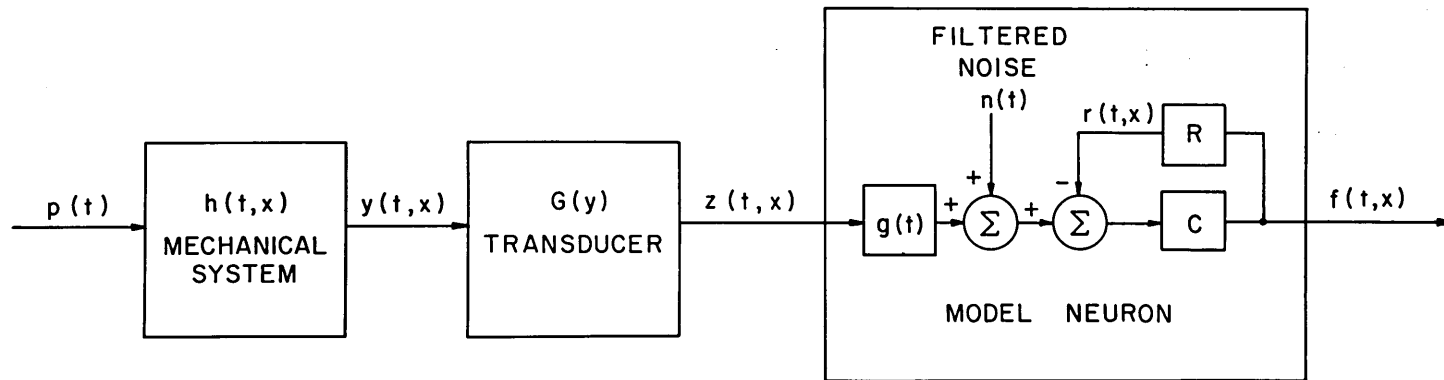
$h(t,x)$ is the impulse response of the mechanical system

$G(y)$ is the transducer function

$g(t)$ is a linear filter

t - time

x - distance from the oval window to a point along the cochlear partition



A MODEL RELATING THE FIRING PATTERNS OF FIBERS IN THE AUDITORY NERVE TO ACOUSTIC STIMULI

reset to some larger value by the box labelled "R".

Figure 16 shows both the noisy membrane potential of the model neuron and the threshold as a function of time. The threshold is reset to some larger value (R_M) upon the occurrence of a spike and decays to its resting value (R_R) with an exponential decay (of time constant τ_R).

A. Summary of Assumptions of the Model

(1) The mechanical part of the peripheral auditory system is assumed to be representable as a linear system over an intensity range of 80 db. The mechanical system encompasses the outer, middle and the mechanical part of the inner ear and relates the displacement of the cochlear partition to acoustic pressure at the ear. Furthermore, the transfer function characterizing this mechanical system is assumed to be determined by the data of von Békésy. Implicit in this assumption is a further assumption that the outer and middle ear have flat frequency responses over the range of validity of this model (approximately 100 cps to 2 Kc).

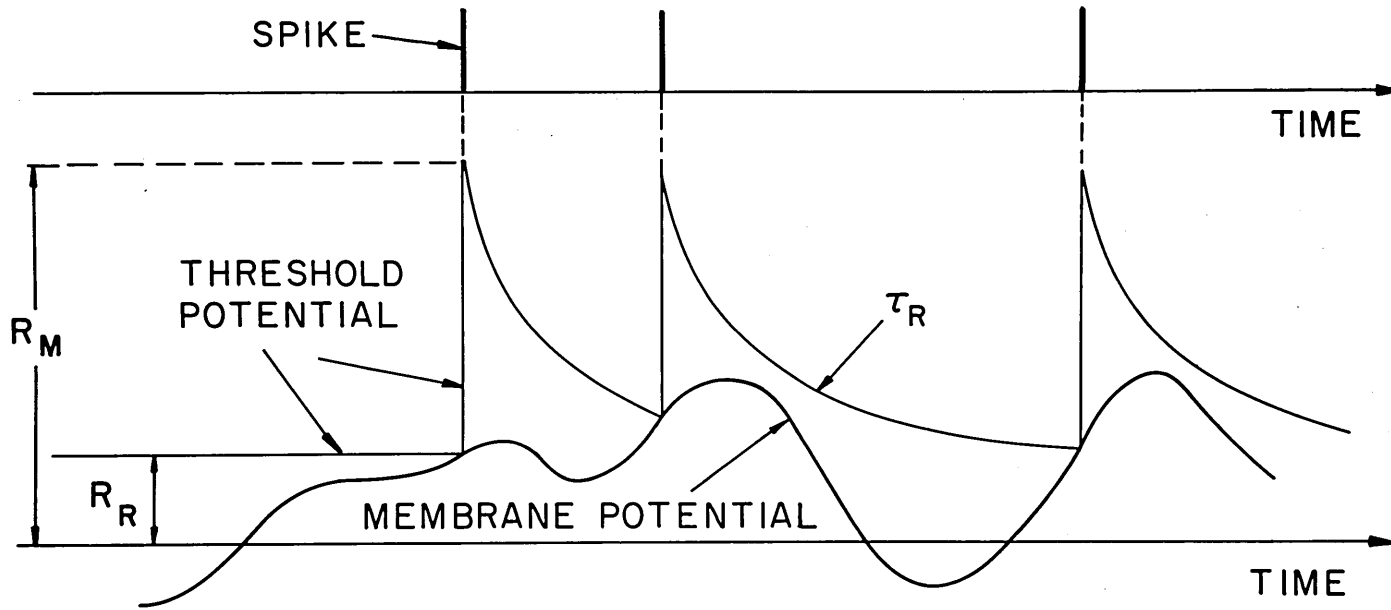
(2) A point-to-point relation between the displacement of the cochlear partition and the neural excitation is assumed. A particular neural fiber is assumed to be excited by a particular hair cell which in turn responds to the displacement of the cochlear partition at a single point along its length.

Figure 16. Diagrammatic representation of membrane potential, threshold potential and spike activity of the model.

R_M is the maximum threshold potential

R_R is the resting threshold potential

τ_R is the time constant of the exponential decay of the threshold from its maximum to its resting value.



DIAGRAMMATIC REPRESENTATION OF MEMBRANE POTENTIAL,
THRESHOLD POTENTIAL AND SPIKE ACTIVITY OF THE MODEL

(3) The process of neural excitation is represented by a simple model neuron. This model is probabilistic and contains both threshold and refractory properties.

(4) The effect of efferent fibers on the spike activity of the afferent fibers of the VIIIth nerve is ignored.

B. Discussion of Assumptions of the Model

(1) Representation of the mechanical system: The validity of representing the mechanical part of the peripheral auditory system by a linear system has been discussed in Chapter III. We, furthermore, assume that the outer and middle ear have flat frequency responses (we ignore 10 db fluctuations in the frequency responses) for frequencies up to 2 Kc. Finally, the transfer function of the mechanical system has been assumed to be simply the transfer function relating the displacement of the stapes to the displacement of the cochlear partition. This transfer function is based upon the observations of von Békésy on the response of the cochlear partition to sinusoidal displacements of the stapes. These data are composed of observations on human cadavers, guinea pigs, cows and even elephants, but not on cats. There is, however, some justification for inferring that the transfer function is similar in cats as in the other species for which it has been measured. The experimentally determined tuning curves⁽⁷²⁾ for all species (including the chicken, which has a very crude cochlea) are very similar. For instance, the sharpness of tuning, Q , varies very little across species. The cochlear maps⁽⁷³⁾ (distributions of maxima of

of displacement of the cochlear partition versus frequency of stimulation), and the elasticity of the cochlear partition as a function of distance along the partition^(74, 75) are all similar in these different species. It seems reasonable, therefore, to assume that the data of von Békésy is valid for the cat. This assumption is strengthened since we are not concerned so much with the details of the tuning curves as with their first order properties, such as their width and asymmetry.

(2) Representation of the sensory cells and their innervation: The point-to-point relation between the displacement of the cochlear partition and the excitation of an adjacent neural fiber assumed in the model is the most parsimonious assumption possible. Anatomically, this assumption appears to be consistent with the radial fiber innervation. A radial fiber is connected at most to two or three hair cells.⁽⁷⁶⁾ The hair cell spacing is estimated to be approximately 2.5μ for outer hair cells and 8.5μ for inner hair cells.* In either case, these distances are negligible compared to the widths of von Békésy's tuning curves (when they are plotted versus position along the cochlear partition).⁽⁷⁸⁾ Therefore, a single radial fiber is essentially

*These values are obtained by dividing the length of the cochlear partition by the number of hair cells. The density of hair cells is assumed to be constant.⁽⁷⁷⁾

sensitive to the pattern of displacement of the cochlear partition over a relatively short length of the partition. The spiral fiber innervation appears not to be as simply structured. Spiral fibers are thought to innervate the hair cells more diffusely (although there appears to be some difference of opinion on this fact in the literature). (79, 80) It is not clear which of these two major groups of fibers contribute predominantly to the VIIIth nerve afferent fibers. The point-to-point relation assumed in the model leads to results that appear to be qualitatively consistent with the electrophysiological data of Kiang, et al. and this assumption also appears to be consistent with the radial fiber innervation.

Initially, the relation between the excitation of a fiber and the displacement of the cochlear partition is assumed to be linear with no energy storage elements. Thus, a hair cell is assumed to generate a current that is proportional to the displacement of the cochlear partition at a point and this current flows through and depolarizes a fiber adjacent to the hair cell. The excitatory process is the subject of a considerable amount of investigation at the present time, (81) but the process is not understood in detail. We are forced to make some rather simple assumptions in the model. The consequences of these assumptions are investigated in the next chapter.

(3) Representation of the nerve excitation process:

The representation of the initiation of action potentials in the fibers of the VIIIth nerve is the most phenomenological part of the model. It would perhaps be possible to include a more complete model of a nerve fiber (such as the Hodgkin-Huxley model)⁽⁸²⁾ in the representation. However, these membrane models are too detailed and cumbersome for our purpose and they are generally based on empirical evidence obtained from non-mammalian and relatively large neural fibers. These fibers show no spontaneous activity and their response to stimulation can be adequately described by deterministic models.* This is not the case for VIIIth nerve fibers in the cat and as a result the more detailed models of the initiation of action potentials are inadequate for our purposes.

(a) The need for a probabilistic neuron model:

The work of Kiang et al. suggests rather strongly that a probabilistic description of the spike activity of VIIIth nerve fibers is necessary. There are two reasons: (1) these fibers exhibit spontaneous spike activity whose origin cannot be related to any controllable stimulus to the cat and (2) the response of a fiber is not the same to each

*A number of simplified models of nerve membrane have been proposed.^(84, 85, 86)

presentation of the acoustic stimulus, but averages of the spike activity appear to be stable. With our current understanding of the peripheral auditory system, it is difficult to account for the origin of the apparent random behavior of the spike activity of the fibers. The cause might be: Brownian motion in any of the acoustic or mechanical parts of the system; fluctuations in osmotic pressure caused by blood pulsation in the surrounding capillaries in the cochlea; fluctuations of ionic potentials across the hair cell and nerve membranes; fluctuations in the amount of the chemical activating substance at the hair cell-neuron junction and/or a number of other possibilities.

At this point we wish to digress from the main discussion to present one possible explanation of the probabilistic behavior of the spike activity in the VIIIth nerve. The unpredictable response behavior of single nerve fibers has been known since the classic work of Pecher⁽⁸⁷⁾ and the more recent work of Verveen.⁽⁸⁸⁾ In both of these experiments, the sciatic nerves of frog were stimulated directly by short electric current pulses. When the amplitude of the current pulses was sufficiently small these single fibers rarely responded. For sufficiently large amplitude pulses the fibers responded to almost every current pulse. The fiber responded to pulses of an intermediate range of amplitude in a seemingly random fashion. Upon more careful investigation it was found that the set of spike responses

to a periodic pulse train (where the period of the train was large compared to the refractory period of the fiber), could be characterized as a set of Bernoulli trials where the probability of a response to a pulse was a sigmoid function of the amplitude of the pulse. This phenomenon was referred to as the fluctuation of excitability of nerve fibers. Typically, the standard deviation (σ) of the threshold potential (difference in potential between threshold for firing and resting value) normalized by the mean threshold (R_R) potential is .01 in sciatic nerve fibers of frogs.

Further empirical evidence, (89, 90) including data obtained from nerve fibers of other species, indicates that the normalized standard deviation of the threshold potential (σ/R_R) is a function of the diameter of the fiber. Small diameter fibers have large values of σ/R_R , an intuitively appealing result. In terms of fluctuations in ionic concentrations, this result means that for large fibers containing a large number of ions, the fluctuation in ionic concentration is small (Law of Large Numbers). The relation Verveen⁽⁹¹⁾ infers from his data is:

$$\sigma/R_R = 0.03 d^{-0.8}$$

where d is the diameter of the fiber in microns. Verveen's data was obtained from fibers with diameters in the range of a few microns up to a few hundred microns. If the relation is extrapolated to smaller values of fiber diameter, then

σ/R_R becomes appreciably large. For $d = 0.1$, $\sigma/R_R = .26$. Therefore, for diameters of fibers approaching those of the terminal endings of the VIIIth nerve fibers near the base of the hair cells, ⁽⁹²⁾ σ/R_R approaches 1/3. This implies that the fluctuations in membrane potential are large enough occasionally to exceed threshold. This argument thus leads to the prediction of the existence of spontaneous activity in fibers as large as VIIIth nerve fibers.

Although this explanation may have some merit, it has not been verified empirically. Nevertheless, the need for a probabilistic mechanism in the model is patent and such a mechanism has been included as a Gaussian noise, added to the input of the neuron.

(b) Threshold and refractory properties of the model neuron: The neuron model contains two other major properties that are intended to represent properties of nerve membrane:* i) There is a threshold for firing and a spike is defined to occur when the sum of the output of the transducer and the noise exceeds this threshold potential. ii) Refractory effects are included in the model by making this threshold depend upon the time of occurrence of the previous spike. The refractoriness of the model can be summarized by stating that the probability of the occurrence of a spike immediately after a spike has occurred is low--

*A linear filter is provided at the input to the neuron to include the effect of membrane capacitance. The time constant of this filter is assumed to be approximately 0.5 milliseconds. (93, 94)

because the threshold is very high. This probability increases as the time intervals between spikes increases and is a function of both the stimulus and the time of occurrence of the last spike. The refractory effect is assumed to last one or perhaps a few milliseconds.

This representation of the excitation of a nerve membrane is considerably simplified and can not account for some of the details of the initiation of action potentials, such as the shape of the spike potential or the detailed recovery properties of a fiber. Nevertheless, some of the first order properties of the excitability of nerve fibers are included and perhaps the coding of information about acoustic events in the VIIIth nerve does not depend upon the details of the initiation of action potentials. This conjecture can only be decided by the descriptive and predictive capabilities of the model.

(4) Efferent systems: The schematic representation of the auditory system, Figure 1, suggests that there are at least two efferent neural pathways to the periphery. The dotted line from the central nervous system to the middle ear represents the two tracts innervating the middle ear muscles. We have mentioned that the primary purpose of the middle ear muscles appears to be the protection of the ear from sustained, high intensity sounds. This is accomplished by a reduction of the transformer ratio provided by the middle ear. It is clear that this action

of the middle ear muscles is inconsequential in both the von Bekesy data and the VIIIth nerve data of Kiang, et al. In the latter case, the barbiturate anaesthesia used during the experiments effectively blocks this action.

The figure shows the efferent fibers that enter the cochlea via the VIIIth nerve as a dotted line going to the inner ear. Several distinct tracts have been identified by Rasmussen.⁽⁹⁵⁾ One of these--the crossed olivo-cochlear tract--has been traced from the neighborhood of the contralateral accessory nucleus of the superior olivary complex into the cochlea. Suggestions that these fibers terminate near the hair cells have been put forward, but the fineness of the fibers has prevented any direct verification of this hypothesis.

There has been considerable speculation concerning the role of these tracts on the processing of sensory information. Galambos⁽⁹⁵⁾ and Fex⁽⁹⁷⁾ have demonstrated that electrical stimulation of this tract (at the floor of IVth ventricle) inhibits both N₁ and single unit activity of the VIIIth nerve afferent fibers. Fex⁽⁹⁸⁾ has also shown that CM is augmented slightly when these fibers are stimulated electrically. He has demonstrated that these efferent fibers (this time the recording electrodes were located in fibers just before their entry into the cochlea) respond to acoustic stimulation of the contralateral ear. It is difficult to interpret the effect of these fibers on the coding of acoustic information in the VIIth nerve, especially in the light of

some of the results of Galambos.⁽⁹⁹⁾ Despite many attempts to interfere with this pathway in various ways, Galambos has not found any systematic effects on behavioral thresholds or discriminations. The effect of the efferent fibers on the coding of acoustic information in the VIIIth nerve remains equivocal and therefore we choose to ignore these fibers in our model.

CHAPTER V: Results of Testing the Model

The model of the peripheral auditory system presented in the previous chapter is based on a number of assumptions. These assumptions in turn are based on inferences derived from physiological data. The process of making these inferences has led to a model that is analytically unwieldy and as a result the derivation of even the simplest statistics of the behavior of the model appears to be quite difficult. For instance, the distribution of intervals between spontaneous spikes generated by the model is equivalent to the distribution of successive crossings of a Gaussian noise process with a function (in this case the threshold function). A special and simple case of this problem is the distribution of intervals between successive crossings of the constant function. The problem is referred to in the literature as the "axis-crossing problem" and it has not been solved for the general case. (100, 101, 102, 103)

The complexity of the analytic problems* involved in testing the model and the desirability for determining its response to a number of stimuli have made machine computation essential. The structure of the equations (multi-dimensional

*Appendix A gives a short discussion of the problem of finding the distribution of successive intervals between spikes generated by the model for a simple case.

integral equations) governing the behavior of the model appears to make a direct solution of the problem more complex than a Monte Carlo scheme. For these reasons, and for reasons of personal bias, a general purpose digital computer (the TX-2 computer of the Lincoln Laboratory)⁽¹⁰⁴⁾ was used to simulate the peripheral auditory system. Appendix C includes a discussion of the programs written for the TX-2 machine. The programs were written to generate the firing patterns of the model and to compute statistics of these firing patterns. Certain of these statistics were chosen to make possible direct comparisons of data obtained from the model with data obtained from VIIIth nerve fibers.

In order to avoid confusing the activity of VIIIth nerve fibers with activity generated by the model, this chapter will refer to the former simply as "spikes", while the latter will be referred to as "events". Furthermore, both the results of the simulation and any analytic arguments to be presented in this work assume a model that generates events at discrete intervals of time. Events, E_k , are defined to occur when signal, s_k , plus noise, n_k , exceeds the threshold, r_k , at time $k(\Delta t)$ where k ranges over the integers and Δt is the fundamental sampling interval. We define $r_k = \alpha_{k-j}$ if the last event occurred at time j , i.e., the value of the threshold is reset upon the occurrence of an event. Moreover, $\alpha_i = R_R + (R_M - R_R)\gamma_R^i$ where

$\gamma_R = \exp(-\Delta t/\tau_R)$. The refractory effect is assumed to be represented by an exponential decay of the threshold from its maximum value to its resting value after the occurrence of an event. The noise, n_k , has a Gaussian distribution with zero mean, standard deviation σ and $E[n_j n_k] = \sigma^2 \rho_{j-k}$ where $\rho_i = \gamma_N^i$ and $\gamma_N = \exp(-\Delta t/\tau_N)$. *

A. Response of the Model Neuron to "Short" Pulses

The response of the model neuron to short pulses is discussed** in order to present a rationale for the assumptions of the nature of the neural noise. This discussion is also intended to verify the results of Verveen's model of the fluctuation of excitability of neural fibers. (106)

Suppose the membrane potential of the model, $m_k = s_k + n_k$ and $\sigma/R_R \ll 1$. For this case the number of spontaneous events per unit time are vanishingly small. Assume that $\{s_k\}$ is a "short" pulse signal that is introduced

*The noise is also filtered by a high-pass filter so that the correlation function of the noise is actually given by:

$$\rho_i = C_1 \gamma_N^i + C_2 \gamma_M^i$$

where $\gamma_N = \exp(-\Delta t/\tau_N)$, $\tau_N \ll \tau_M$

and $\gamma_M = \exp(-\Delta t/\tau_M)$

$f_h = 1/\tau_N$ is the high frequency 3 db point

$f_l = 1/\tau_M$ is the low frequency 3 db point

**This discussion is similar to a discussion presented by Verveen. (105)

at $k = 0$. A "short" pulse is defined to be a pulse whose duration is short compared to all the other important time constants in the model. That is, if $\delta(\Delta t)$ is the duration of the pulse then $\delta(\Delta t) \ll \tau_R$, $\delta(\Delta t) \ll \tau_N$. The pulse is short compared both to the time over which the noise is correlated and to the refractory time constant. These assumptions are equivalent to assuming: (1) there can be at most one event in response to a pulse and (2) the noise is a constant over the duration of the pulse.

The event E is defined to occur when there is an event E_k for $0 \leq k \leq \delta$ or $E = E_0 \cup E_1 \cup \dots \cup E_\delta$. But $\Pr[E] = 1 - \Pr[\bar{E}]$ where \bar{E} is the complementary event, no firing occurs during the interval of the pulse.

$$\Pr[\bar{E}] = \Pr[n + s_k < R_R] \quad k = 0, 1, 2, \dots, \delta$$

By assumption the noise is a constant for $k = 0, 1, 2, \dots, \delta$ and

$$\Pr[\bar{E}] = \Pr[n + s_k < R_R] \quad k = 0, 1, 2, \dots, \delta$$

$$= \Pr[\sup(n + s_k) < R_R]$$

$$= \Pr[n < R_R - \sup(s_k)]$$

$$p = \Pr[E] = 1 - \Pr[\bar{E}]$$

$$= 1 - \int_{-\infty}^{R_R - \sup(s_k)} (1/\sqrt{2\pi}\sigma) \exp(-n^2/2\sigma^2) dn$$

By further manipulation this can be put in the form:

$$p = \int_{-\infty}^{\sup(s_k)} (1/\sqrt{2\pi}\sigma) \exp(-(n - R_R)^2/2\sigma^2) dn$$

Therefore, the probability, p , of a response to a pulse $\{s_k\}$ as a function of the amplitude of s_k is an integrated Gaussian function with mean R_R (resting threshold) and standard deviation σ . The response of the model neuron to a periodic train of identical pulses of amplitude $\sup s_k$ forms a set of Bernoulli trials with probability of success p . This result is valid under the assumption that the period of the train is large compared to both the refractory period of the model neuron and the correlation time of the noise. This description is consistent with the empirical findings of Verveen on the response of sciatic nerve fibers. Figure 17 shows the results of the response of the computer-simulated model neuron. The ratio of the number of responses of the model to the number of stimuli is plotted as a function of the amplitude of the pulses. The figure also shows the same function plotted on Gaussian distribution coordinate paper.

A histogram of the distribution of intervals, I_k , between events, E , in response to a train of short pulses is given in Figure 18. The number of intervals equal to an integral number of periods (T) of the stimulus, i.e.,--the number of intervals of length $T, 2T, 3T, \dots$, where T is the period of the train of pulses, form the distribution of success runs in a set of Bernoulli trials. This distribution is the geometric distribution and the predicted interval distribution is: $\Pr[I_k = kT] = p(1-p)^{k-1}$ $k = 1, 2, \dots$ where I is the length of an interval.

Figure 17. Number of responses of the model to a train of short pulses as a function of the amplitude of the pulses.

$$R_R = 1000$$

$$R_M = 1200$$

$$\tau_R \doteq 1 \text{ msec}$$

$$f_l \doteq 20 \text{ cps}$$

$$f_h \doteq 2 \text{ kc}$$

$$\sigma \doteq 10$$

Number of pulses = 1000
Pulse duration = 0.3 msec
Pulse period = 5.0 msec

~58~

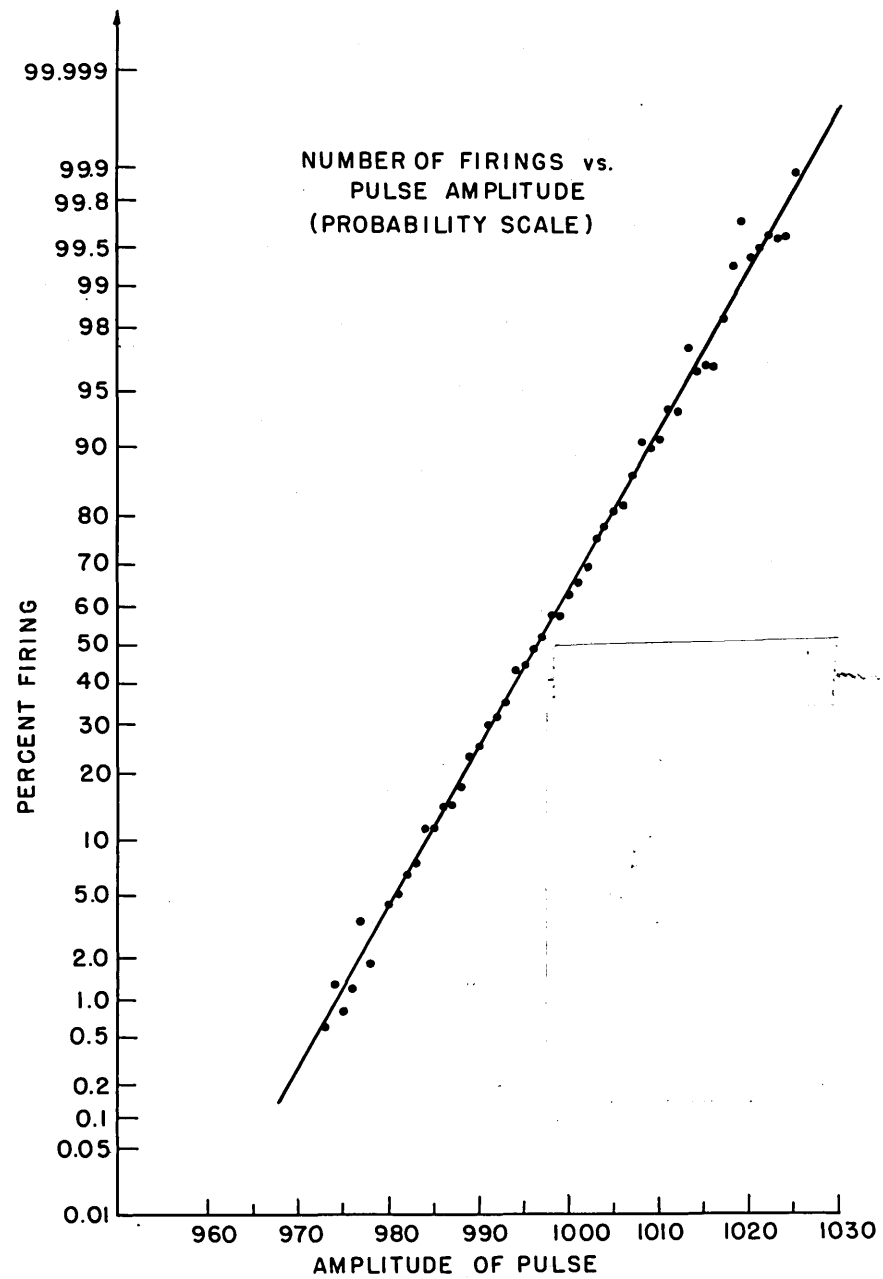
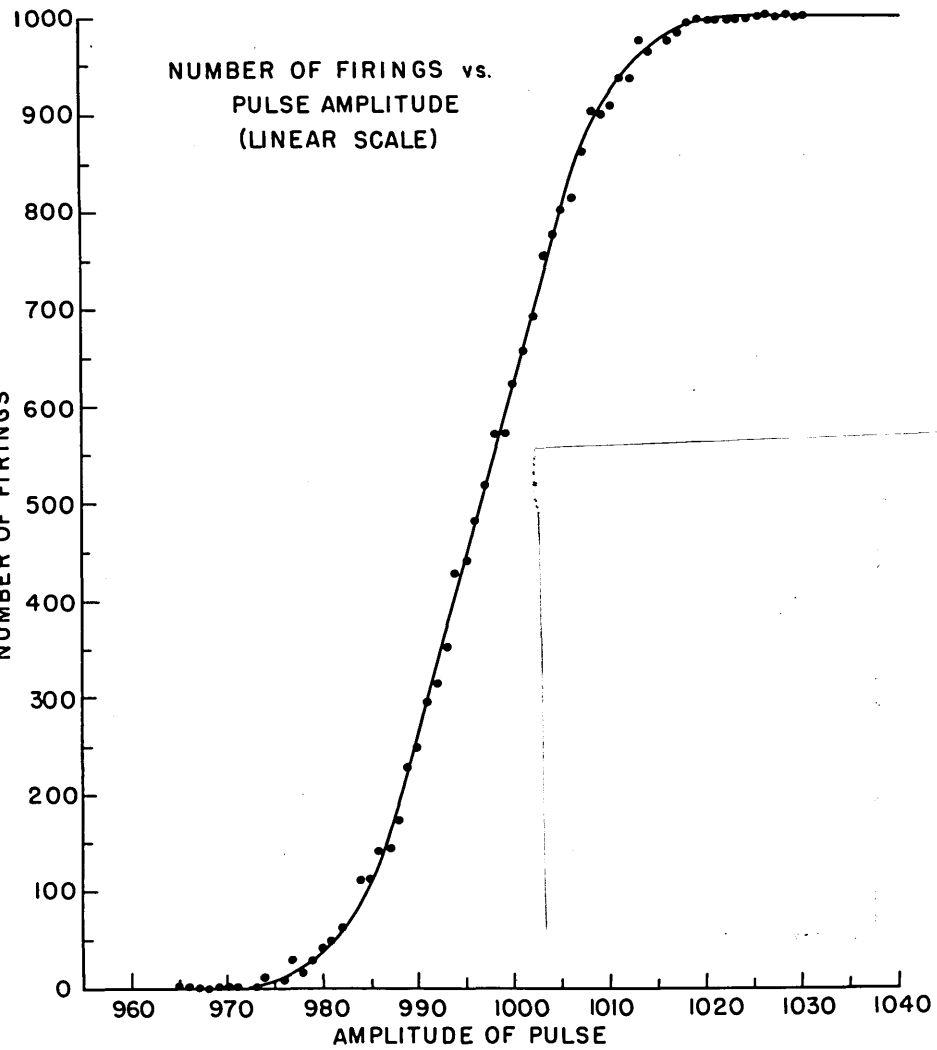


Figure 18. Histogram of intervals of time between responses of model to a periodic train of short pulses.

$$R_R = 10000$$

$$R_M = 100000$$

$$\tau_R \doteq 0.3 \text{ msec}$$

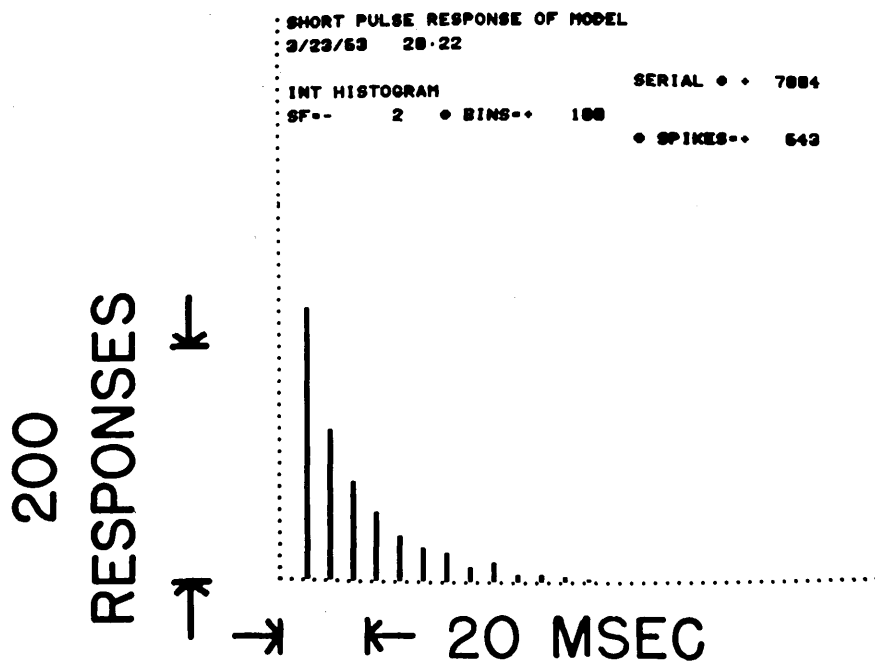
$$f_h \doteq 5 \text{ kc}$$

$$f_l \doteq 5 \text{ cps}$$

$$\sigma \doteq 100$$

Pulse duration	= 0.1 msec
Pulse period	= 5.0 msec
Pulse amplitude	= 9950
Number of pulses	= 2000
Number of responses	= 643

HISTOGRAM OF INTERVALS OF TIME BETWEEN RESPONSES OF MODEL TO A PERIODIC TRAIN OF SHORT PULSES



PULSE AMPLITUDE = 9950

$R_R = 10000$

$\sigma = 100$

Table 1 shows both the predicted intervals and the set of intervals generated by the computer for the distribution shown in Figure 18. The predicted set of intervals were obtained by estimating p from the data computed in the same run.

Table 1

Number of pulses = 2000
 Number of events = N = 643
 Estimated value of p = .322
 I_k is the number of intervals of length k
 $\hat{I}_k = Np_k = Np(1-p)^{k-1}$ is the estimated mean number of intervals of length k
 $\sigma_k = \sqrt{Np_k(1-p_k)}$ is the estimated standard deviation of the number of intervals of length k

k	I_k	\hat{I}_k	k
1	232	207	11.8
2	129	140	10.5
3	84	95.2	9.0
4	58	64.3	7.6
5	38	43.8	6.4
6	28	29.7	5.3
7	24	20.1	4.4
8	12	13.7	3.7
9	16	9.3	3.3
10	7	6.3	2.5
11	7	4.3	2.1
12	4	2.9	1.7

Figure 19 shows the distribution of intervals between events as a function of the amplitude of the pulse. For large pulse amplitudes the probability of getting long intervals approaches zero, i.e., events occur in response to almost every pulse.

Figure 19. Histograms of intervals of time between responses of the model to periodic trains of short pulses as a function of pulse amplitude.

$$R_R = 10000$$

$$R_M = 100000$$

$$\tau_R \doteq 0.3 \text{ msec}$$

$$f_h \doteq 5 \text{ Kc}$$

$$f_\ell \doteq 5 \text{ cps}$$

$$\sigma \doteq 100$$

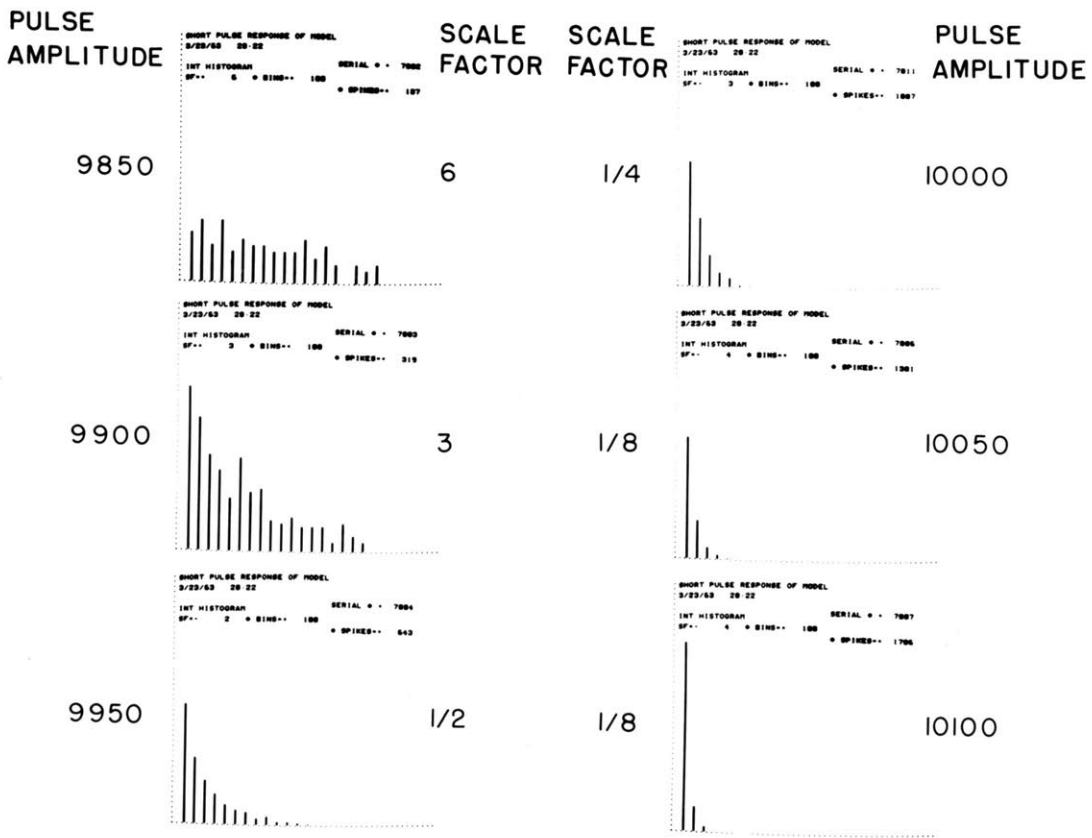
Pulse duration = 0.1 msec

Pulse period = 5.0 msec

Number of pulses = 2000

(The spacing between dots along the ordinate represents a number of entries in the histogram equal to 5/scale Factor.)

INTERVAL HISTOGRAMS OF THE RESPONSE OF THE
MODEL TO PERIODIC TRAINS OF SHORT PULSES



→ 20 MSEC

PULSE DURATION = 100 μSEC
PERIOD OF PULSE TRAIN = 5 MSEC
NUMBER OF PULSES = 2000

B. Spontaneous Activity of the Model

As the ratio of the standard deviation of the noise to the resting threshold, σ/R_R , increases, the probability that the model exhibits spontaneous events in the absence of an input increases. For small values of σ/R_R , the probability of a spontaneous event, E_k at time $k\Delta t$ is given approximately by:

$$\begin{aligned} \Pr[E_k] &= p[n_k \geq r_k] \leq p[n_k \geq R_R] \\ \Pr[E_k] &\leq \int_{R_R}^{\infty} (1/\sqrt{2\pi}\sigma) \exp(-n^2/2\sigma^2) \, dn \\ &\leq \int_{R_R/\sigma}^{\infty} (1/\sqrt{2\pi}) \exp(-n^2/2) \, dn \end{aligned}$$

The equality holds in the limit as σ/R_R goes to zero, i.e., when the probability of an event is small and the threshold r_k decays essentially to the resting value R_R between events.

We are interested in a statistical description of the set of events $\{E_k\}$. First, it is clear that the events can not be described as "recurrent events"⁽¹⁰⁷⁾ in the general case. By a "recurrent event" process we mean a statistical process that generates events where the probability of an event at time $k(\Delta t)$ is dependent only on the time of occurrence of the last event, i.e., after an event has occurred the statistics are reset. Figure 20 shows the spontaneous activity of the model for different noise spectra. For values of the bandwidth of the noise that are large compared to $1/\tau_R$ the noise appears uncorrelated between events, while for small values of noise bandwidth several events may occur

Figure 20. Membrane potential and threshold potential of model. The same data is shown on three time scales for each of two values of f_h . In each picture, the upper trace shows the threshold potential, the center trace shows the membrane potential, and the lower trace shows the times of occurrence of events. The threshold potential and the membrane potential are on the same amplitude scale.

$$R_R = 40$$

$$R_M = 100$$

$$\tau_R \doteq 0.3 \text{ msec}$$

$$f_h \doteq 100 \text{ cps (left-hand figures)}$$

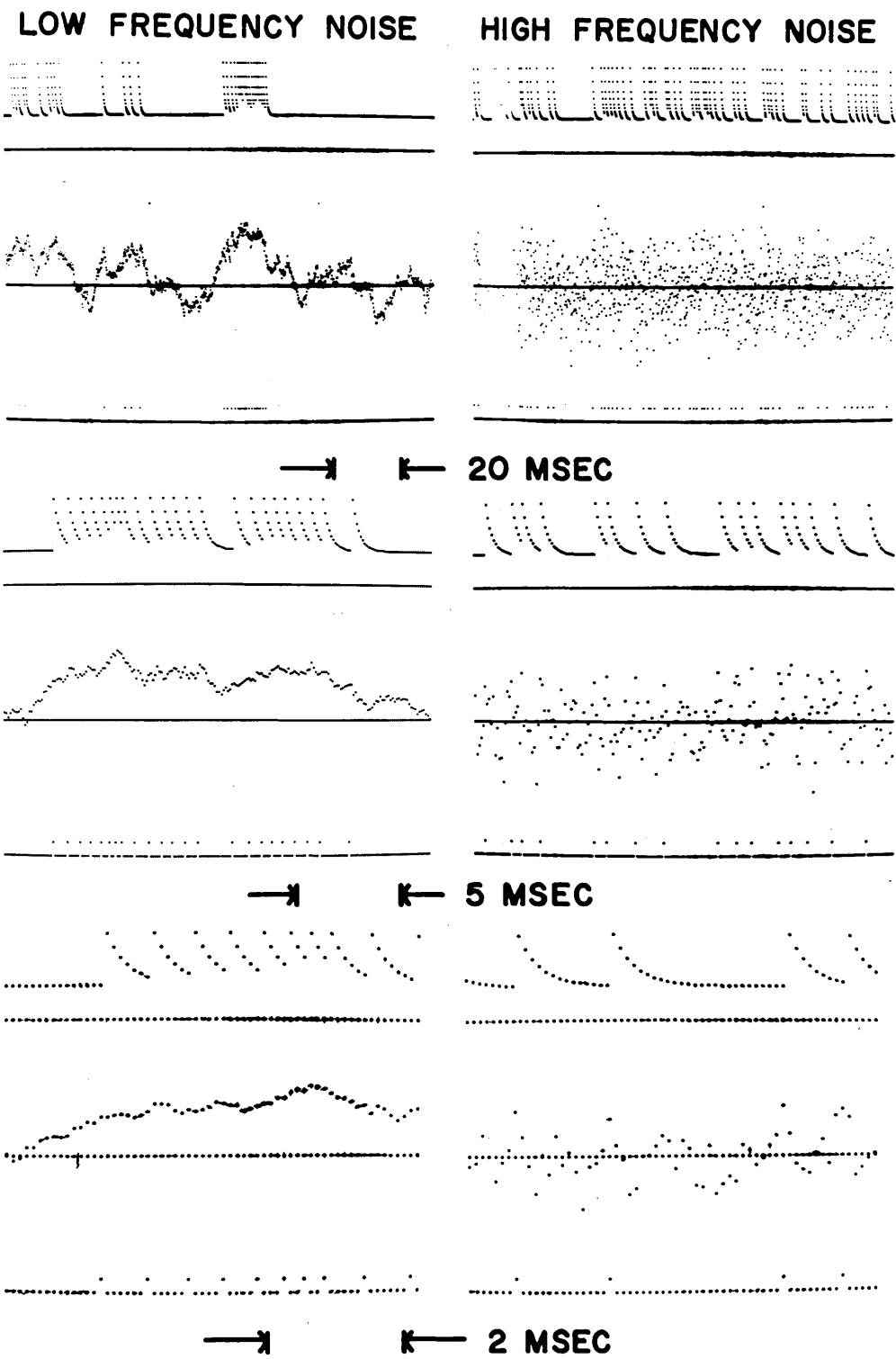
$$f_h \doteq 10 \text{ kc (right-hand figures)}$$

$$f_l \doteq 10 \text{ cps}$$

$$\sigma \doteq 30$$

$$\Delta t = 100 \text{ } \mu\text{sec}$$

MEMBRANE POTENTIAL AND THRESHOLD POTENTIAL OF MODEL



on one large excursion of the noise.

A short interval occurring between events implies that a relatively large value of noise has occurred at the end of the interval because a large value of noise is needed to exceed the relatively large value of the threshold. But if the noise is varying slowly with respect to the decay time of the threshold then a relatively short interval will tend to occur again. In other words, there is a correlation between successive intervals between events such that short intervals tend to be followed by short intervals. The existence of this statistical dependence is due to the fact that while the threshold is reset upon the occurrence of an event the noise is not reset.

To a first-order approximation, the parameters which determine the degree of statistical dependence between successive inter-event intervals are the time constant of the threshold decay, τ_R , and the bandwidth of the noise, $1/\tau_N$. If $\tau_R \gg \tau_N$, then the correlation of the noise between events approaches zero. Consider the expected value of the noise k units of time after an event at which the value of the noise was n_0 .

$$E[n_k/n_0] = n_0 \rho^k = n_0 (\exp(-\Delta t/\tau_N))^k = n_0 \exp(-k\Delta t/\tau_N)$$

For $k\Delta t > \tau_R$

$$E[n_k/n_0] < n_0 \exp(-\tau_R/\tau_N)$$

$$\lim_{(\tau_R/\tau_N) \rightarrow \infty} E[n_k/n_0] = 0$$

Therefore, successive intervals between events become uncorrelated for noise whose correlation time, τ_N , is short relative to the time constant of the threshold decay, τ_R . Figure 21 shows the mean inter-event interval given the previous interval I_1 , $(\bar{I}_2)_{I_1}$, as a function of I_1 , for different values of $f_h = 1/\tau_N$. Note that the degree of correlation between successive intervals (as indicated by the estimate of the conditional mean interval given in the figure) decreases as f_h increases. For an f_h approximately 2 Kc, successive intervals are only slightly correlated. Similar statistics computed from the firing patterns of VIIIth nerve fibers (in the absence of acoustic stimuli) indicate only a slight amount of correlation between successive inter-spike intervals. This correlation is of the same form as the correlation of successive intervals shown by the model, i.e., short intervals tend to be followed by short intervals. Therefore, we have fixed the bandwidth of the noise in the model at approximately 2 to 5 Kc. This value is consistent with the findings of a number of workers who have attempted to estimate such a figure. (108, 109)

Figure 21. Conditional average interspike intervals of the spontaneous activity generated by the model as a function of noise spectrum.

$$R_R = 10000$$

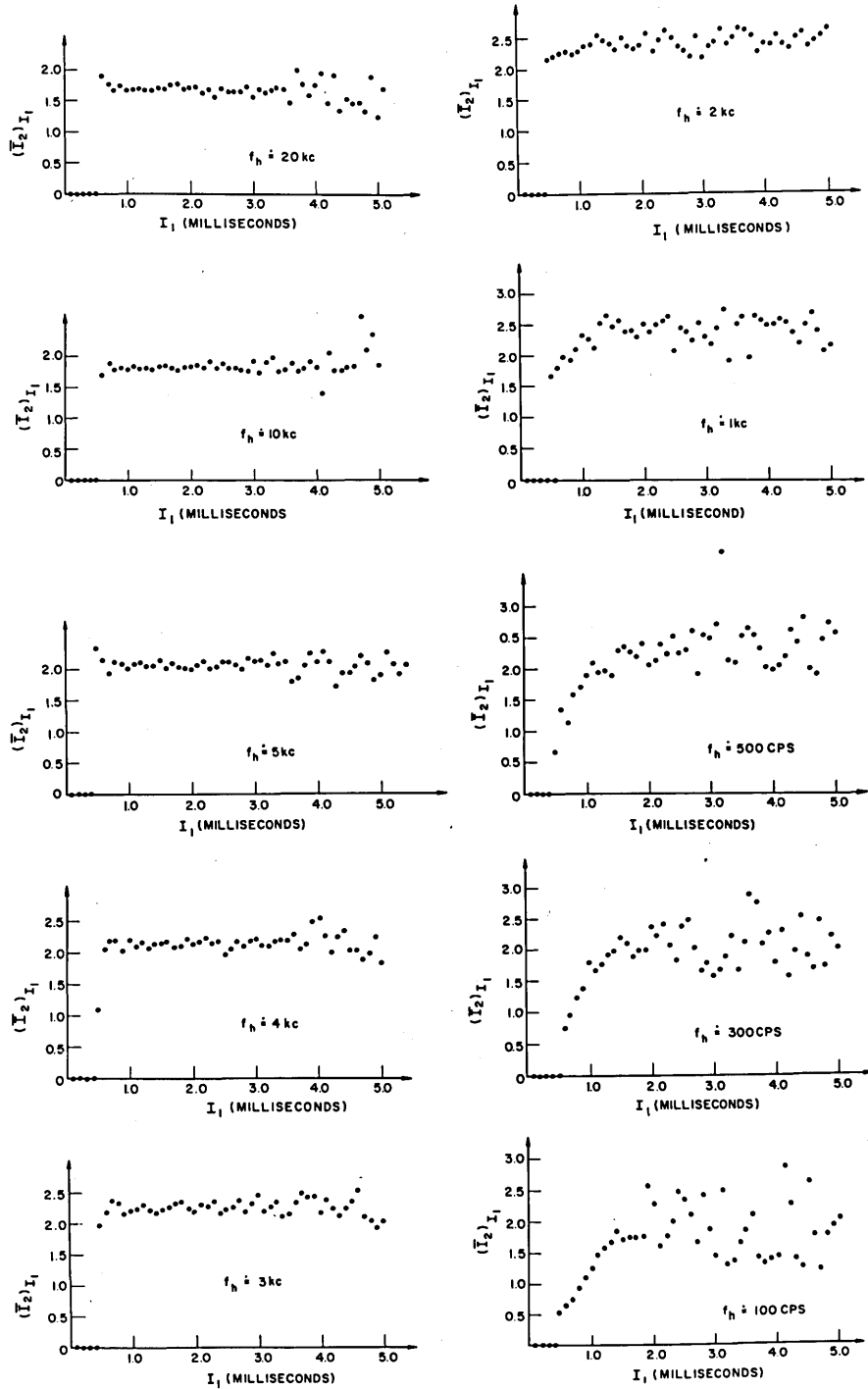
$$R_M = 100000$$

$$\tau_R \doteq 0.3 \text{ msec}$$

$$\sigma \doteq 10000$$

$$f_l \doteq 5 \text{ cps}$$

CONDITIONAL AVERAGE INTERSPIKE INTERVALS OF
 SPONTANEOUS ACTIVITY GENERATED BY THE MODEL
 AS A FUNCTION OF NOISE SPECTRUM



$(\bar{I}_2)_{I_1}$ IS THE AVERAGE INTERSPIKE INTERVAL I_2 GIVEN THE PREVIOUS INTERVAL IS I_1
 f_h IS THE HIGH FREQUENCY LIMIT OF THE NOISE SPECTRUM

Figure 22 shows interval histograms calculated for the same data used to obtain the results of Figure 21. As f_h decreases, not only does the statistical dependence between successive intervals increase, but a larger proportion of short intervals occur (as Figure 22 indicates). Figure 23 shows some of the same interval histograms plotted in semi-logarithmic co-ordinates. For values of the bandwidth of noise greater than 2 Kc the tails of the distribution of intervals are clearly linear on these co-ordinates or are exponential on linear co-ordinates. Figure 24 shows the rate of spontaneous events generated by the model as a function of the bandwidth of the noise.

Figure 25 shows interval histograms of the spontaneous activity of the model as a function of the standard deviation of the noise. These histograms are all exponential for large values of time intervals. Figure 26 shows the rate of spontaneous firing of the model as a function of σ/R_R . The rate of firing is strongly dependent on the value of σ/R_R . A 50% change in σ/R_R is seen to change the rate of firing by as much as 500%.

Further investigations have shown that the general features of these interval histograms are attained under a large variety of parameter values of the model. The histograms show an exponential function for large, inter-event intervals and a dead time for very short intervals, with a smooth transition between these limits. For values of $\tau_R \doteq 1$ millisecond and $\tau_N \doteq 1/5$ millisecond, the histograms appear quite similar to interval histograms computed from VIIIth nerve data.

Figure 22. Interval histograms of the spontaneous activity generated by the model as a function of noise spectrum.

$$R_R = 10000$$

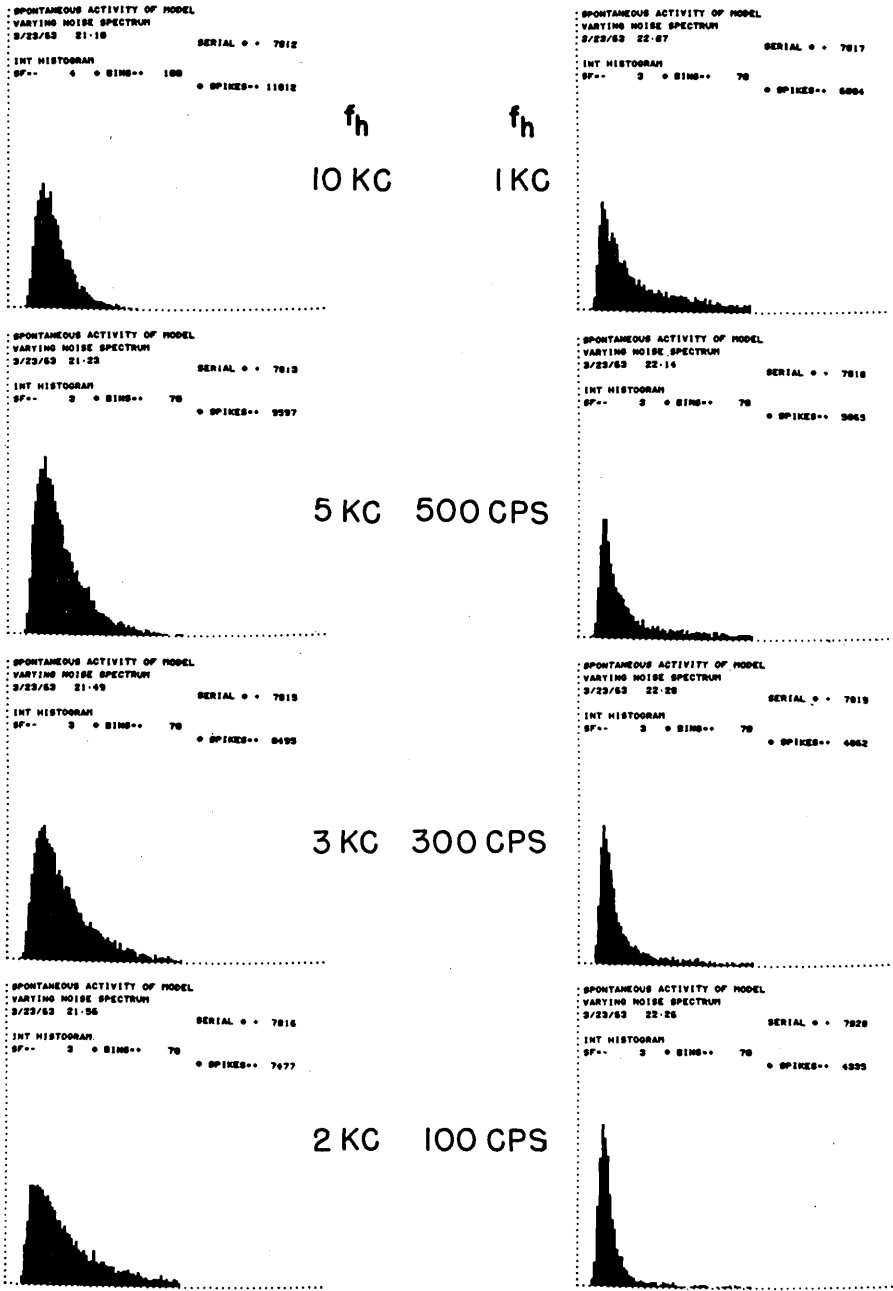
$$R_M = 100000$$

$$\tau_R \doteq 0.3 \text{ msec}$$

$$\sigma \doteq 10000$$

$$f_l \doteq 5 \text{ cps}$$

INTERVAL HISTOGRAMS OF SPONTANEOUS ACTIVITY GENERATED BY THE MODEL AS A FUNCTION OF NOISE SPECTRUM



→ ← 2 MSECS

f_h IS THE HIGH FREQUENCY LIMIT OF THE NOISE SPECTRUM

Figure 23. Interval histograms of the spontaneous activity generated by the model as a function of noise spectrum (plotted in semi-logarithmic coordinates).

$$R_R = 10000$$

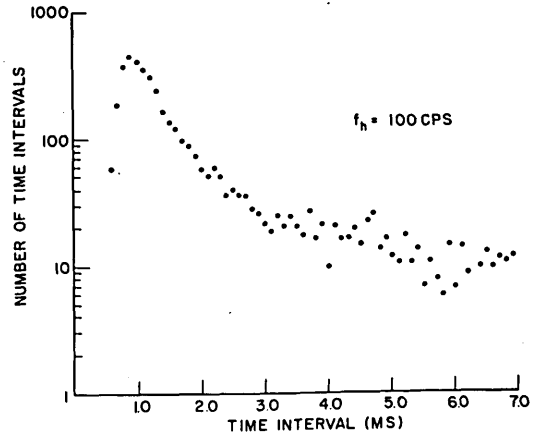
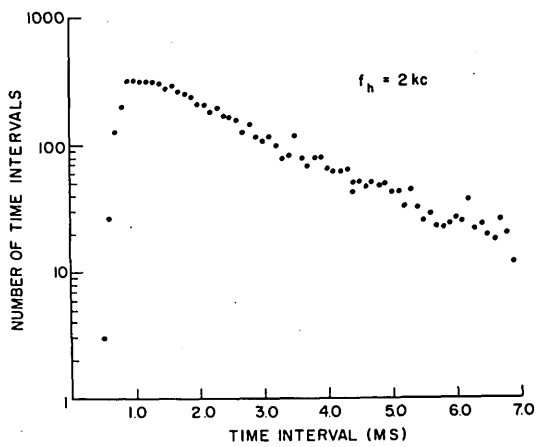
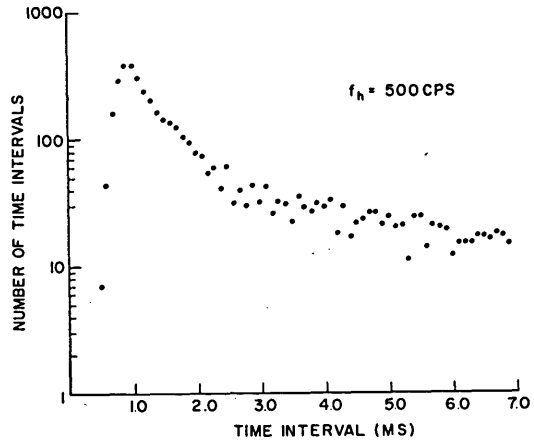
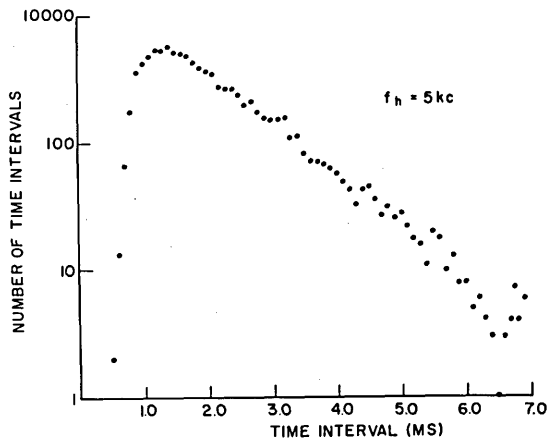
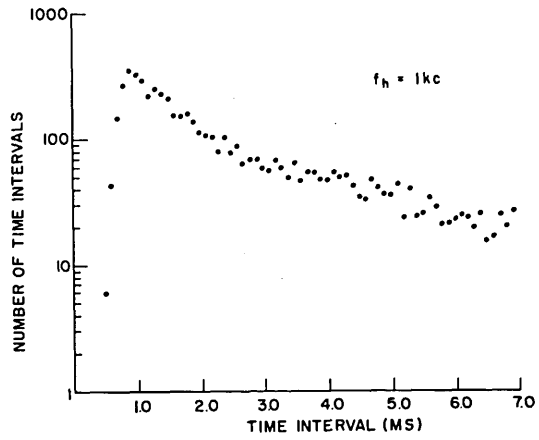
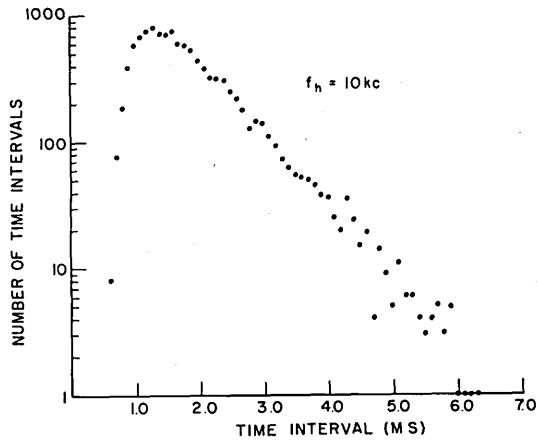
$$R_M = 100000$$

$$\tau_R \doteq 0.3 \text{ msec}$$

$$\sigma \doteq 10000$$

$$f_l \doteq 5 \text{ cps}$$

SPONTANEOUS
HISTOGRAM OF INTER-SPIKE INTERVALS
GENERATED BY THE MODEL AS A
FUNCTION OF NOISE SPECTRUM



f_h IS THE HIGH FREQUENCY LIMIT OF THE NOISE SPECTRUM

Figure 24. Spontaneous rate of firing of the model versus the high frequency limit of the noise.

$$R_R = 10000$$

$$R_M = 100000$$

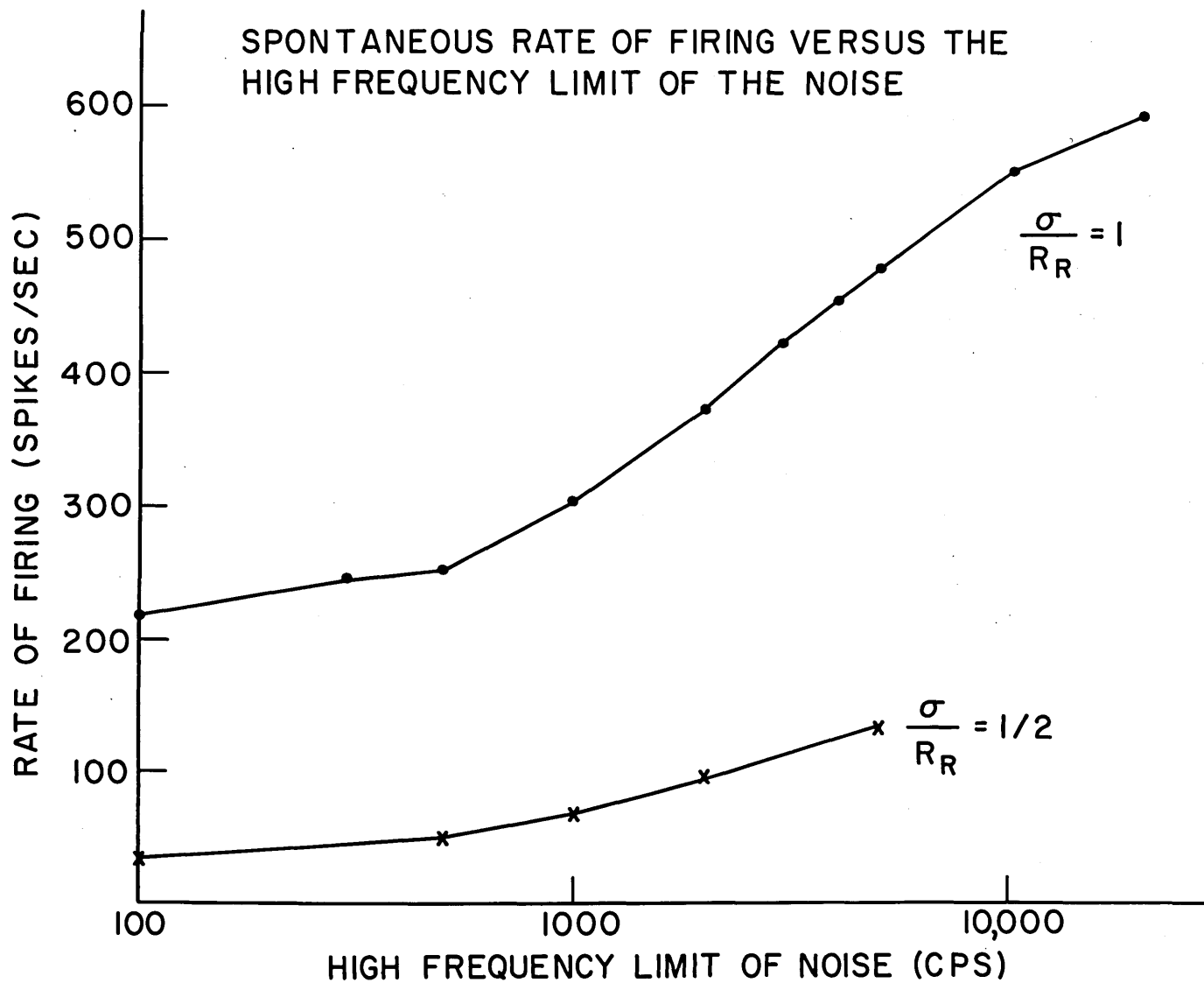
$$\tau_R \doteq 0.3 \text{ msec}$$

$$\sigma \doteq 10000 \text{ (for } \sigma/R_R \doteq 1)$$

$$\sigma \doteq 5000 \text{ (for } \sigma/R_R \doteq 1/2)$$

$$f_l \doteq 5 \text{ cps}$$

SPONTANEOUS RATE OF FIRING VERSUS THE
HIGH FREQUENCY LIMIT OF THE NOISE



102-

Figure 25. Interval histograms of the spontaneous activity generated by the model versus the standard deviation of the noise.

$$R_R = 10000$$

$$R_M = 100000$$

$$\tau_R \doteq 0.3 \text{ msec}$$

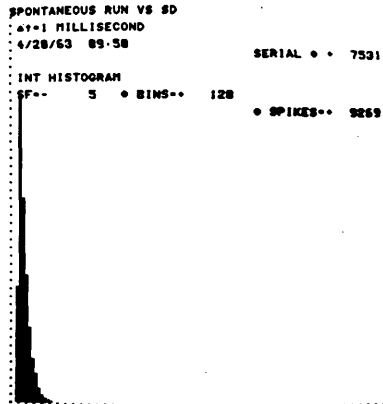
$$f_h \doteq 5 \text{ Kc}$$

$$f_l \doteq 5 \text{ cps}$$

INTERVAL HISTOGRAMS OF SPONTANEOUS ACTIVITY VERSUS STANDARD DEVIATION OF NOISE

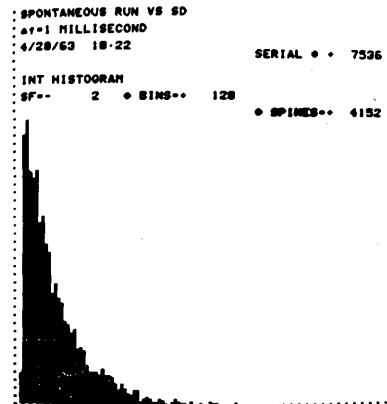
SCALE
FACTOR

1/16



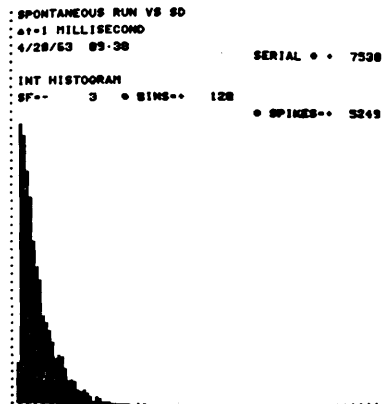
STANDARD
DEVIATION

7000 4500



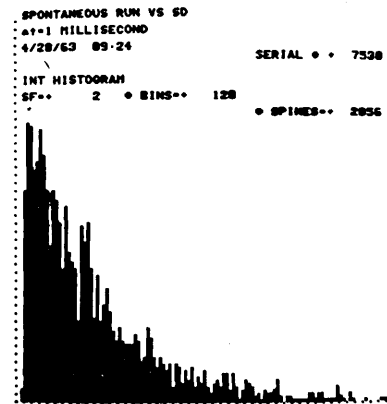
SCALE
FACTOR

1/2



1/4

5000 4000



2

→ ← 2 MSEC

Figure 26. Spontaneous rate of firing of the model versus the ratio of the standard deviation of the noise to the resting threshold (σ/R_R).

$$R_R = 10000$$

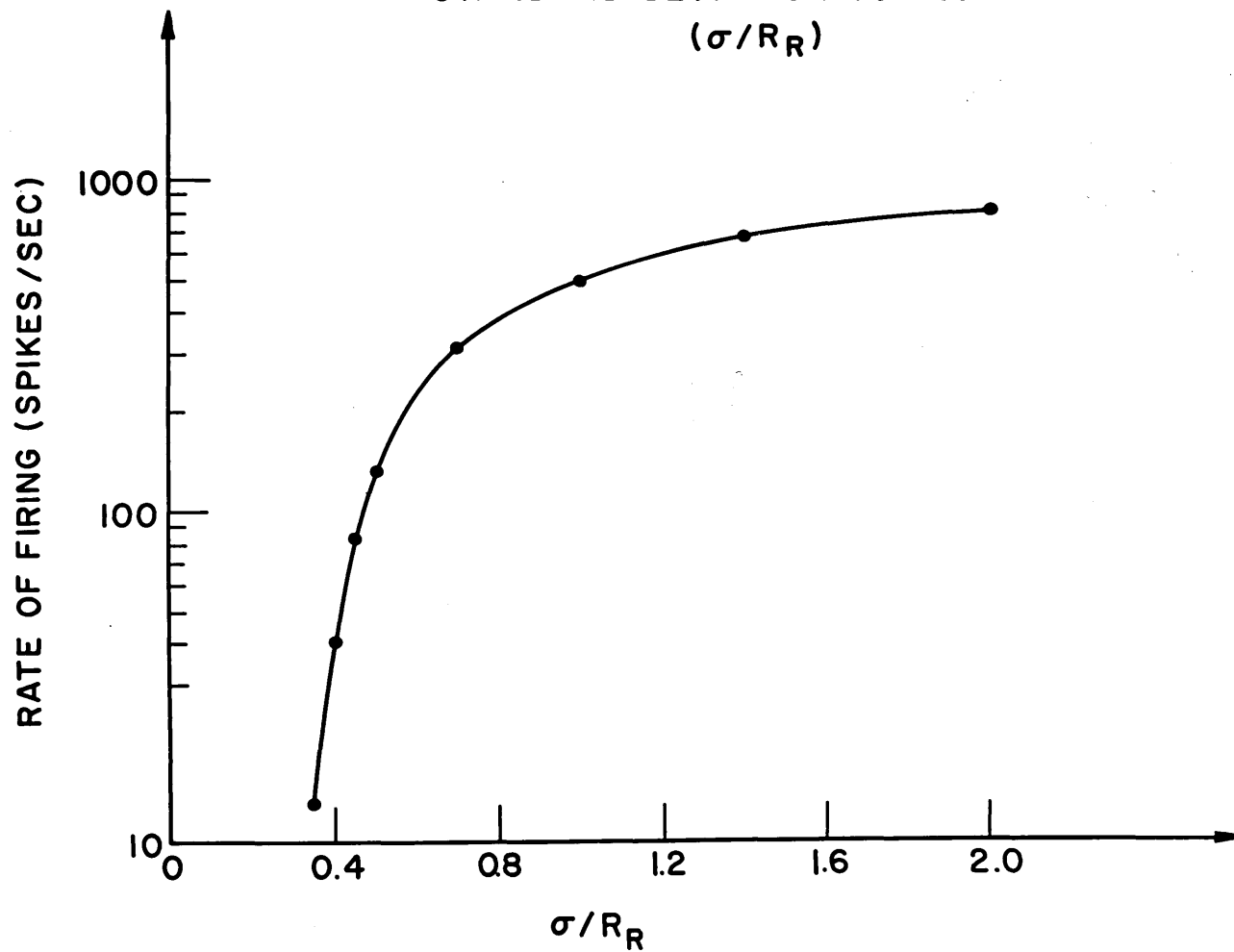
$$R_M = 100000$$

$$\tau_R \doteq 0.3 \text{ msec}$$

$$f_h \doteq 5 \text{ Kc}$$

$$f_l \doteq 5 \text{ cps}$$

SPONTANEOUS RATE OF FIRING VERSUS RATIO OF
NOISE STANDARD DEVIATION TO RESTING THRESHOLD
(σ/R_R)



C. Response of the Model to Sinusoidal Stimuli

The fibers of the VIIIth nerve respond selectively to different frequencies of sinusoidal stimuli. Each fiber is tuned (i.e., is maximally sensitive) to a particular frequency, which shall be referred to as the characteristic frequency (CF) of the fiber. "Neural tuning curves" for a representative group of VIIIth nerve fibers are presented in Figure 13. These tuning curves are graphs of the threshold of firing of a fiber in response to a sinusoidal stimulus as a function of the frequency of the stimulus. The threshold of firing of a fiber has been defined by Kiang et al. as the intensity of the stimulus required to increase the rate of firing of the fiber by 20% above the spontaneous rate of firing. This criterion for threshold was utilized for fibers with a high rate of spontaneous activity. For fibers exhibiting a low rate of spontaneous activity, the threshold was defined as the intensity of the stimulus to which the fiber responded in a time-locked manner, as determined visually.

There is a second aspect to the frequency response of VIIIth nerve fibers. Figure 13 indicates that the threshold of firing of VIIIth nerve fibers in response to sinusoids whose frequencies are equal to the CF varies as a function of CF. The most sensitive points in the tuning curves of the most sensitive fibers shown in the Figure constitute what we shall refer to as a "neural sensitivity curve". The neural sensitivity curve for the data shown

in Figure 13 shows a minimum at a frequency of about 2 Kc. For frequencies below 2 Kc the "neural sensitivity curve" shows a rate of decrease of sensitivity of about 40 db/decade. At frequencies above 2 Kc, the sensitivity also decreases.

It is perhaps already clear that we assume that a relation exists between the frequency response curves of the cochlear partition (as shown in Figure 8) and the tuning curves of VIIIth nerve fibers (as shown in Figure 13). A particular neural fiber with a CF equal to f_0 is assumed to be stimulated by the displacement of the cochlear partition at a point x_0 which responds maximally to a frequency, f_0 , of sinusoidal stimulation presented to the ear. Furthermore, we are assuming the existence of a correspondence between the "neural sensitivity curve" and the "mechanical sensitivity curve" (shown in Figure 9). The mechanical sensitivity curve relates the amplitude of the displacement of the stapes required to achieve some fixed maximum amplitude of displacement of a point on the cochlear partition as a function of frequency.

In this section we will first consider the sensitivity curves generated by the model vis-a-vis the neural sensitivity curve. We will then discuss the tuning curves of VIIIth nerve fibers.

(1) Sensitivity of the model at low frequencies:
Much of the empirical data of Kiang, et al. on the response of VIIIth nerve fibers to sinusoidal stimuli depends upon

a determination of the "threshold of firing" of a fiber to a stimulus. Before we can discuss the data generated by the model, we feel that it is essential to discuss the concept of a threshold of firing in response to a stimulus.

The "threshold of firing" of a neuron to a stimulus is an old concept in neurophysiology. Pecher⁽¹¹⁰⁾ was one of the first to recognize that the response to electrical stimulation of a sciatic nerve fiber in a frog could not be described by a simple threshold below which the fiber never fired and above which the fiber always fired. Pecher was able to demonstrate that a probabilistic description of the firing of a fiber was a more accurate description. For the sciatic nerve fibers, a threshold can be defined arbitrarily as the intensity of stimulation which produces a response to 50% (or any other percent) of the number of stimuli. With such a definition of threshold, equal response curves can be determined, under a variety of physiological conditions.

For fibers that exhibit spontaneous activity (such as VIIIth nerve fibers) the problem of defining a threshold of firing to a stimulus is more complicated and perhaps irrelevant. It appears to be unreasonable to identify some spikes with the response to a stimulus and other spikes as spontaneous activity. Results obtained from the model indicate that there is time-locked activity present in the response for every intensity of stimulus. For any particular

intensity of stimulation there is a resultant perturbation of the average rate of firing of the model. In a sufficiently long record this time-locked activity can be seen as a perturbation in the PST histogram.*

Despite the difficulty in defining the concept of "threshold", one still opts for a metric of the spike activity of fibers which permits equal response or relative sensitivity curves, if not absolute sensitivity curves, to be obtained. Clearly, if a model of the system were sufficiently accurate and sufficiently manipulatable, metrics of the spike activity could be derived that would be appropriate in some sense.

A somewhat arbitrary choice of metrics must be made, in the absence of more appropriate metrics. Kiang et al. have used an arbitrary criterion for defining the threshold of firing of VIIIth nerve fibers to sinusoidal stimuli. They chose the intensity required to increase the rate of firing by 20% over the spontaneous firing rate as the definition of threshold for fibers having a relatively high spontaneous rate. For fibers exhibiting a low spontaneous rate, the threshold was defined as the intensity at which the fiber fired in a time-locked manner (determined visually) to the stimulus.

*Long and stable records of data cannot be obtained and therefore such behavior in neural fibers cannot be demonstrated.

In order to compare results obtained from the model with data obtained from VIIIth nerve fibers, we shall adopt the same criteria for threshold to tonal stimuli. In addition to investigating the rate of firing of the model as a function of stimulus parameters, we shall also investigate a metric which is closely related to the amount of time-locked activity. This same metric can be used to define a threshold and, as is discussed below, the thresholds obtained by using this definition are lower than those obtained using the 20% change of rate as a criterion for threshold.

In order to define this metric, first consider the PST histogram obtained from an experiment (on model or fiber) to consist of η_i firings in the i th bin at time $i(\Delta t)$ following the onset of a stimulus, where Δt is the width of a bin in the PST histogram. Suppose this record contains a total of N firings distributed in the n bins, i.e., $i = 1, \dots, n$. D^2 is defined as follows:

$$D^2 = (1/n) \sum_{i=1}^n (\eta_i - E[\eta_i])^2$$

$E[\eta_i]$ is the average number of firings per bin.

The expected value of D^2 for the case of N firings placed at random into n bins is given by

$$E[D^2] = (N/n) (1 - (1/n)) = \text{var}[\eta_i]$$

One can further determine that

$$\text{var}[D^2] = 2N(N-1)(n-1)/n^4 = [2(N-1)/n^2] E [D^2]$$

A full discussion of these and other derivations are given in Appendix B. D_n is defined as follows:

$$D_n = \frac{(1/n) \sum_{i=1}^n (\eta_i - (N/n))^2}{(N/n)(1-(1/n))}^{1/2}$$

The expected value of this function is 1 when there is no time-locked activity and the value increases as the amount of time-locked activity increases. The expression for the variance of D_n yields an estimate of the significant variations of D_n from the value $D_n = 1$ for different values of N and n . Both of the definitions of threshold, the 20% change of rate of firing and the D_n criterion will be utilized in the discussion of the sensitivity of the model to sinusoidal stimuli.

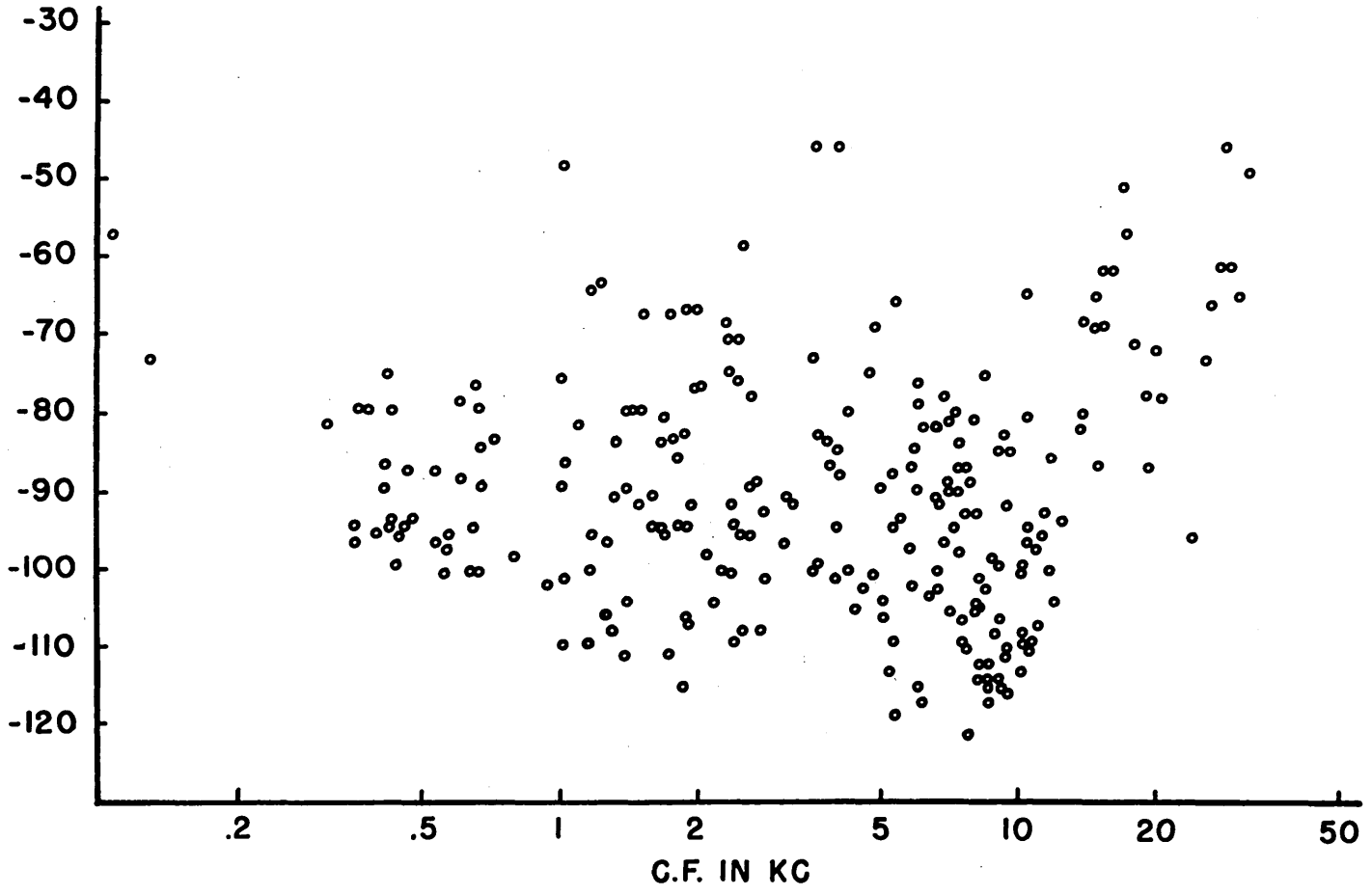
To continue the discussion of the sensitivity curves generated by the model as compared to the results obtained from VIIIth nerve fibers: A graph showing the intensity required to achieve the "threshold of firing" at the CF as a function of the CF for a number of VIIIth nerve fibers is shown in Figure 27. A curve composed of the lowest points in the figure shows the 40 db/decade change in sensitivity at low frequencies.

Figure 9 shows that the mechanical system exhibits a decrease of sensitivity of between 10 and 15 db/decade in the same range of frequencies. Therefore, if the model is assumed to be a valid representation of the peripheral

Figure 27. Threshold of firing of VIIIth nerve fibers (of cats) to tone bursts (delivered at the CF of the fiber) as a function of CF.

-411-

THRESHOLD INTENSITY FOR TONE BURSTS AT C.F.
IN DB RE 200V P-P INTO CONDENSER EARPHONE



auditory system then it must account for a change in sensitivity in excess of the 10 or 15 db/decade change in sensitivity exhibited by the mechanical part of the system. More specifically, in the frequency range of 200 cps to 2 Kc, the transducer and model neuron of the overall model must account for a change in sensitivity of approximately 25 to 30 db/decade.

We shall consider two properties of the response of the transducer and model neuron* to a sinusoidal stimulus--(1) the amount of time-locked activity as given by the value of D_n and (2) the rate of firing of the model.

The response of the model to sinusoidal stimuli for two different values of frequency is shown in Figure 28. The response is displayed in the form of a post-zero-crossing (PZC) histogram. This histogram is essentially a PST histogram where the onset of the stimulus is assumed to occur at the positive-going zero-crossing of the input sinusoid. The PZC histogram shows the number of firings that occur at time, t , after the positive-going zero-crossing of the sinusoid as a function of time, t .

The histogram corresponding to a frequency of 208 cps and an intensity of -12 db shows an increase in the rate of firing of less than 8% over the spontaneous rate,

*For the remainder of this section we shall consider the response of the transducer and model neuron; for simplicity, we shall use the word "model" to refer to this part of the overall model of the peripheral auditory system.

Figure 28. Response of model to sinusoidal stimuli as a function of intensity.

$$R_R = 25000$$

$$R_M = 100000$$

$$\tau_R \doteq 0.3 \text{ msec}$$

$$\sigma \doteq 10000$$

$$f_h \doteq 5 \text{ Kc}$$

$$f_l \doteq 5 \text{ cps}$$

$$\Delta t = 100 \text{ } \mu\text{sec}$$

Rate of spontaneous events $\doteq 40$ events/sec

0 db corresponds to a sinusoid whose amplitude is 10000 units

SINUSOIDAL RESPONSE OF MODEL

1250 cps

208 cps

SCALE
FACTOR

INTENSITY
(DB)

SCALE
FACTOR

1/16



0

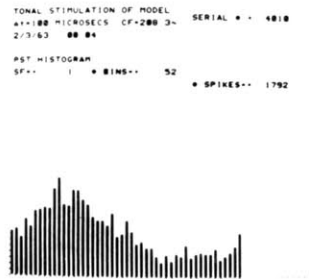


1/2

1/4



-12

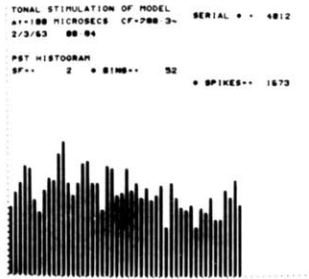


1

1/2



-24

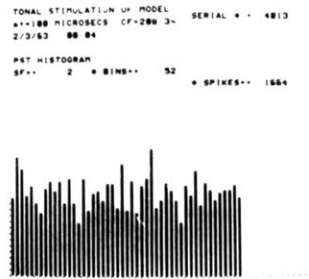


2

1/2



-∞



2

$\Delta t = 100 \mu \text{sec}$

yet a considerable amount of time-locked activity can easily be seen in the histogram. The value of $D_n = 3.05$ for this run. This value of D_n indicates that the root-mean-square value of the histogram is three times the value that would be expected for a spontaneous run given the same number of firings. This value is highly significant and it can be shown that the probability of getting a value of $D_n = 3.05$ in the spontaneous case is vanishingly small (the 3σ level of significance in the variation of the sample standard deviation can be shown to yield values of D_n between 0.885 and 1.09 for this run). We mention in passing that using the criterion $D_n = 3.05$ to define threshold yields a lower threshold than the one attained by defining the threshold as the intensity required to increase the rate of firing by 20% over the spontaneous level.

Figure 29 shows the rate of firing of the model as a function of the intensity of sinusoidal stimulation for six different frequencies. For any given intensity the rate increases with increasing frequency. For a fixed rate of firing, a higher intensity is required at low frequencies than at high frequencies of sinusoidal stimulation. Similarly, Figure 30 shows that the same trend holds if D_n is plotted as a function of intensity for different frequencies. D_n is a measure of the amount of time-locked activity and it can be seen that a higher intensity is required at low frequencies to achieve some fixed value of D_n .

Figure 29. Rate of firing of model versus amplitude of sinusoidal stimulation.

$$R_R = 10000$$

$$R_M = 100000$$

$$\tau_R \doteq 0.3 \text{ msec}$$

$$\sigma \doteq 10000$$

$$f_h \doteq 5 \text{ Kc}$$

$$f_l \doteq 5 \text{ cps}$$

Rate of spontaneous events $\doteq 490$ events/sec

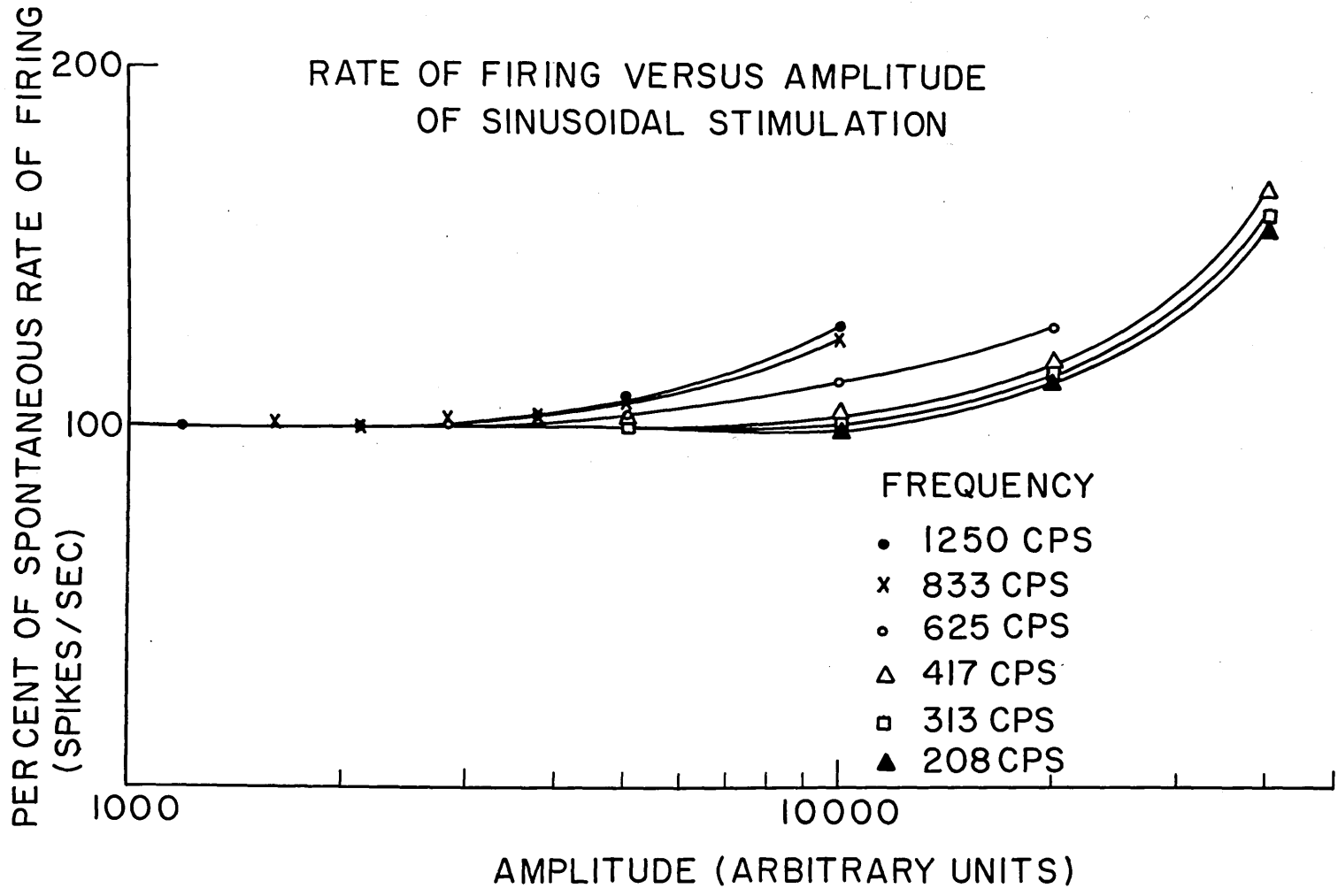


Figure 30. D_n versus amplitude of sinusoidal stimulation of the model.

$$R_R = 10000$$

$$R_M = 100000$$

$$\tau_R \doteq 0.3 \text{ msec}$$

$$\sigma \doteq 10000$$

$$f_h \doteq 5 \text{ Kc}$$

$$f_l \doteq 5 \text{ cps}$$

$$\text{Rate of spontaneous events} \doteq 490 \text{ events/sec}$$

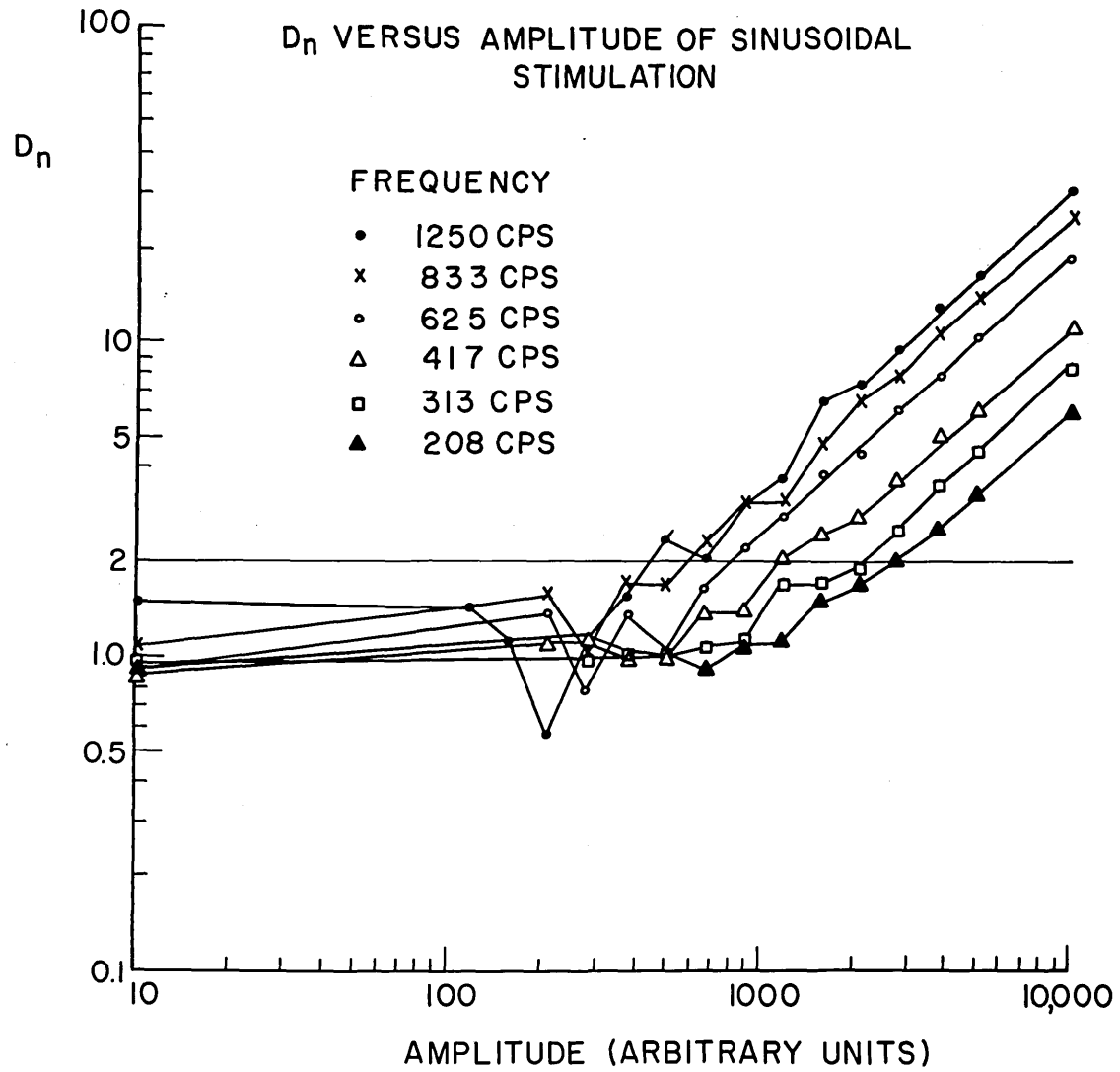


Figure 31 summarizes these data in a set of sensitivity functions generated by the model. The ordinate is the amplitude of the sinusoidal stimulus required to achieve the threshold criterion. The abscissa is the frequency of the sinusoid. The three definitions of threshold, or rather the three equal-response criteria, are: 1) a 20% increase in the rate of firing above the spontaneous level; 2) $D_n = 2$; and 3) $D_n = 5$. In each case the sensitivity of the model is higher for higher frequencies. Furthermore, the sensitivity decreases at low frequencies at a rate of approximately 12 db/decade to 20 db/decade, depending on which criterion for threshold is utilized.

It is perhaps a little difficult to see why the model should exhibit such a frequency sensitivity. In order to gain some insight into the reasons for this result, consider the case* for which the model exhibits no spontaneous activity. Assume that the intensity of the sinusoid is large enough to exceed the value of the resting threshold, R_R . Then in the limit of high frequencies, the model fires at a rate determined entirely by the properties of the refractory period and the amplitude of the sinusoid. The sinusoid acts effectively as an increase in the average value of the membrane potential. The model fires, therefore, as

*We are indebted to Professor W.M. Siebert for suggesting this particular explanation of the frequency sensitivity of the model.

Figure 31. "Threshold" of firing of the model versus frequency of sinusoidal stimulation.

$$R_R = 10000$$

$$R_M = 100000$$

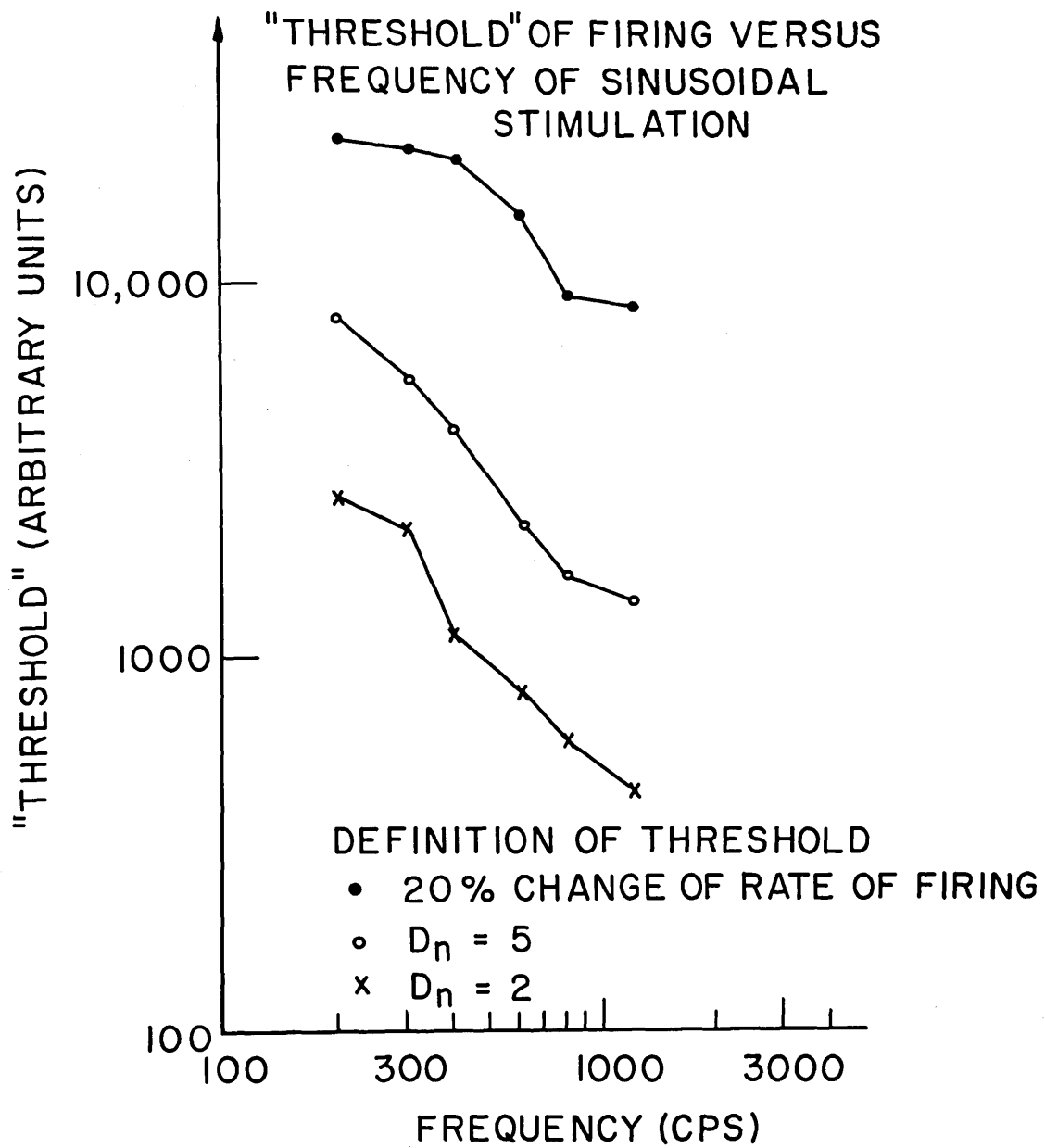
$$\tau_R \doteq 0.3 \text{ msec}$$

$$\sigma \doteq 10000$$

$$f_h \doteq 5 \text{ Kc}$$

$$f_l \doteq 5 \text{ cps}$$

$$\text{Rate of spontaneous events} \doteq 490 \text{ events/sec}$$



soon as the threshold r_k has decayed to a sufficiently small value. In the limit of low frequencies, the sinusoidal input effectively acts as a square wave. In half of this cycle the model fires at a rate determined almost entirely by the refractory period and by the amplitude of the sinusoid; in the other half cycle the model does not fire. Therefore, the model fires at approximately twice the rate in response to the high frequency sinusoid as it does in response to the low frequency sinusoid. The frequency sensitivity of the model is not as easy to understand in the presence of spontaneous activity.

Figure 32 indicates that this decrease of sensitivity of the model for low frequencies exists for a large range of rates of spontaneous firing. The figure shows the rate of firing of the model as a function of intensity of sinusoidal stimulation for two frequencies and three different rates of spontaneous firing. The different rates of spontaneous firing have been achieved by varying σ/R_R . The model is seen to respond at a higher rate to high frequency sinusoids than to low frequency sinusoids for each rate of spontaneous firing.

Further investigations of a similar nature indicate that the model always has a higher sensitivity at high frequencies than at low frequencies. This trend is independent of the definitions of the equal-response criteria that we have used. These results are also valid for all the values of the rate of spontaneous firing which we have investigated

Figure 32. Rate of firing of the model versus amplitude of sinusoidal stimulation for different rates of spontaneous firing.

$$R_R = 10000 \text{ (for the 490 spikes/sec curves)}$$

$$R_R = 20000 \text{ (for the 135 spikes/sec curves)}$$

$$R_R = 25000 \text{ (for the 40 spikes/sec curves)}$$

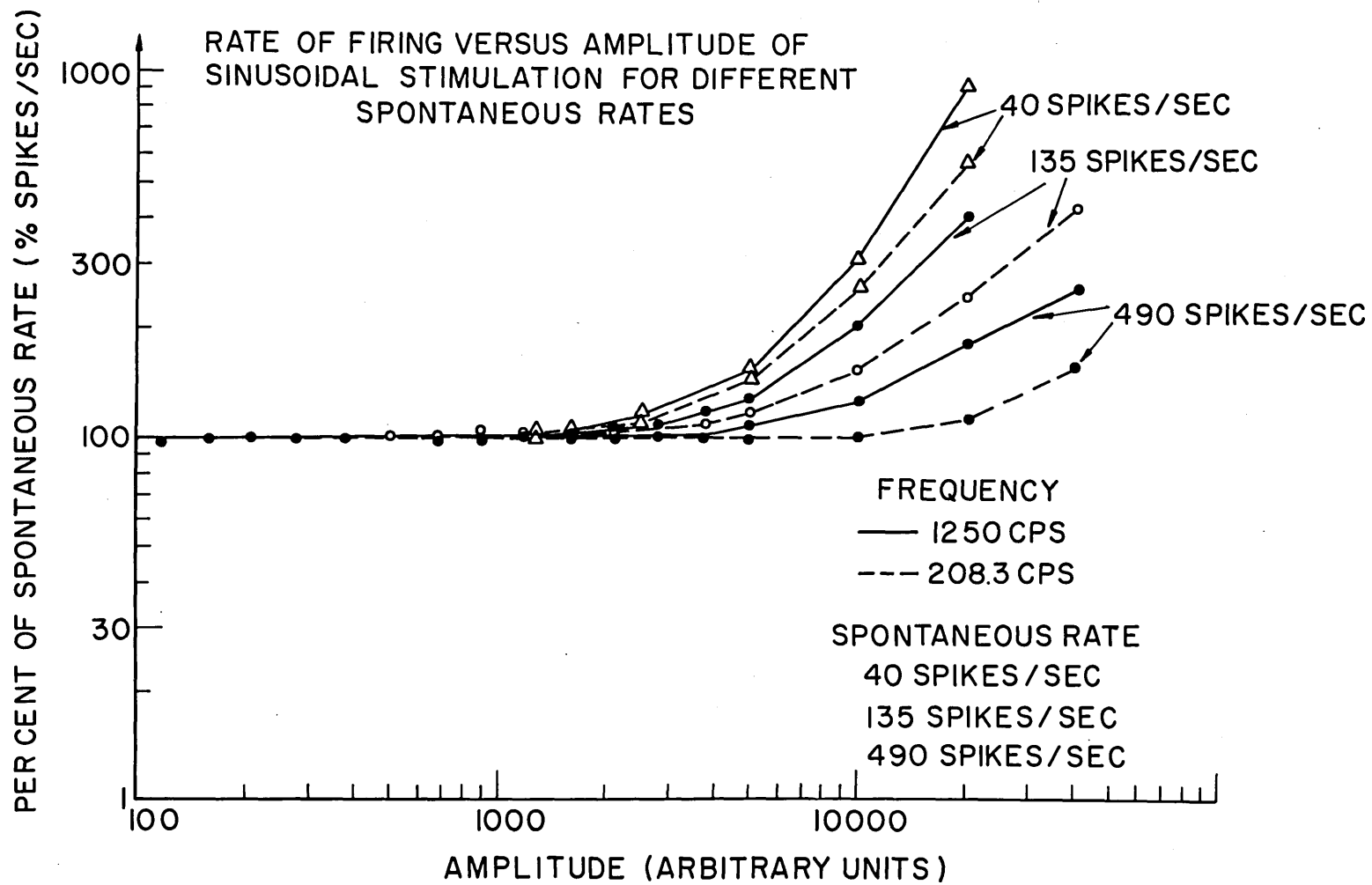
$$R_M = 100000$$

$$\tau_R \doteq 0.3 \text{ msec}$$

$$\sigma \doteq 10000$$

$$f_h \doteq 5 \text{ Kc}$$

$$f_l \doteq 5 \text{ cps}$$



(a range of 500 events/sec to 10 events/sec). The rate of change of sensitivity over the frequency range of 100 cps to 1250 cps is, however, a function of all of these variables. In general, the slope of the sensitivity curve decreases as the rate of spontaneous firing of the model is decreased, i.e., as σ/R_R is decreased. For rates of spontaneous firing comparable to the largest values seen in VIIIth nerve fibers (approximately 150 spikes/sec) the change in sensitivity produced by the model is not large enough to account for a 40 db/decade change nor even a 20 db/decade change in sensitivity.

Although the sensitivity of the model to sinusoidal stimuli is qualitatively in agreement with comparable results obtained from VIIIth nerve fibers, the quantitative agreement is poor. Thus far we have assumed that the transducer element of the model serves no essential functional purpose except to convert the output of the mechanical system into the input to the model neuron, without distorting this signal in any way. Now suppose that the transducer could be characterized by a non-linear function. Suppose, furthermore, that this function increased monotonically with a slope that was positive but monotonically decreasing. For instance, $G(y) = (k_1 y) (k_2 / (k_2 + |y|))$ for $y \geq 0$ is such a function. To a first-order approximation, the effect of the introduction of such a function upon the sensitivity curves shown in Figure 31 can be thought of as an expansion of the ordinate (threshold) scale. Therefore, given complete freedom to choose a

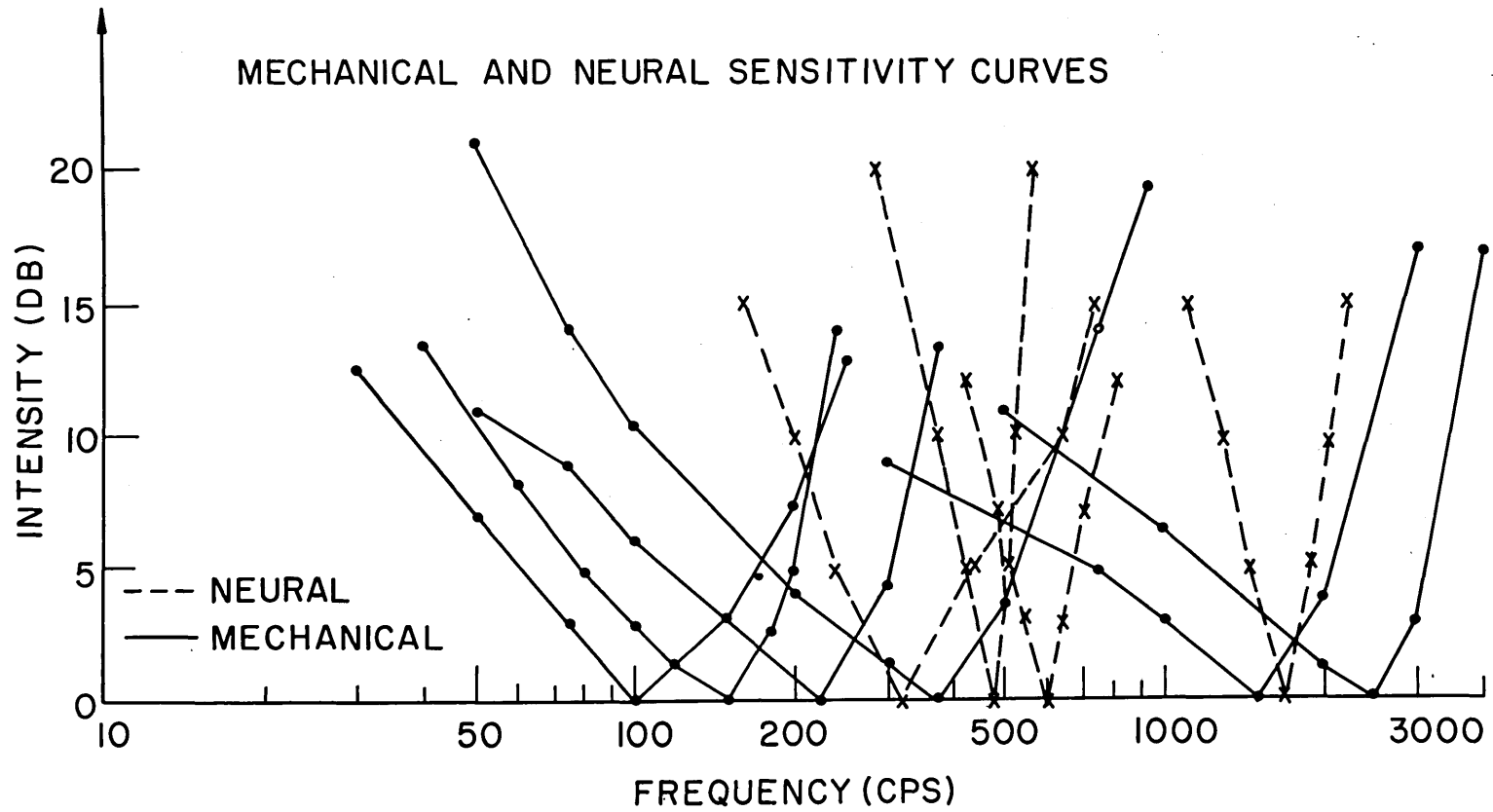
non-linear transducer function, the slope of the sensitivity curves shown in Figure 31 can be adjusted to any desired value. This is clearly too much freedom and we shall defer a discussion of the transducer to the section on the acoustic click response of the model.

(2) A discussion of the shape of the tuning curves: Figure 33 shows the frequency response curves of the cochlear partition (Figure 8) plotted as tuning curves. A representative set of neural tuning curves are also shown in the figure. The absolute sensitivities of the neural curves have been normalized to make the thresholds of the fibers at their CFs equal.

Both sets of tuning curves are very steep at high frequencies. Both sets of tuning curves are less steep at low frequencies, but the neural tuning curves are steeper than the mechanical tuning curves at low frequencies. The mechanical tuning curves are wider than the neural tuning curves. Both sets of curves can be shown to be essentially constant-Q curves for the range of frequencies shown in the figure.

We have shown that the transducer and model neuron part of our overall model of the peripheral auditory system exhibits a decrease in sensitivity for low frequencies. We have not been able to demonstrate that this part of the model accounts entirely for the additional 25 or 30 db/decade change in sensitivity which is needed to approximate the VIIIth nerve data. We have indicated that this discrepancy

Figure 33. Mechanical and neural tuning curves. The mechanical tuning curves are derived from the curves shown in Figure 8, which are based on data obtained from human cadavers. The curves shown in Figure 8 can be represented as $|H(f, x_0)| / |H(f_0, x_0)|$ for different values of x_0 . The mechanical tuning curves are defined as $-20 \log(|H(f, x_0)| / |H(f_0, x_0)|)$. f_0 is the CF for a point x_0 centimeters from the stapes. The neural tuning curves were obtained from the VIIIth nerve fibers of cats by Kiang et al.



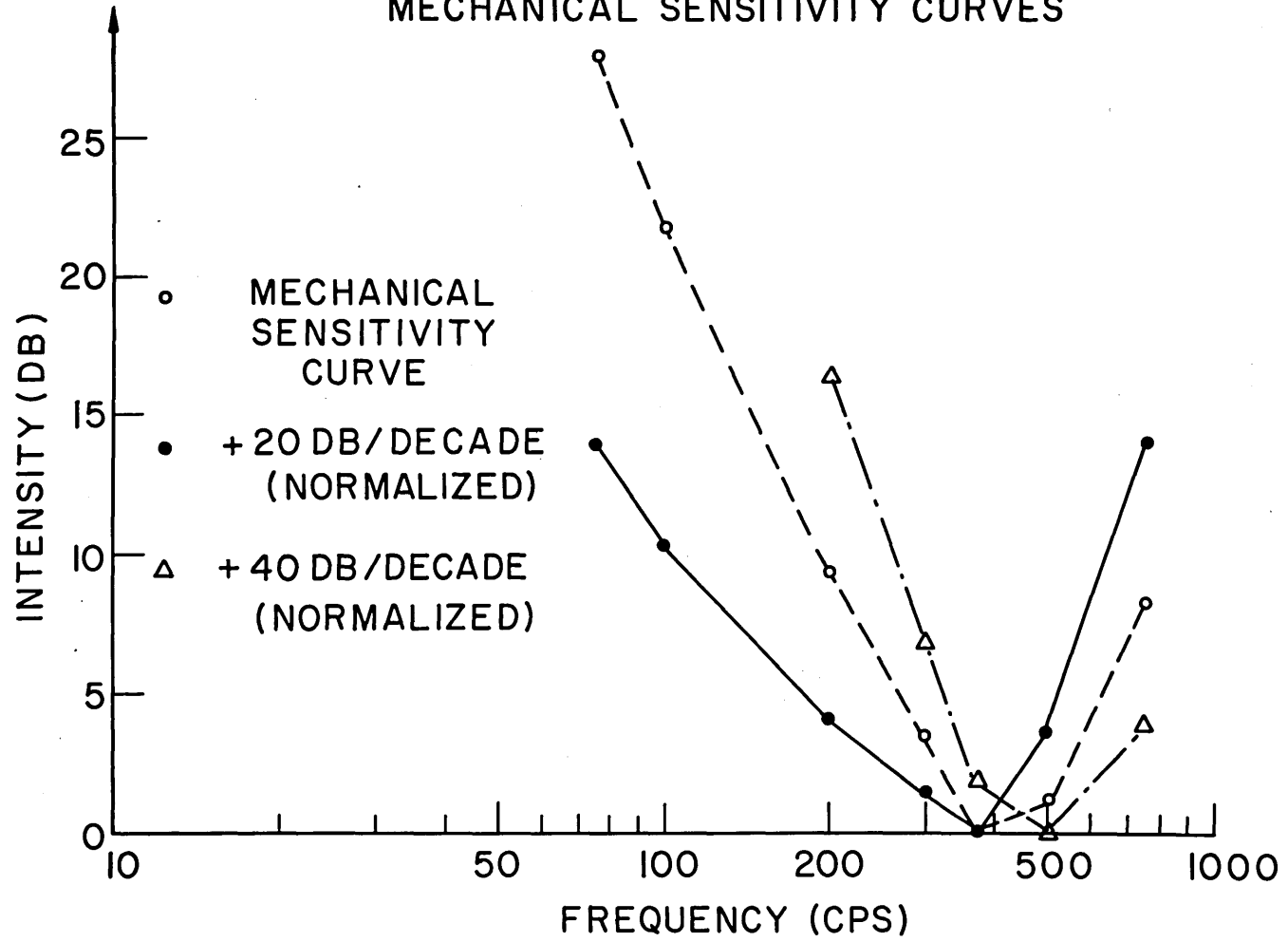
may be due to ignorance of the nature of the proper transducer function of the hair cells.

In order to discuss the shape of the tuning curves, we shall assume that the transducer and model neuron exhibit a rate of change of sensitivity of 25 to 30 db/decade of frequency. Figure 34 shows tuning curves constructed by adding both a 20 and a 40 db/decade change in sensitivity to a typical mechanical tuning curve. The results have been normalized to make the minima of the curves equal. Note that although the resultant curves are still slightly wider than the neural tuning curves, they are in closer agreement with them. Furthermore, the slopes of these augmented mechanical tuning curves are steeper at low frequencies than the slopes of the mechanical curves. We think it reasonable to say that the augmented mechanical tuning curves correspond more closely to the neural tuning curves than do the mechanical tuning curves. Any further discrepancies between mechanical and neural tuning curves may be attributed to the differences in species and preparations used to obtain the two sets of data as well as to the degree of approximation of the argument presented in this section.

We have attempted to show that the tuning curves generated by the model are similar to the tuning curves of VIIIth nerve fibers, although we have not demonstrated these results directly.

Figure 34. Mechanical tuning curves. The augmented mechanical tuning curves were obtained by adding a 20 db/decade and a 40 db/decade change in sensitivity to a typical mechanical tuning curve.

MECHANICAL SENSITIVITY CURVES



D. Response of the Model to Acoustic Clicks

The responses of a number of VIIIth nerve fibers to periodic trains of acoustic clicks (100 μ sec pulses applied to a condenser earphone) are shown in Figure 14. The responses are in the form of post-stimulus-time (PST) histograms, i.e., histograms of the times of occurrence of spike potentials following the onset of the last stimulus. The PST histograms shown in the figure have been ordered according to the characteristic frequencies of the fibers. All histograms of fibers whose CF's are less than approximately 4 Kc exhibit multiple peaks. The intervals between the peaks are equal to $1/CF$. Figure 35 shows the displacement of the cochlear partition and the PST histogram for two polarities of acoustic clicks as generated by the model*. The results shown in the figure correspond to a point along the partition whose $CF = 500$ cps. Note that in each case shown, the PST histograms exhibit peaks at intervals of 2 milliseconds and these peaks occur at the positive deflections of the impulse response of the cochlear partition. Several peaks can be seen in the PST histograms, while only a few are discernable in the response of the cochlear

*The conditions for obtaining the results shown in this figure are discussed later in this section. The click response of the cochlear partition corresponds to the impulse response ($F_3(t)$) shown in Figure 10.

Figure 35. Response of the cochlear partition and model for two different polarities of acoustic clicks. The dotted curves are the response of the cochlear partition to positive (left) and negative (right) polarities of clicks. The responses are equal to $F_3(t)$, (after Flanagan) for a point along the partition with a $CF = 500$ cps.

Transducer function is:

$$G(y) = (k_1 y) (k_2 / k_2 + |y|)$$

$$k_1 = 1$$

$$k_2 = 20000$$

$$R_R = 10000$$

$$R_M = 100000$$

$$\tau_R \doteq 1 \text{ msec}$$

$$f_h \doteq 5 \text{ Kc}$$

$$f_\ell \doteq 5 \text{ cps}$$

$$\sigma \doteq 5000$$

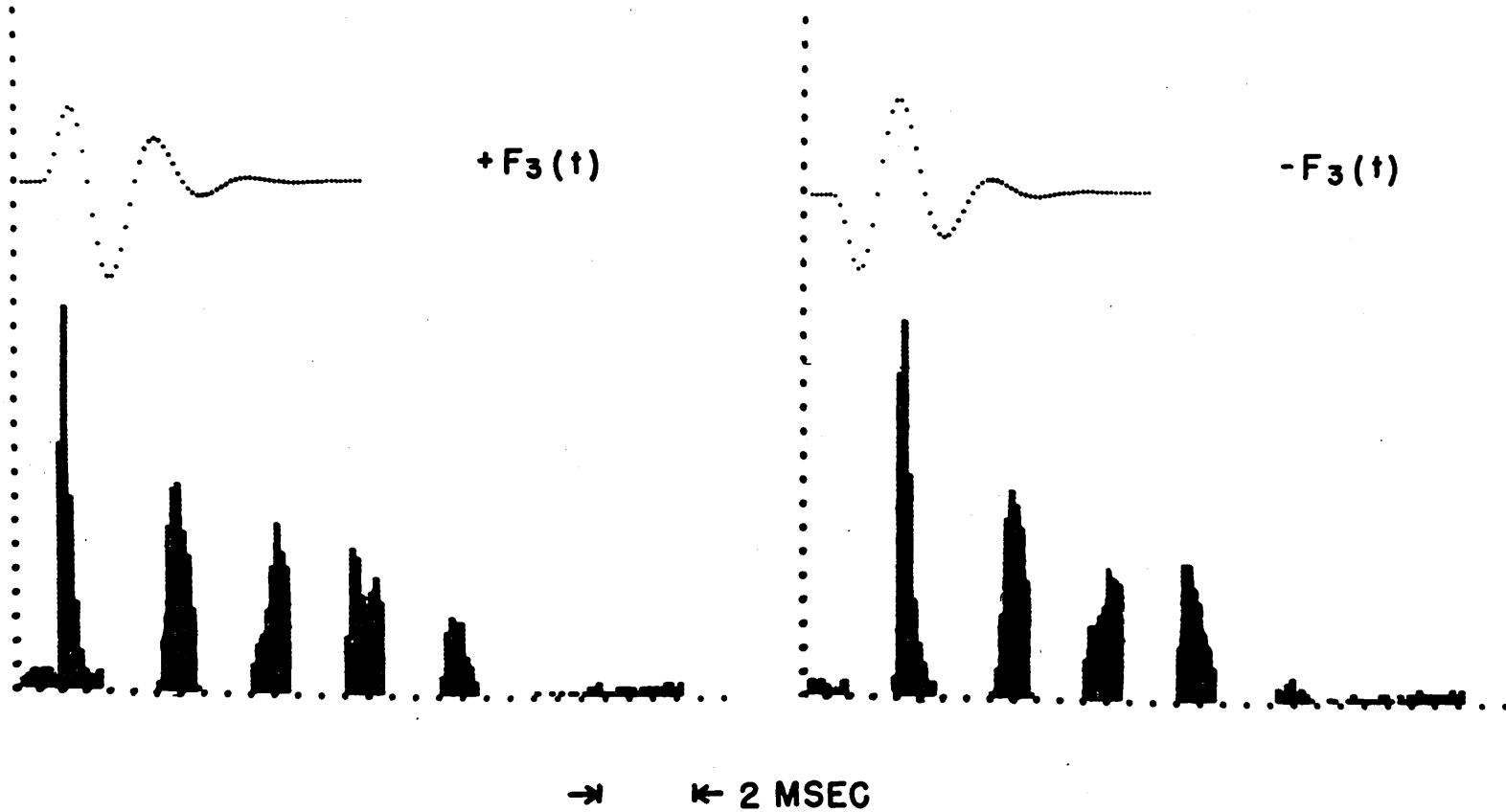
Spontaneous rate of firing $\doteq 90$ events/sec

ACOUSTIC CLICK RESPONSE OF THE COCHLEAR PARTITION
AND MODEL NEURON FOR TWO CLICK POLARITIES

G.F. = 500 CPS

(NON-LINEAR TRANSDUCER)

-138-



partition. Successive peaks of the response of the cochlear partition decrease in amplitude at a rate of not less than 20 db/cycle of oscillation. As a result, the fourth, fifth and later peaks are too small to be seen in the figure.

Figure 36 shows the response of a typical VIIIth nerve fiber to rarefaction and condensation* clicks as a function of intensity. The intervals between peaks equals $1/CF$ and these intervals remain relatively constant as a function of intensity. Furthermore, the peaks of the response to a rarefaction click occur at the troughs of the response to a condensation click and vice-versa. The times of occurrence of the peaks in the PST histogram for condensation and rarefaction clicks as a function of intensity for the VIIIth nerve fiber are shown in Figure 37. The almost perfect interleaving of peaks is readily apparent.

Figure 38 shows the response of the model to acoustic clicks as a function of intensity (the intensity

*The two polarities of clicks used in the VIIIth nerve data are referred to as condensation and rarefaction clicks. The two polarities of clicks used to test the model are referred to as positive and negative clicks. This distinction is drawn in order to avoid a discussion of which direction of displacement of the cochlear partition is effective in depolarizing the nerve fibers. The correspondence between positive and negative clicks versus rarefaction and condensation has been avoided.

Figure 36. Response of an VIIIth nerve fiber to condensation and rarefaction clicks as a function of intensity.

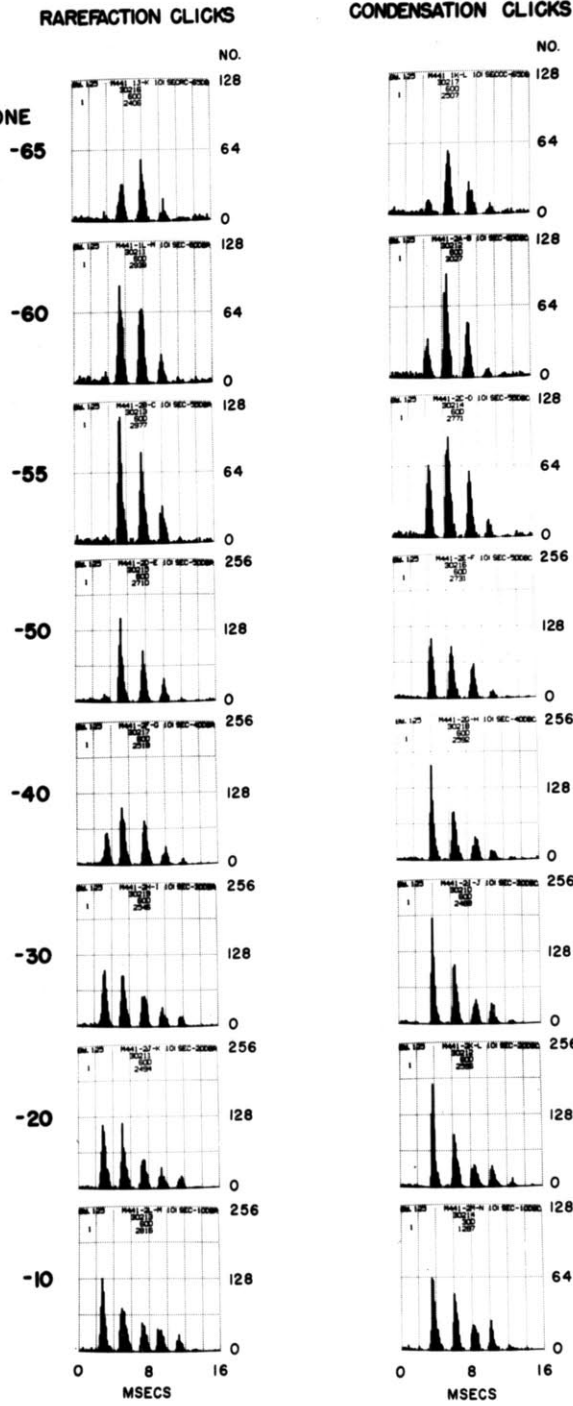
CF = 472 cps

Rate of spontaneous firing = 52.5 spikes/sec.

Rate of presentation of clicks = 10/sec.

UNIT 300-21
PST HISTOGRAMS

CLICK INTENSITY
IN DB RE 100V INTO
CONDENSER EARPHONE



CLICK RATE: 10/SEC

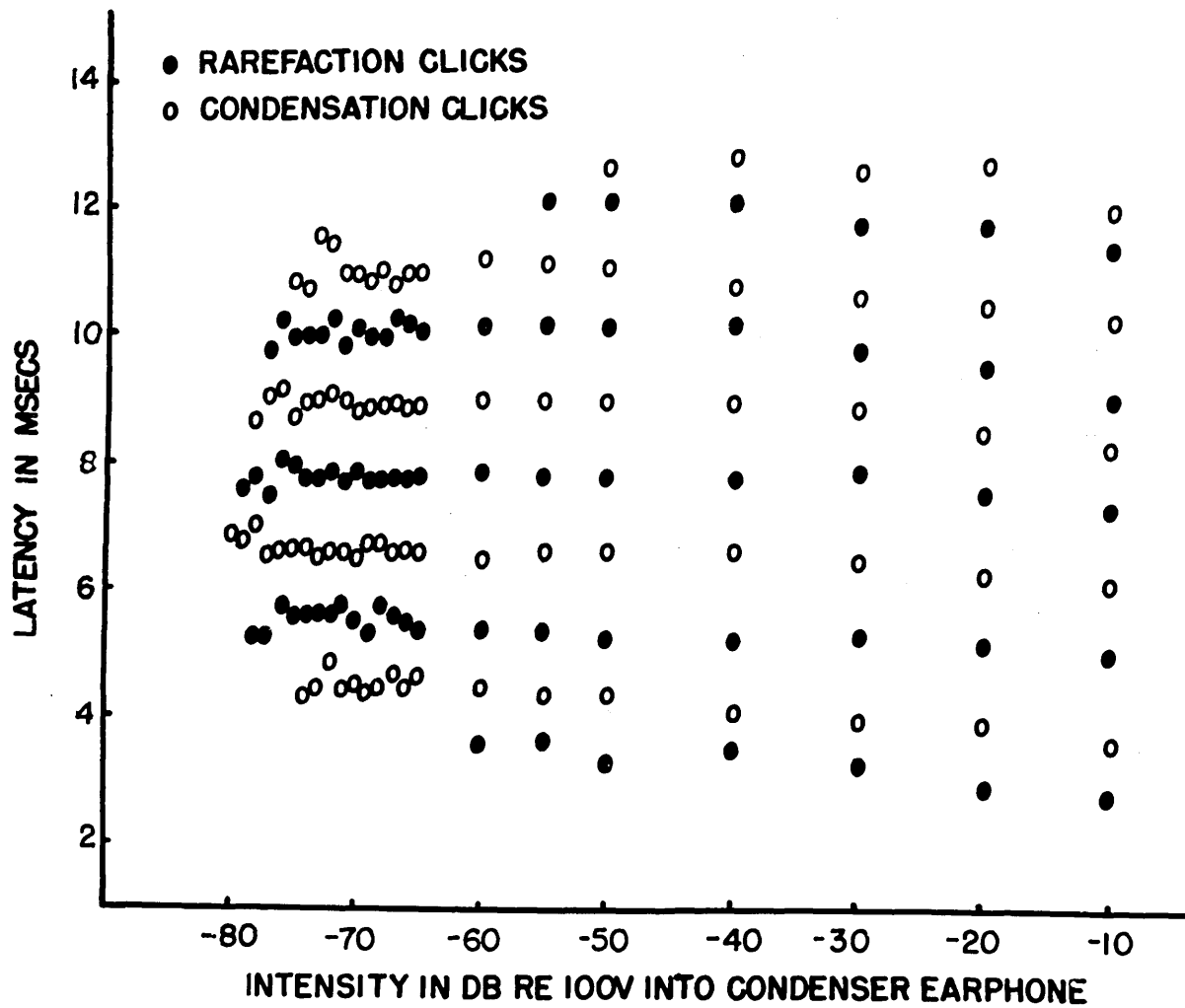
Figure 37. Times of occurrence of peaks in the PST histogram of the response of an VIIIth nerve fiber to condensation and rarefaction clicks as a function of intensity.

CF = 472 cps.

Rate of spontaneous firing = 52.5 spikes/sec.

Rate of presentation of clicks = 10/sec.

UNIT 300-21



-143-

Figure 38. Acoustic click response of the model for a linear (left) and non-linear (right) transducer as a function of intensity.

$$CF = 500 \text{ cps}$$

$$G(y) = y \text{ (for linear transducer)}$$

$$G(y) = y (20000/20000+|y|) \text{ (for non-linear transducer)}$$

$$R_R = 10000$$

$$R_M = 100000$$

$$\tau_R \doteq 1 \text{ msec}$$

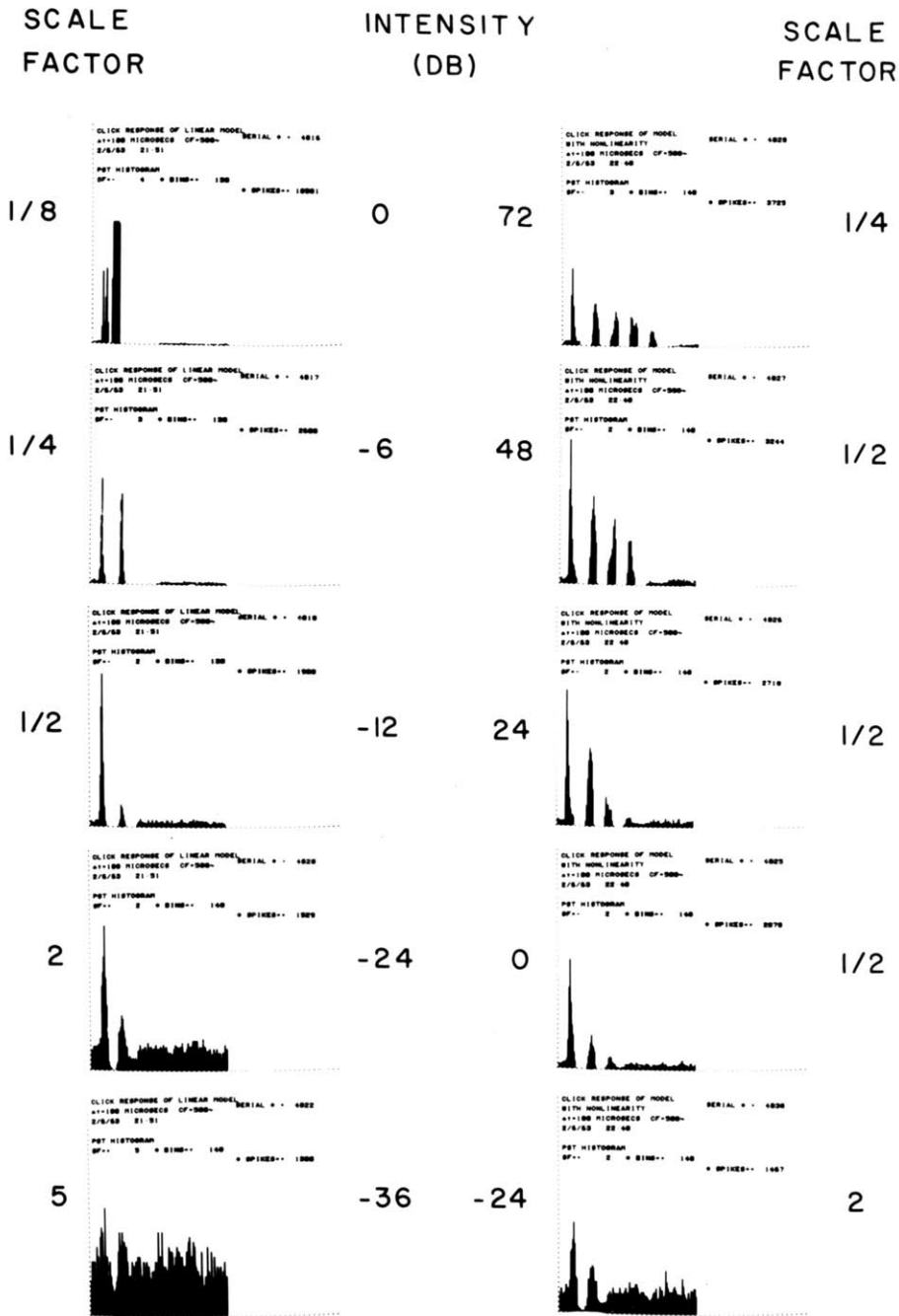
$$\sigma \doteq 5000$$

$$f_h \doteq 5 \text{ Kc}$$

$$f_l \doteq 5 \text{ cps}$$

$$\text{Rate of spontaneous firing} \doteq 90 \text{ events/sec.}$$

ACOUSTIC CLICK RESPONSE OF MODEL



LINEAR TRANSDUCER NON-LINEAR TRANSDUCER
 $\Delta t = 100 \mu\text{sec}$
 CF = 500 cps

scale has an arbitrary reference level and only relative intensities should be considered meaningful). The PST histograms in the left hand column were obtained by using a linear transducer function. Note that there is a 36 db range between the intensity at which a response is first visible in the PST histogram and the intensity at which the response of the model becomes stereotyped (i.e., the model responds to the largest positive deflection of the cochlear partition every time a stimulus is presented in a manner unlike the response of VIIIth nerve fibers). Since the envelope of the impulse response of the cochlear partition decays at a rate exceeding 20 db per cycle of oscillation, there can be at most two or three peaks in the PST histogram when a linear transducer is used. These results are clearly at variance with the empirical data of Kiang, et al.

It is clear that the peaks of the PST histogram grow too rapidly as a function of intensity. The right side of Figure 38 shows the PST histograms of the click response of the model for a non-linear transducer function. The function chosen in this case is $G(y) = k_1 y (k_2 / (k_2 + |y|))$. This function has the following limiting behavior:

$$G(y) \sim k_1 y \text{ for small values of } y \text{ and}$$

$$G(y) \sim k_1 k_2 (y/|y|) \text{ for large values of } y.$$

The effect of this function is to saturate the large peaks in the deflections of the cochlear partition and to allow the smaller peaks to increase as a function of intensity.

Figure 39 shows the click response of the model for both positive and negative clicks. The same non-linear function was used to obtain the results shown in Figure 39 as in the right side of the previous figure. Figure 40 shows the time of occurrence of the peaks in the PST histogram in response to clicks of opposite polarity as a function of intensity. The intervals between peaks (for each polarity of click) are 2 milliseconds. The peaks resulting from the response to positive and negative clicks are seen to interleave.

Figure 41 shows PST histograms generated by the model for four different values of CF. The intervals between peaks are seen to correspond to $1/CF$ in each case. The data for values of CF equal to 4 Kc and 8 Kc were computed at a resolution of 12.5 μ sec. The large statistical fluctuations shown in the figure result from the limited sample size used for the high resolution runs. This figure indicates that the model can resolve separate peaks of the impulse response of the cochlear partition for a CF as high as 8 Kc.

Figures 42 and 43 are included to show the responses produced when a different non-linear transducer function is used. $G(y) = k_1(y / |y|) \log|y|$ in these two cases. Both figures show the PST histograms of the click response of the model as a function of intensity. Figure 42 shows these results for a CF equal to 500 cps and Figure 43 is for a CF equal to 1 Kc. The results obtained by using the

Figure 39. Response of the model to positive and negative clicks as a function of the intensity of click stimulation. The response to positive (left) and negative (right) clicks is shown.

$$CF = 500 \text{ cps}$$

$$G(y) = y(20000/20000 + |y|)$$

$$R_R = 10000$$

$$R_M = 100000$$

$$\tau_R \doteq 1 \text{ msec}$$

$$\sigma \doteq 5000$$

$$f_h \doteq 5 \text{ Kc}$$

$$f_l \doteq 5 \text{ cps}$$

Rate of spontaneous firing $\doteq 90$ events/sec.

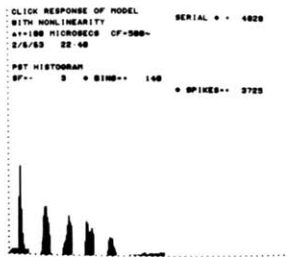
ACOUSTIC CLICK RESPONSE OF MODEL

SCALE
FACTOR

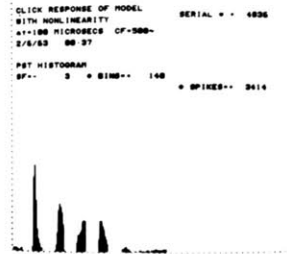
INTENSITY
(DB)

SCALE
FACTOR

1/4

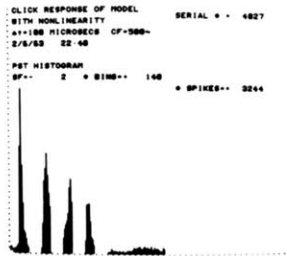


+72

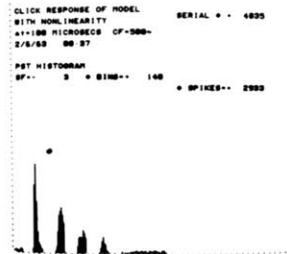


1/4

1/2

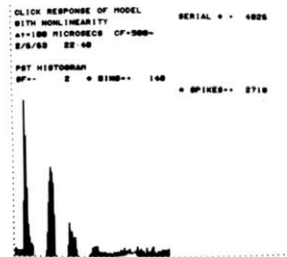


+ 48

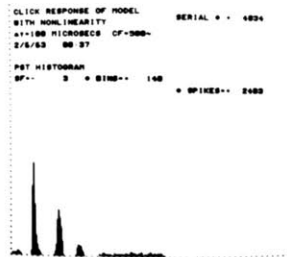


1/4

1/2

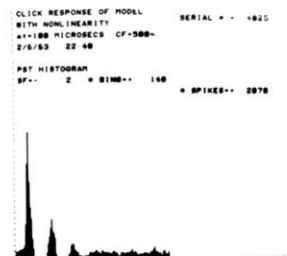


+ 24

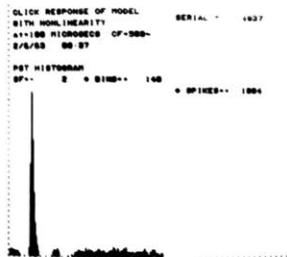


1/4

1/2

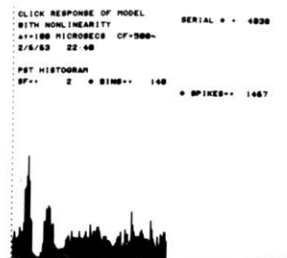


0



1/2

2



-24



2

$\Delta t = 100 \mu \text{sec}$

CF = 500 cps

Figure 40. Times of occurrence of peaks in the PST histograms of the response of the model to acoustic clicks.

$$CF = 500 \text{ cps}$$

$$G(y) = y(20000/20000 + |y|)$$

$$R_R = 10000$$

$$R_M = 100000$$

$$\tau_R \doteq 1 \text{ msec}$$

$$\sigma \doteq 5000$$

$$f_h \doteq 5 \text{ Kc}$$

$$f_l \doteq 5 \text{ cps}$$

Rate of spontaneous firing $\doteq 90$ events/sec.

TIME OF OCCURRENCE OF PEAKS IN PST HISTOGRAM OF CLICK RESPONSE

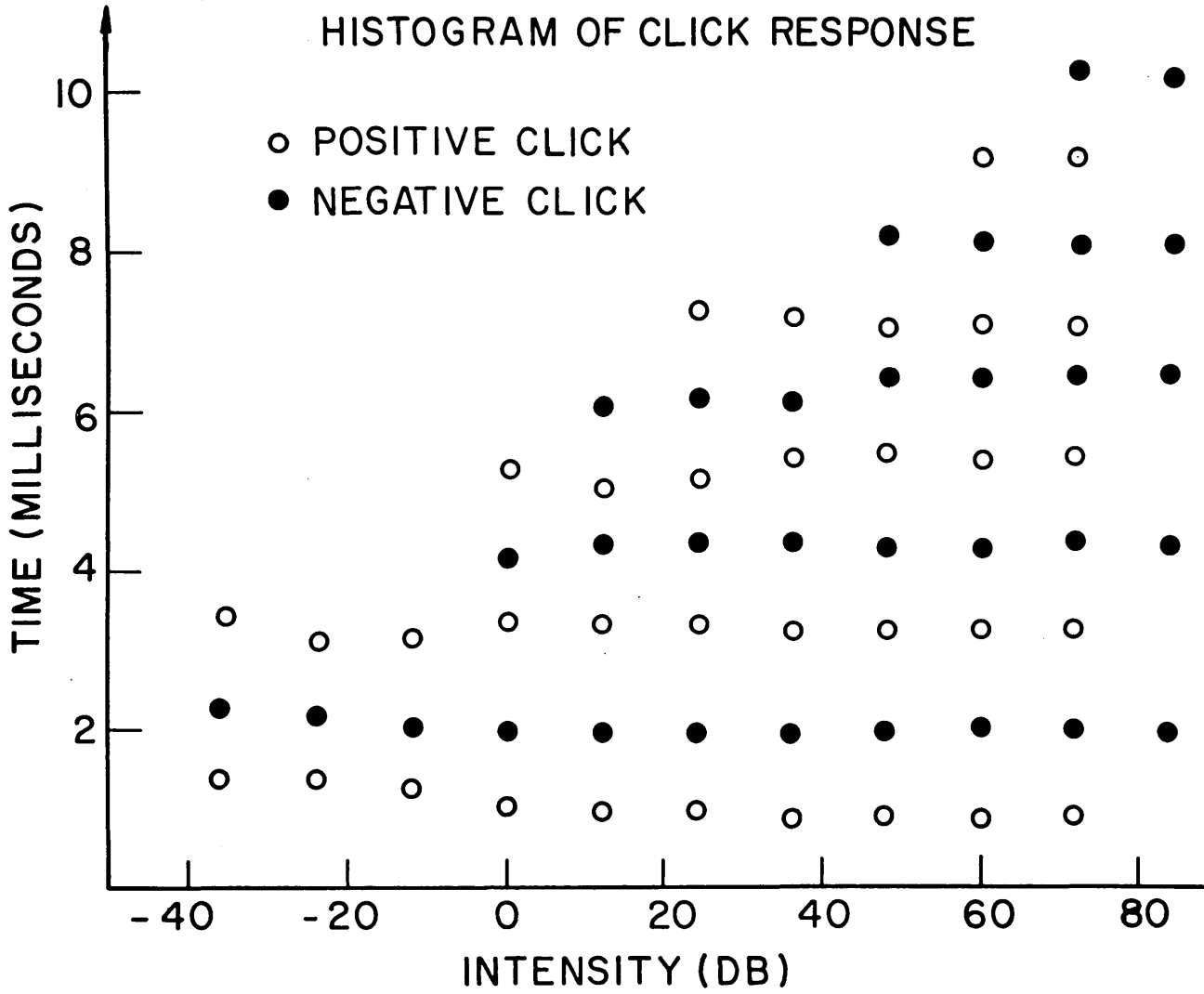


Figure 41. Acoustic click response of the model for different values of CF.

$$G(y) = y(20000/(20000+|y|))$$

$$R_R = 10000$$

$$R_M = 100000$$

$$\tau_R \doteq 1 \text{ msec}$$

$$\sigma \doteq 5000$$

$$f_h \doteq 5 \text{ Kc}$$

$$f_l \doteq 5 \text{ cps}$$

Rate of spontaneous firing $\doteq 90$ events/sec.

ACOUSTIC CLICK RESPONSE OF MODEL (NON-LINEAR TRANSDUCER)

SCALE
FACTOR

CLICK RESPONSE OF MODEL WITH
NONLINEARITY *1 K1=1.K2=20000
*1=100 MICROSECS CF=250~ SERIAL * * 7536
4/20/63 11-34
PST HISTOGRAM
SF-- 3 * BINS-- 128 * SPIKES-- 8717

C.F.

C.F.

CLICK RESPONSE OF MODEL WITH
NONLINEARITY *1 K1=1.K2=20000
*1=12.5 MICROSECS CF=4000~ SERIAL * * 7685
4/22/63 23-28
PST HISTOGRAM
SF-- 4 * BINS-- 128 * SPIKES-- 1964

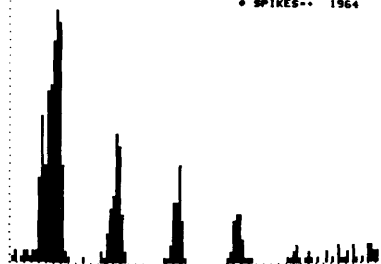
SCALE
FACTOR

1/4

250 CPS

4 KC

4



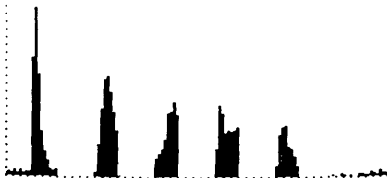
CLICK RESPONSE OF MODEL WITH
NONLINEARITY *1 K1=1.K2=20000
*1=100 MICROSECS CF=500~ SERIAL * * 7538
4/20/63 11-53
PST HISTOGRAM
SF-- 3 * BINS-- 128 * SPIKES-- 7917

500 CPS

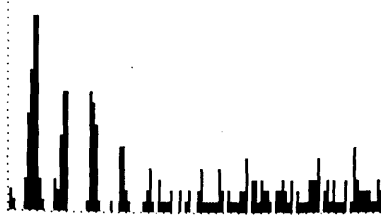
8 KC

7

1/4



CLICK RESPONSE OF MODEL WITH
NONLINEARITY *1 K1=1.K2=20000
*1=12.5 MICROSECS CF=8000~ SERIAL * * 7686
4/22/63 23-52
PST HISTOGRAM
SF-- 7 * BINS-- 128 * SPIKES-- 1856



← 2 MSEC

← 0.25 MSEC

Figure 42. Acoustic click response of model as a function of intensity.

$$CF = 500 \text{ cps}$$

$$G(y) = 0.1(y/|y|) \log_2 |y|$$

$$R_R = 10000$$

$$R_M = 100000$$

$$\tau_R \doteq 0.3 \text{ msec}$$

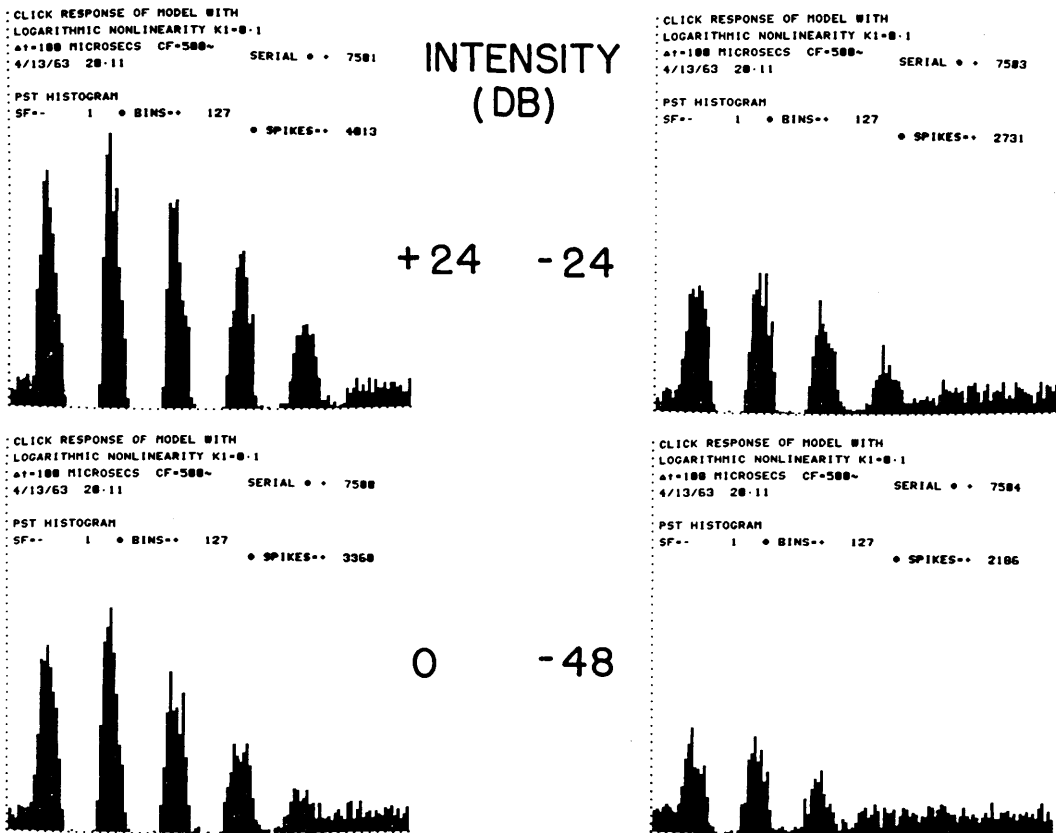
$$\sigma \doteq 5000$$

$$f_h \doteq 5 \text{ Kc}$$

$$f_l \doteq 5 \text{ cps}$$

Rate of spontaneous firing \doteq 135 events/sec.

ACOUSTIC CLICK RESPONSE OF MODEL (NONLINEAR TRANSDUCER)



-155-

Figure 43. Acoustic click response of model as a function of intensity.

$$CF = 1000 \text{ cps}$$

$$G(y) = 0.1(y/|y|) \log_2|y|$$

$$R_R = 10000$$

$$R_M = 100000$$

$$\tau_R \doteq 0.3 \text{ msec}$$

$$\sigma \doteq 5000$$

$$f_h \doteq 5 \text{ Kc}$$

$$f_l \doteq 5 \text{ cps}$$

Rate of spontaneous firing \doteq 135 events/sec.

ACOUSTIC CLICK RESPONSE OF MODEL (NONLINEAR TRANSDUCER)

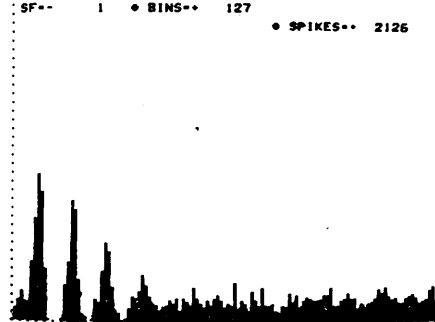
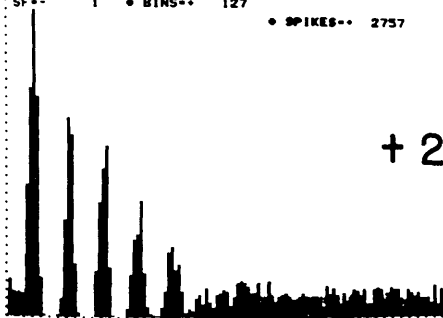
CLICK RESPONSE OF MODEL WITH
LOGARITHMIC NONLINEARITY K1=0.1
Δt=100 MICROSECS CF=1000~
4/13/63 20:57 SERIAL • • 7507

INTENSITY
(DB)

CLICK RESPONSE OF MODEL WITH
LOGARITHMIC NONLINEARITY K1=0.1
Δt=100 MICROSECS CF=1000~
4/13/63 20:57 SERIAL • • 7508

PST HISTOGRAM
SF-- 1 • BINS-- 127
• SPIKES-- 2757

PST HISTOGRAM
SF-- 1 • BINS-- 127
• SPIKES-- 2126



+ 24 - 24

CLICK RESPONSE OF MODEL WITH
LOGARITHMIC NONLINEARITY K1=0.1
Δt=100 MICROSECS CF=1000~
4/13/63 20:57 SERIAL • • 7506

CLICK RESPONSE OF MODEL WITH
LOGARITHMIC NONLINEARITY K1=0.1
Δt=100 MICROSECS CF=1000~
4/13/63 20:57 SERIAL • • 7509

PST HISTOGRAM
SF-- 1 • BINS-- 127
• SPIKES-- 2302

PST HISTOGRAM
SF-- 1 • BINS-- 127
• SPIKES-- 1071



0 - 48

→ K ← 2 MSEC
C.F. = 1000 CPS

-157-

logarithmic non-linearity are similar to the results obtained by using the previously-mentioned non-linearity. The general features of the PST histograms are in close agreement with the VIIIth nerve data. The peaks in the PST histogram occur at intervals of time separated by $1/CF$. These peaks interleave for the response to positive and negative clicks. The intervals of time between peaks remain constant as a function of intensity. The intervals of time between the onset of the stimulus and each peak decrease slightly as the intensity of stimulation is increased.

There are, however, at least two discrepancies between the response of the model and the response of VIIIth nerve fibers to acoustic clicks. One is a somewhat trivial discrepancy: A careful study of the response of VIIIth nerve fibers to rarefaction clicks of high intensity reveals that a new peak appears early in the PST histogram. Similarly, a new trough appears early in the PST histogram of the response to condensation clicks of high intensity. For instance, the early peak can be clearly seen to appear at -40 db in Figure 36. This peak appears at an interval of time equal to $1/CF$ with respect to the next peak (or what was previously the first peak). This early peak is never seen in data generated by the model. The peaks in the PST histograms generated by the model correspond to the positive displacements of the impulse response of the cochlear partition. Since the impulse response (due

to Flanagan) which we have utilized in this model exhibits no such early peak, neither does the PST histogram of the model. Our conclusion is that the inaccuracies of the approximation to the impulse response of the cochlear partition are probably responsible for the discrepancy.

There is, however, a more serious difficulty with the model. Too large a dynamic range of intensity is required to obtain results from the model similar to those generated by VIIIth nerve fibers. For instance, a 70 db range of intensity is required to obtain the results shown in Figure 37. Further data indicate that the patterns of firing of VIIIth nerve fibers require a range of intensity of about 50 to 70 db from threshold to an intensity at which the PST histograms no longer change much (i.e., no new peaks appear). For the non-linearities tested thus far, the comparable range of intensity for the model appears to be about 100 db. Furthermore, additional peaks appear at uniform intervals of intensity in this 100 db range (i.e., the peaks appear at approximately 24 db intervals in Figure 39). A smaller range of intensities is required to obtain a full complement of peaks for the VIIIth nerve data.

These facts suggest that either: 1) a fundamental assumption of the model is invalid, or 2) the non-linearities tested thus far are not the correct ones. The latter alternative, together with the results attained thus far, suggest a class of non-linear functions that have a sigmoid shape.

$$G(y) = k\left[\left(\int_{-\infty}^y \exp(-ax^2) dx\right) - 1/2\right] \text{ is such a function.}$$

In conclusion, the model predicts a number of features of the response of VIIIth nerve fibers to clicks. The peaks in the PST histograms appear at the proper intervals of time. These intervals remain fixed as a function of intensity. The times of occurrence of these peaks interleave for positive and negative clicks and these times of occurrence decrease slightly (less than $1/(4CF)$) as the intensity of click stimulation is increased. The dynamic range of intensity required to achieve these results in the model is larger than a comparable range for VIIIth nerve fibers. A knowledge of the transducer function of the sensory cells would aid in eliminating this discrepancy.

CHAPTER VI: Concluding Remarks

A. Comparison of the Data Generated by the Model with Data Obtained from VIIIth Nerve Fibers

We have considered three experimental conditions in order to compare results produced by the model with results obtained from VIIIth nerve fibers.* These conditions are: 1) the spontaneous activity of the model, 2) the response of the model to sinusoidal stimuli, and 3) the response of the model to simulated acoustic clicks.

Both the qualitative and quantitative results generated by the model for the case of spontaneous activity are in agreement with the results obtained from the fiber data. The interval histograms of the spontaneous activity of both model and fiber can be described as exponential in the limit of large intervals. The interval histograms exhibit a refractory effect for short intervals of time with a smooth transition between these two regions. Both model and fiber data show a small amount of statistical dependence between successive inter-spike intervals. This dependence indicates that short intervals tend to be followed by short intervals. Successive intervals of time between events are uncorrelated if the preceding interval is long. The critical parameters

*The VIIIth nerve fiber data, to which we refer, is the electrophysiological data of Kiang, et al. In most, but not all, respects these data are in agreement with results obtained by other investigators.

for determining this dependence are the time course of the refractory period and the band pass of the noise. These results are achieved for a duration of the refractory period of approximately one millisecond and a noise band pass of two to five kilocycles. The duration of the primary refractory effects of neural fibers is one or perhaps a few milliseconds and the value of the bandwidth of the noise is consistent with estimates of this figure obtained by others. (108, 109)

The response of the model to sinusoidal stimuli is qualitatively similar to data obtained from VIIIth nerve fibers. Arguments were presented to show that the tuning curves generated by the model approximate the tuning curves of VIIIth nerve fibers. The post-zero-crossing histograms (histograms of the times of occurrence of spikes after each positive-going zero-crossing of the sinusoid) of the response of model and fiber to sinusoidal stimuli appear to be similar in some rather gross respects. The sensitivity curves* generated by model and fiber in response to sinusoidal stimuli (delivered at the characteristic frequencies) show the same trend as a function of frequency. For frequencies below 2 Kc both model and fiber exhibit a decrease of sensitivity. The fibers of the VIIIth nerve exhibit a change of sensitivity

*This term is defined on page 107.

of approximately 40 db/decade of frequency. The model exhibits a change of sensitivity of approximately 25 or 30 db/decade in the same range of frequency. The part of the model that represents the mechanical part of the ear accounts for approximately a 15 db/decade change in sensitivity. The remaining 10 or 15 db/decade change in sensitivity is due to the rest of the model. We have presented arguments that show that the differences between the sensitivity curves derived from model and fiber data can be attributed to our not knowing the proper transducer function of the sensory cells.

We have shown that using a linear, memoryless function to represent the transducer action of the sensory cells yields responses of the model to simulated acoustic clicks that are at variance with the VIIIth nerve data of Kiang, et al. For instance, the PST histograms (histograms of the times of occurrence of spikes after the onset of a stimulus) generated by the model do not show the multiple peak structure that is evident in the fiber data. A non-linear transducer function can be shown to improve the agreement between model and fiber data. For the non-linear transducer functions tested thus far, the form of the PST histogram in response to clicks is qualitatively quite similar to the results obtained from fibers. These similarities include: 1) the appearance of a number of peaks in the histograms; 2) the intervals of time between peaks equal

1/CF*; 3) the values of these intervals are relatively insensitive to changes of the intensity of the stimulus; 4) the times of occurrence of peaks in the response of the model to clicks of opposite polarity interleave in time; and 5) the times of occurrence of these peaks relative to the onset of the stimulus decrease (by a duration less than $1/(4 \text{ CF})$) when the intensity of the stimulus is increased. The intensity range required for the appearance of successive peaks in the PST histogram is larger for the model than for the VIIIth nerve data. We feel that this discrepancy can also be accounted for by our not knowing the proper non-linear transducer function of the hair cells. Furthermore, the same form of transducer function appears capable of improving the discrepancies of the response of model and fiber to sinusoidal as well as to click stimuli. This function appears to be a sigmoid function.

Data generated by the model appear to approximate the fiber data for the three experimental conditions that we have considered. At this stage in the research, the agreement is, for the most part, qualitative, but this agreement holds for a relatively broad class of stimulus conditions and parameters.

B. Appraisal of the Model and Suggestions for Further Study

This study suggests that the peripheral auditory system can be represented to a first-order approximation by a model

*CF is the characteristic frequency and is defined on page 107.

which consists of three functional constituents: 1) a linear mechanical system; 2) a non-linear transducer; and 3) a probabilistic threshold device with refractory properties. Such a model appears to be consistent with much of the known anatomy and physiology of the peripheral system. In particular, this model generates both spontaneous events and responses to stimuli that appear to be in agreement with some of the data obtained from VIIIth nerve fibers. As might be expected, the parts of the model that appear to be responsible for the quantitative discrepancies that exist between model and fiber data correspond to the parts of the peripheral auditory system that are least understood. More precisely, the excitation process involving the hair cell-neuron junction is very poorly understood. We propose to extend our studies of models of the excitation process. For instance, we are considering a model which attributes the probabilistic mechanism in the peripheral system to "synaptic noise" rather than to noise in the membrane potential of the fiber as we have assumed in the model presented here.

The results obtained from the model have suggested some new ways to analyze the spike activity generated by nerve fibers. The D_n criterion, discussed in Chapter V, Part C, is a measure of the amount of time-locked spike activity present in a record of data. This measure is somewhat independent of the spontaneous rate of firing. A "threshold of firing" to a stimulus can be defined using

the D_n measure, and the significant variations of D_n from its mean value can be computed.

One further method of analysis of the spike activity of VIIIth nerve fibers has suggested itself as a result of the model work. The interaction between the refractory effects of the model neuron and the non-linearities in the system (both those included in the transducer model and those in the model neuron) have led to many conceptual difficulties in this study. Both the refractory effects and the non-linearities affect the rate and form of the firing of the model in response to stimuli. The separation of the effects of these two components on the response of the model to stimuli would simplify the study of the model. One procedure for eliminating the refractory effects and studying only the effects of the rest of the system is to consider only those events (in the model) or spikes (generated by a fiber) that are preceded by long intervals of time during which no firing occurs. For instance, a PST histogram of the response to acoustic clicks could be generated by counting only those firings that are preceded by intervals of time equivalent to the time needed for a fiber to recover from the last firing. Such modified PST histograms of the response of model and fiber to acoustic stimuli would, we feel, lead to interesting insights on the nature of the excitation process.

There are clearly many and more general extensions of this work. The primary goal remains the same: To find a model of the peripheral auditory system that predicts the data obtained from VIIIth nerve fibers.

C. A Note on Models and Digital Computer Simulations

The research discussed here is patterned after a style of scientific investigation which we would like to state more explicitly. First, we believe that precise answers to scientific questions can be obtained only when the questions themselves are precise. Furthermore, we find it desirable to phrase these questions in some context. We think of this context as a formal or a conceptual structure: The word "model" is now in vogue to describe such a structure.

With the advent of the general purpose digital computer, it has become possible to investigate models which do not necessarily lend themselves to more formal and analytic treatments. A much richer class of conceptual structures can thus be studied. This has particular importance in neurophysiology because few problems in this area have been reduced to an analytically manipulatable form.

It is unfortunately true that most contemporary digital machines are taxed by even relatively simple models of relatively simple parts of the nervous system (such as the model of the peripheral auditory system presented here). This is primarily a consequence of both the design and

administration of these machines. Many of the large, general purpose machines have been designed for business or military use, and this has made them somewhat unsuitable as research tools. Access to these machines has been limited largely to computer operators carrying punched cards.

This study has been made possible because of the existence of the TX-2 computer. This machine was designed and is administered as a research tool. Relatively large amounts of time (hours instead of minutes) have been made available to individual investigators. An investigator can thus operate the machine in very much the same manner as he might perform an experiment in the laboratory. Computations can be modified on the basis of results obtained. In addition, the TX-2 has a flexible order code, high speed memories and a rich selection of input-output devices. We hopefully expect that bigger and better machines of this kind will be built to the needs of the biological investigator.

APPENDIX A: A Discussion of the Distribution of Spontaneous Events

The problem of finding the distribution of intervals between events generated by the model (for the spontaneous event case) is similar to the problem of finding the distribution of axis crossings of a Gaussian process, where the axis is not constant but is some function of time. The axis crossing problem has not been solved in general, although considerable attention has been directed to this problem.

The distribution of intervals between spontaneous events generated by the model for a white noise process is discussed in this section. Consider the set of events $\{E_k\}$ occurring at times $k(\Delta t)$, where k is an integer. The event E_k is defined to occur at k if the noise exceeds the threshold, $n_k \geq r_k$. The noise has a Gaussian distribution with

$$E[n_k] = 0 \text{ and}$$

$$E[n_j n_k] = \begin{cases} 0 & \text{if } j \neq k \\ \sigma^2 & \text{if } j = k \end{cases}$$

The value of the threshold r_k is determined by the time of occurrence of the last event. If the previous event occurred at j , then the threshold is a function only of the time elapsed since the last event, $r_k = \alpha_{k-j}$. The probability of the occurrence of an event at $k+j$ given an event occurred at time k is:

$$(p_{k+j})_k = P_r [n_{k+1} < r_{k+1}, n_{k+2} < r_{k+2}, \dots, n_{k+j-1} < r_{k+j-1}, n_{k+j} \geq r_{k+j} / n_k \geq r_k]$$

An event occurred at k and the noise is assumed stationary, therefore:

$$(p_{R_{ij}})_k = p_j = P_r [n_1 < \alpha_1, n_2 < \alpha_2, \dots, n_{j-1} < \alpha_{j-1}, n_j \geq \alpha_j / n_0 \geq \alpha_i]$$

The noise process is white, therefore:

$$p_j = \int_{-\infty}^{\alpha_1} p[n_1] dn_1 \int_{-\infty}^{\alpha_2} p[n_2] dn_2 \dots \int_{-\infty}^{\alpha_{j-1}} p[n_{j-1}] dn_{j-1} \int_{\alpha_j}^{\infty} p[n_j] dn_j$$

The n_k 's are identically distributed and, therefore,

$$p_j = \prod_{k=1}^{j-1} \left[\int_{-\infty}^{\alpha_k/\sigma} d\Phi \right] \left[\int_{\alpha_j/\sigma}^{\infty} d\Phi \right]$$

$$p_j = \prod_{k=1}^{j-1} \left[\Phi(\alpha_k/\sigma) \right] \left[1 - \Phi(\alpha_j/\sigma) \right]$$

where
$$\Phi(x) = \int_{-\infty}^x \left(\frac{1}{\sqrt{2\pi}} \right) e^{-y^2/2} dy$$

$$p_j = \Phi^{j-1}(\alpha_j/\sigma) \left[1 - \Phi(\alpha_j/\sigma) \right] \prod_{k=1}^{j-1} \left[\Phi(\alpha_k/\sigma) / \Phi(\alpha_j/\sigma) \right]$$

Assume $\lim_{j \rightarrow \infty} \alpha_j = \alpha$ and $\alpha_1 > \alpha_2 > \dots > \alpha_j > \alpha$

therefore $\lim_{j \rightarrow \infty} \Phi(\alpha_j / \sigma) = g$ (a constant)

Then for large j

$$p_j = g^{j-1} (1-g) \prod_{k=1}^{j-1} \left[\frac{\Phi(\alpha_k / \sigma)}{\Phi(\alpha_j / \sigma)} \right]$$

and $\prod_{k=1}^{j-1} \left[\frac{\Phi(\alpha_k / \sigma)}{\Phi(\alpha_j / \sigma)} \right]$ is a monotone,

bounded sequence and, therefore, converges to a limit as $j \rightarrow \infty$

Therefore,

$$p_j \sim g^{j-1} (1-g) \quad \text{as } j \rightarrow \infty$$

and the distribution of intervals between events approaches the Geometric distribution (exponential) in the limit of large intervals.

APPENDIX B: Derivation of Statistics of D_n^2

Consider a histogram with η_i elements in the i^{th} bin, $i=1, \dots, n$ and a total number of elements equal to $\sum_{i=1}^n \eta_i = N$.

Define the counting random variable,

$$x_{ij} = \begin{cases} 1 & \text{if the } j^{\text{th}} \text{ element goes into the } i^{\text{th}} \text{ bin} \\ 0 & \text{otherwise} \end{cases}$$

Consider the case where the probability that the j^{th} element goes into the i^{th} bin is independent of j and i and equals $p = 1/n$. Then the number of elements in i^{th} bin is given by the Bernoulli distribution. The mean and variance of η_i are then simply given by

$$E[\eta_i] = Np = N(1/n)$$

$$\text{var}[\eta_i] = Np(1-p) = (N/n)(1 - 1/n)$$

or they can be derived by means of the counting random variables as follows:

$$\eta_i = \sum_{j=1}^N x_{ij}$$

$$E[\eta_i] = E\left[\sum_{j=1}^N x_{ij}\right] = \sum_{j=1}^N E[x_{ij}]$$

$$\text{but } E[x_{ij}] = 1 \cdot p + 0 \cdot (1-p) = p$$

$$\text{therefore, } E[\eta_i] = Np = N/n$$

Similarly,

$$\text{var}[\eta_i] = \text{var}\left[\sum_{j=1}^N x_{ij}\right]$$

but the x_{ij} are a set of independent random variables. Therefore,

$$\text{var}[\eta_i] = \sum_{j=1}^N \text{var}[x_{ij}]$$

$$\text{var}[x_{ij}] = E[x_{ij}^2] - E^2[x_{ij}]$$

$$E[x_{ij}^2] = 1^2 \cdot p + 0^2(1-p) = p$$

$$\text{var}[x_{ij}] = p - p^2 = p(1-p)$$

$$\text{var}[\eta_i] = Np(1-p) = (N/n)(1 - 1/n)$$

Define,

$$D^2 = (1/n) \sum_{i=1}^n (\eta_i - E[\eta_i])^2$$

$$E[D^2] = E\left[(1/n) \sum_{i=1}^n (\eta_i - E[\eta_i])^2\right]$$

$$= (1/n) \sum_{i=1}^n E[(\eta_i - E[\eta_i])^2]$$

$$= (1/n) \sum_{i=1}^n \text{var}[\eta_i] = \text{var}[\eta_i]$$

$$= (N/n)(1 - 1/n)$$

$$\text{var}[D^2] = E[(D^2)^2] - E^2[D^2]$$

$$E[(D^2)^2] = (1/n^2) \sum_{i=1}^n \sum_{k=1}^n E[(\eta_i - E[\eta_i])(\eta_k - E[\eta_k])]$$

Expansion of the term in the bracket yields terms such as $E[\eta_i^2 \eta_k^2]$. Using the counting random variables, this term can be expanded as

$$E[\eta_i^2 \eta_k^2] = \sum_{j,p,l,m}^N E[X_{ij} X_{ip} X_{kl} X_{km}]$$

There are several cases to be considered in order to evaluate this sum:

Case 1. All terms different $j \neq p \neq l \neq m$

$$\begin{aligned} E[X_{ij} X_{ip} X_{kl} X_{km}] &= E[X_{ij}] E[X_{ip}] E[X_{kl}] E[X_{km}] \\ &= p^4 \end{aligned}$$

There are $(N)(N-1)(N-2)(N-3) = (N!)/(N-4)!$ such terms.

Case 2. All terms equal $j=p=l=m$

$$\begin{aligned} E[X_{ij} X_{ip} X_{kl} X_{km}] &= E[X_{ij}^2 X_{kj}^2] \\ &= \begin{cases} 0 & \text{if } i \neq k \\ E[X_{ij}^4] = p & \text{if } i = k \end{cases} \end{aligned}$$

There are N such terms.

Case 3. Only one pair of equal terms

a) Pair corresponds to same bin, i.e.,

$j=p, l \neq m, j \neq l \neq m$

$$\begin{aligned} E[X_{ij} X_{ip} X_{kl} X_{km}] &= E[X_{ij}^2 X_{kl} X_{km}] \\ &= E[X_{ij}^2] E[X_{kl}] E[X_{km}] \\ &= p^3 \end{aligned}$$

There are $(N)(N-1)(N-2) = (N!)/(N-3)!$ such terms and two ways to pick the equal pair.

b) Pair corresponds to different bins, i.e.,

$$j \neq p \neq m$$

$$\begin{aligned} E[X_{ij} X_{ip} X_{Aj} X_{Am}] &= E[X_{ij} X_{kj}] E[X_{ip}] E[X_{Am}] \\ &= \begin{cases} 0 & \text{if } i \neq k \\ p^3 & \text{if } i = k \end{cases} \end{aligned}$$

There are $(N)(N-1)(N-2) = (N!)/(N-3)!$ such terms and four ways to pick the equal pair.

The other cases can be dealt with in a similar fashion.

Case 4. Two pairs of two equal terms

Case 5. Three equal terms

The other terms in the equation for $E[(D^2)]^2$ can be similarly expanded. When all these terms are expanded and the results collected, the variance reduces to:

$$\begin{aligned} \text{var}[D^2] &= \frac{2N(N-1)}{n^3} \left[1 - \frac{1}{n}\right] \\ &= \frac{2(N-1)}{n^2} \frac{N}{n} \left[1 - \frac{1}{n}\right] \\ &= \frac{2(N-1)}{n^2} E[D^2] \\ \sigma[D^2] &= \frac{\sqrt{2(N-1) E[D^2]}}{n} \end{aligned}$$

APPENDIX C: A Description of the Computer Programs

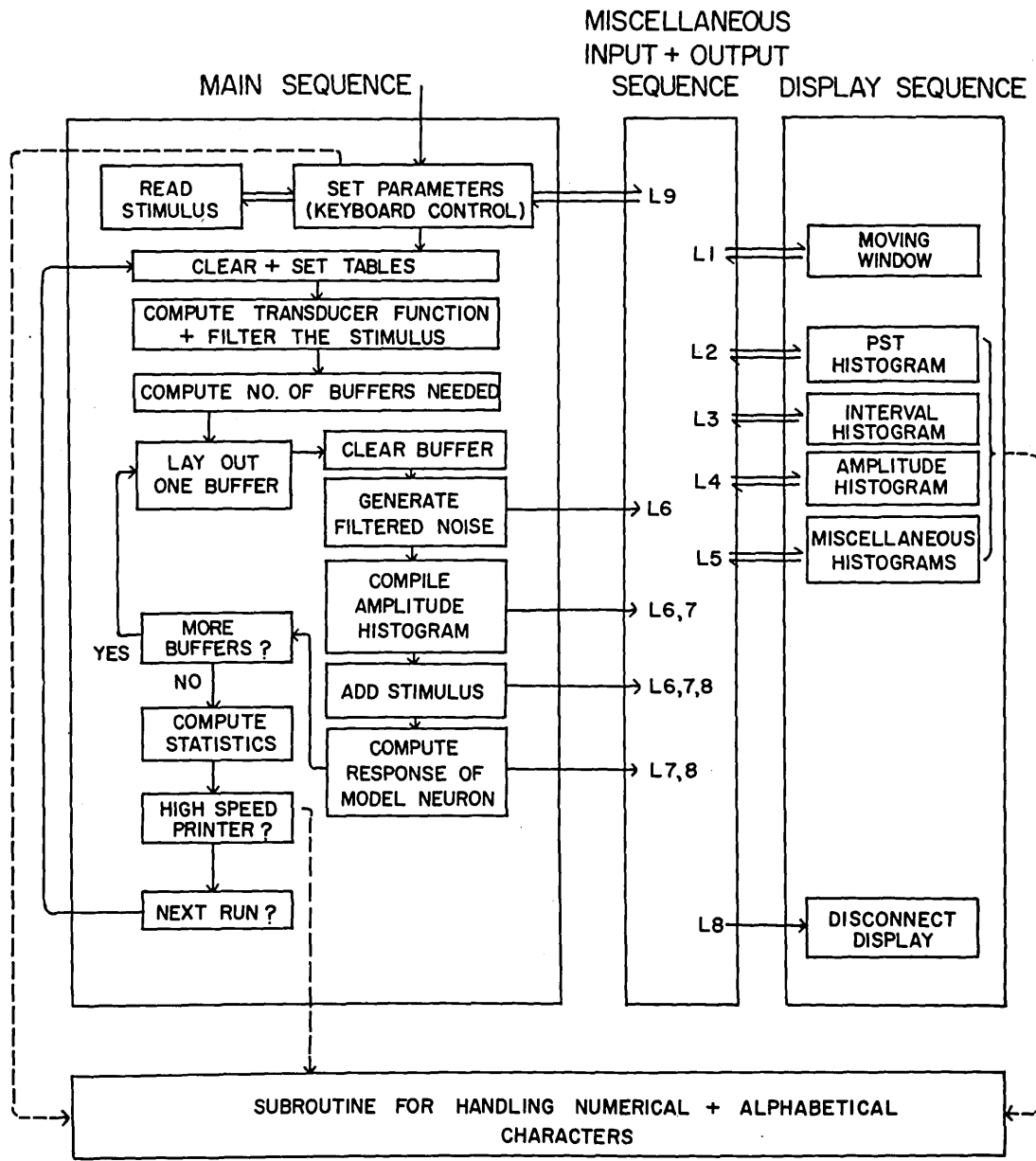
When a choice was necessary, the computer programs used in this study were written to achieve greater flexibility of the programs, rather than to decrease the time required to run them. The programs are flexible in two different senses. First, there is a great deal of program control available to the operator of the machine. This control includes typewriter control of the parameters of the computation, toggle switch control of various options in the computation, toggle switch control of the initiation of a series of runs to be done automatically, push button control of various displays of the computations which can be shown while the computations proceeds, etc. Secondly, it is relatively simple to make program modifications that accommodate rather gross changes in the model. Thus a wide variety of models of the peripheral auditory system can be studied with relatively minor changes of program. Flexibility is an essential feature in the type of research presented here. It is important for the research worker to interact with the machine directly, since the problems do not remain static, but change as the system under investigation is further explored.

The TX-2 machine was chosen for this project for a number of reasons: Foremost among these is the philosophy of its design and administration. It has been regarded primarily as a research tool rather than as an overgrown

calculating device. As such, it incorporates a highly flexible order-code, a multiplicity of easily manipulatable input and output devices, together with a large, high-speed memory. Furthermore, computer time has been made available for intervals of time large enough to make on-line concept formation possible.

No discussion of computer programs can be complete without a presentation of a logical flow diagram of the programs. Figure 44 is such a diagram. The programs are divided into four major blocks: (1) a main sequence, (2) a miscellaneous input and output sequence, (3) a display sequence and (4) a subroutine for handling numerical and alphabetical characters. The main sequence controls all the computation associated with generating the required data. The miscellaneous input and output sequence can be used to select the desired display mode (without essentially interrupting the computation) or to stop the computation at any desired time. The display sequence is controlled by the miscellaneous input and output sequence and can be used to display a number of the results of the computation. The subroutine for handling characters (written by Lt. C.E. Molnar) is used in a variety of ways whenever alphabetical, numerical or other characters are to be manipulated by the machine. For instance, this subroutine can be used to display characters on the oscilloscopic display tube in order to provide a title for the particular computation that

Figure 44. Logical flow diagram of the computer programs. The computer programs, L1, L2, ..., L9 are a set of lights and push buttons. The lights and push buttons are independent. The lights can be used as indicators from the machine to the operator, and the push buttons can be used as indicators from the operator to the machine. The Moving Window display program (written by Lt. C.E. Molnar) is used to view the contents of memory of the machine. Figure 20 shows six pictures of data generated by the machine as displayed on the oscilloscopic display tube using the Moving Window program.



is being displayed. Examples of the use of this subroutine are shown in many of the figures in Chapter V. This subroutine is also utilized by a program which sets the parameters of the computation according to the keys struck on a keyboard. All of these sequences can be run virtually concurrently in the machine. That is, the computations can be viewed and/or printed out as they are produced. This is achieved in the TX-2 computer by the existence of interleaved programs. The control of the interleaving is done almost automatically by the machine.

Then the main sequence is actuated, control can be transferred to a program that is used 1) to set the parameters of the computation (parameters are set according to keys struck on the keyboard), 2) to read stimuli into the memory via a photoelectric tape reader, and 3) to add any desired titles associated with the run or set of runs. The next step involves clearing an area of the memory that is used to hold the results of the computation and setting up table locations to hold the results of the computation (such as histograms, mean firing rates and other statistics), etc. At the next step, a specified non-linear function of the stimulus (displacement of the basilar membrane) can be computed. The stimulus (which exists as a table of numbers stored in the memory) is then filtered by a low pass filter. Several different nonlinear functions have been used and the program has been written so that these different nonlinear functions can be selected by toggle switches.

The program now computes the number of buffers needed to compute the number of data points called for by the operator. Several distinct computations are performed on each buffer of data. First, the buffer is cleared; filtered Gaussian noise is next loaded into the buffer. (The filtered noise is obtained by sampling a noise generator, which produces noise with a uniform distribution. Several samples of this uniform distribution noise are added and the sum is then filtered in two stages-- a high pass stage followed by a low pass stage. Both of these filtering operations are accomplished by difference equations that simulate RC filters.) When the buffer is filled with noise an amplitude histogram of the noise is compiled. The transformed and filtered stimulus is added to the noise. Finally, the subroutine that is used to determine the response of the model neuron to this signal is activated. This subroutine compares the value of the signal plus noise to the value of the threshold at each point in time. The threshold value is determined by a table look-up scheme and the computer determines the value of the threshold by retaining the amount of time that has elapsed since the last event. An event occurs when the value of the signal plus the noise exceeds the threshold value. When an event occurs the appropriate entries are made in tables representing the PST histogram, the interval histogram, and the two-dimensional interval histogram. The counter,

which is used to retain the value of the time elapsed since the last event, is reset, thus effectively resetting the threshold to its maximum value. If the threshold value is larger than the sum of signal and noise, no event occurs and the counter is indexed; this effectively changes the value of the threshold to its new value.

When these computations are completed on one buffer, the process is continued until the specified number of data points have been completed. At the end of these computations various further statistics are derived. The results can then be printed (in plotted form when desirable) on a high speed printer. The high speed printer has been used to obtain a fast, permanent record of each run. An example of a typical display available on the high speed printer is shown in Figure 45.

After (or while) the data for one run is printed the next run can be started automatically. A number of options are available. For instance, a series of runs with varying intensity of stimulation can be automatically accomplished, using a set of toggle switches to specify the change in signal intensity. Similarly a series of runs for different spontaneous rates can be actuated, etc.

The time required for a typical run is of the order of two or three minutes. This run generates data equivalent to approximately one minute of similar data obtained from the physiological preparation. The time required to obtain

Figure 45. High speed printer display of the results of a typical computation. The figure at the bottom of the page shows a list of the parameters of the computation: $t_{REST} = R_R$, $t_{MAX} = R_M$, $t_{INC} = \exp(\Delta t / \tau_R)$, $STMNUM =$ number of stimuli presented, $STMPER =$ period of the stimulus, $STDEV = \sigma$, etc. In addition, the response of the cochlear partition is shown (for a point tuned to 1000 cps, in this case). The figure in the center of the page shows the PST histogram and the figure at the top of the page shows the interval histogram.

CLICK RESPONSE OF MODEL WITH
 LOGARITHMIC NONLINEARITY K100.1
 47100 MICROSECS CF10000
 4/13/63 20-57

SERIAL # = 7300

I REST = 10000
 I MAX = 100000
 I INC = 10000
 STIMUM = 1000
 STIMPER = 100
 S SPIRES = 1000
 S = 100
 RATE = 1000
 ST DEV = 5000
 PSIY = 100/200
 LPIY = 100/200
 HPIY = 1000/2000

STIMULUS SF # = 40

STIMULUS	SF #	40
1	0	0
2	0	0
3	0	0
4	0	0
5	0	0
6	0	0
7	0	0
8	0	0
9	0	0
10	0	0
11	0	0
12	0	0
13	0	0
14	0	0
15	0	0
16	0	0
17	0	0
18	0	0
19	0	0
20	0	0
21	0	0
22	0	0
23	0	0
24	0	0
25	0	0
26	0	0
27	0	0
28	0	0
29	0	0
30	0	0
31	0	0
32	0	0
33	0	0
34	0	0
35	0	0
36	0	0
37	0	0
38	0	0
39	0	0
40	0	0
41	0	0
42	0	0
43	0	0
44	0	0
45	0	0
46	0	0
47	0	0
48	0	0
49	0	0
50	0	0
51	0	0
52	0	0
53	0	0
54	0	0
55	0	0
56	0	0
57	0	0
58	0	0
59	0	0
60	0	0
61	0	0
62	0	0
63	0	0
64	0	0
65	0	0
66	0	0
67	0	0
68	0	0
69	0	0
70	0	0
71	0	0
72	0	0
73	0	0
74	0	0
75	0	0
76	0	0
77	0	0
78	0	0
79	0	0
80	0	0
81	0	0
82	0	0
83	0	0
84	0	0
85	0	0
86	0	0
87	0	0
88	0	0
89	0	0
90	0	0
91	0	0
92	0	0
93	0	0
94	0	0
95	0	0
96	0	0
97	0	0
98	0	0
99	0	0
100	0	0

CLICK RESPONSE OF MODEL WITH
 LOGARITHMIC NONLINEARITY K100.1
 47100 MICROSECS CF10000
 4/13/63 20-57

SERIAL # = 7300

PST HISTOGRAM SF # = 2
 = 1000 = 100
 = 1000 = 1000
 = 100

PST HISTOGRAM	SF #	2
1	2	
2	2	
3	2	
4	2	
5	2	
6	2	
7	2	
8	2	
9	2	
10	2	
11	2	
12	2	
13	2	
14	2	
15	2	
16	2	
17	2	
18	2	
19	2	
20	2	
21	2	
22	2	
23	2	
24	2	
25	2	
26	2	
27	2	
28	2	
29	2	
30	2	
31	2	
32	2	
33	2	
34	2	
35	2	
36	2	
37	2	
38	2	
39	2	
40	2	
41	2	
42	2	
43	2	
44	2	
45	2	
46	2	
47	2	
48	2	
49	2	
50	2	
51	2	
52	2	
53	2	
54	2	
55	2	
56	2	
57	2	
58	2	
59	2	
60	2	
61	2	
62	2	
63	2	
64	2	
65	2	
66	2	
67	2	
68	2	
69	2	
70	2	
71	2	
72	2	
73	2	
74	2	
75	2	
76	2	
77	2	
78	2	
79	2	
80	2	
81	2	
82	2	
83	2	
84	2	
85	2	
86	2	
87	2	
88	2	
89	2	
90	2	
91	2	
92	2	
93	2	
94	2	
95	2	
96	2	
97	2	
98	2	
99	2	
100	2	

CLICK RESPONSE OF MODEL WITH
 LOGARITHMIC NONLINEARITY K100.1
 47100 MICROSECS CF10000
 4/13/63 20-57

SERIAL # = 7300

INT HISTOGRAM SF # = 8

INT HISTOGRAM	SF #	8
1	8	
2	8	
3	8	
4	8	
5	8	
6	8	
7	8	
8	8	
9	8	
10	8	
11	8	
12	8	
13	8	
14	8	
15	8	
16	8	
17	8	
18	8	
19	8	
20	8	
21	8	
22	8	
23	8	
24	8	
25	8	
26	8	
27	8	
28	8	
29	8	
30	8	
31	8	
32	8	
33	8	
34	8	
35	8	
36	8	
37	8	
38	8	
39	8	
40	8	
41	8	
42	8	
43	8	
44	8	
45	8	
46	8	
47	8	
48	8	
49	8	
50	8	
51	8	
52	8	
53	8	
54	8	
55	8	
56	8	
57	8	
58	8	
59	8	
60	8	
61	8	
62	8	
63	8	
64	8	
65	8	
66	8	
67	8	
68	8	
69	8	
70	8	
71	8	
72	8	
73	8	
74	8	
75	8	
76	8	
77	8	
78	8	
79	8	
80	8	
81	8	
82	8	
83	8	
84	8	
85	8	
86	8	
87	8	
88	8	
89	8	
90	8	
91	8	
92	8	
93	8	
94	8	
95	8	
96	8	
97	8	
98	8	
99	8	
100	8	

the results of a computation on the model is thus equivalent to the time required to obtain and process the physiological data. No particular significance is attached to this result except in a comparative sense. Furthermore, programming changes calling for a change of speed of at least a factor of five are envisioned at present. The bulk of the two minute time interval is consumed by the programs that generate the filtered noise and this time can be reduced in a number of ways. For instance, the filtered noise could be stored on digital tape and read into the machine on command.

At present the programs occupy approximately 5000 registers of core memory. The bulk of this storage is required for the programs concerned with input and output devices, including the programs used for the various displays, the programs used to print the results on the high speed printer, the programs used to read information into the machine via the photoelectric tape reader, the programs used to decode information coming into the machine via the keyboard, and the programs used to type information on a typewriter.

BIBLIOGRAPHY

1. Polyak, S.L. The Human Ear in Anatomical Transparencies. Elmsford, New York: Sonotone Corporation (1946).
2. Gacek, R.R. and Rasmussen, G.L. "Fiber analysis of the statoacoustic nerve of guinea pig, cat and monkey". Anat. Rec., 139, 1961: 455-463.
3. Polyak, S.L., loc. cit., p. 103.
4. Fernandez, C. "The innervation of the cochlea (guinea pig)". Laryngoscope, 61, 1951: 1152-1172.
5. Ibid.
6. Ibid.
7. Ibid.
8. Polyak, S.L., loc. cit., p. 107.
9. Ruben, R.J., Fisch, U., and Hudson, W. "Properties of the eighth nerve action potential". J. Acoust. Soc. Am., 34, 1962: 99-102.
10. Gacek, R.R. and Rasmussen, G.L., loc. cit.
11. Rasmussen, G.L. "Efferent fibers of the cochlear nerve and cochlear nucleus". Pp. 105-115 in Neural Mechanisms of the Auditory and Vestibular Systems (G.L. Rasmussen and W. Windle, Eds.) Springfield: Charles C. Thomas, Publisher (1960).
12. Wever, E.G. and Lawrence, M. Physiological Acoustics. Princeton University Press (1954).
13. Ibid., p. 113.
14. Von Békésy, G. Experiments in Hearing (E.G. Wever, Ed.) New York: McGraw-Hill Book Company, Inc. (1960) p. 101.
15. Ibid., p. 102.
16. Ibid., p. 113.
17. Wever, E.G. and Lawrence, M., loc. cit., p. 154.
18. Ibid., p. 195.
19. Wiener, F.M. and Ross, D.A. "The pressure distribution in the auditory canal in a progressive sound field". J. Acoust. Soc. Am., 18, 1946: 401-408.

20. Von Békésy, G., loc. cit., pp. 99-100.
21. Ibid., p. 432.
22. Wever, E.G. and Lawrence, M., loc. cit., p. 218.
23. Møller, A. "Bilateral contraction of the tympanic muscles in man", Report No. 18, Speech Transmission Laboratory, Royal Institute of Technology, Stockholm (February 20, 1961).
24. Møller, A. "Network model of the middle ear". J. Acoust. Soc. Am., 33, 1961: 168-176.
25. Zwizlocki, J. "Some impedance measurements on normal and pathological ears". J. Acoust. Soc. Am., 29, 1957: 1312-131
26. Flanagan, J.L. "Computational model for basilar membrane displacement". J. Acoust. Soc. Am., 34, 1962: 1370-1376.
27. Møller, A., personal communication.
28. Von Békésy, G., loc. cit., pp. 472-473.
29. Ibid., pp. 476, 510.
30. Ibid., pp. 466-469.
31. Ibid., p. 407.
32. Ibid., pp. 408, 460.
34. Ibid., pp. 447, 464.
35. Ibid., pp. 447-448.
36. Ibid., pp. 442, 500-508.
37. Ibid., p. 454.
38. Ibid., p. 455.
39. Ibid., p. 448.
40. Ibid., p. 461.
41. Ibid., pp. 510-524, 543-533.
42. Wever, E.G. and Lawrence, M., loc. cit., pp. 271-282.
43. Zwizlocki, J. "Theorie der Schneckenmechanik", Acta Oto-Laryngologica, Supplement LXXII, 1948.

44. Fletcher, H. "On the dynamics of the cochlea". J. Acoust. Soc. Am., 23, 1951: 637-645.
45. Zwislocki, J. "Review of recent mathematical theories of cochlear dynamics". J. Acoust. Soc. Am., 25, 1953: 743-751.
46. Ranke, O.F. "Physiologie des gehors" in Gehor, Stimme Sprache (Lehrbuch der Physiologie, Trendelenburg, W. and Schutz, E., Eds.) Berlin: Springer-Verlag (1953).
47. Oetinger, R. and Hauser, H. "Ein elektrischer kettenleiter zur untersuchung der mechanischen schwingungsvorgange in innenohr". Acustica, 11, 1961: 161-177.
48. Wansdronk, C. "On the Mechanism of Hearing". (Ph.D. Thesis, University of Leyden, November, 1961) Philips Research Reports Supplements, No. 1, Philips Research Laboratories, Netherlands, 1962.
49. Flanagan, J.L., loc. cit.
50. Flanagan, J.L. "Models for approximating basilar membrane displacement". Bell Syst. Tech. J., 39, 1960: 1163-1192.
51. Siebert, W.M. "Models for the dynamic behavior of the cochlear partition". Quarterly Progress Report No. 64, Research Laboratory of Electronics, M.I.T., January 15, 1962, pp. 242-258.
52. Von Békésy, G., loc. cit., pp. 651-654.
53. Stevens, S.S. and Davis, H. Hearing. New York: John Wiley & Sons, Inc. (1938) pp. 310-332.
54. Wever, E.G. and Lawrence, M., loc. cit., p. 154.
55. Ibid., p. 167.
56. Peake, W.T. "An analytic study of electric responses at the periphery of the auditory system". Technical Report 365, Research Laboratory of Electronics, M.I.T., March 17, 1960.
57. Von Békésy, G., loc, cit., pp. 680-684.
58. Davis, H. "A mechano-electrical theory of cochlear action". Ann. Otol., Rhinol., Laryngol., 67, 1958: 789-802.
59. Davis, H. "Biophysics and physiology of the inner ear". Physiol. Rev., 37, 1957: 1-49.
60. Davis, H. "Some principles of sensory receptor action". Physiol. Rev., 41, 1961: 391-416.

61. Tasaki, I., Davis, H., and Legouix, J.P. "The space time pattern of the cochlea microphonics (guinea pig), as recorded by differential electrodes". J. Acoust. Soc. Am., 24, 1952: 502-519.
62. Teas, D.C., Eldredge, D.H., and Davis, H. "The processing of acoustic transients by the inner ear". To be published in J. Acoust. Soc. Amer.
63. Davis, H. "Biophysics and physiology . . .", loc. cit.
64. Davis, H. Deatherage, B.H., Eldredge, D.H., and Smith, C.A. "Summating potentials of the cochlea". Am. J. Physiol., 195, 1958: 251-261.
65. Derbyshire, A.J. and Davis, H. "The action potentials of the auditory nerve". Am. J. Physiol., 113, 1935: 476-504.
66. Frishkopf, L.S. "A probability approach to certain neuro-electric phenomena". Technical Report 307, Research Laboratory of Electronics, M.I.T., March 1, 1956.
67. Peake, W.T., loc. cit.
68. Tasaki, I. "Nerve impulses in individual auditory nerve fibers of guinea pig". J. Neurophysiol., 17, 1954: 97-122.
69. Katsuki, Y. "Neural mechanism of hearing in cats and insects". Pp. 53-75 in Electrical Activity of Single Cells (Y. Katsuki, Ed.) Tokyo: Igaku Shoin (1960).
70. Kiang, N. Y-s., Watanabe, T., Thomas, E.C., Clark, L.F. "Stimulus coding in the cat's auditory nerve". Ann. Otol., Rhinol., Laryngol., 71, 1962: 1009-1027.
71. Gerstein, G.L. and Kiang, N.Y.S. "An approach to the quantitative analysis of electrophysiological data from single neurones". Biophysical J., 1, 1960: 15-28.
72. Von Békésy, G., loc. cit., pp. 454, 461, 504-509.
73. Ibid., pp. 442, 504-508.
74. Ibid., pp. 476, 510.
75. Greenwood, D.D. "Critical bandwidth and the frequency coordinates of the basilar membrane". J. Acoust. Soc. Am., 33, 1961: 1344-1356.

76. Fernandez, C., loc. cit.
77. Schuknecht, H.F. "Neuroanatomical correlates of auditory sensitivity and pitch discrimination in the cat". Pp. 86-87 in Neural Mechanisms of the Auditory and Vestibular Systems (G.L. Rasmussen and W. Windle, Eds.) Springfield: Charles C. Thomas, Publisher (1960).
78. Von Békésy, G., loc. cit., pp. 448, 462.
79. Polyak, S.L., loc. cit., p. 109.
80. Fernandez, C., loc. cit.
81. Davis, H. "Some principles...", loc. cit.
82. Hodgkin, A.L., and Huxley, A.F. "A quantitative description of membrane current and its application to conduction and excitation in nerve". J. Physiol., 117, 1952: 500-544.
83. Harmon, L.D. "Studies with artificial neurons, I: properties and functions of an artificial neuron". Kybernetik, 1, 1961: 89-101.
84. Kupfmüller, K., and Jenik, F. "Über die nachrichtenverarbeitung in der nervenzelle". Kybernetik, 1, 1961: 1-6.
85. Viernstein, L.J., and Grossman, R.G. "Neural discharge patterns in the transmission of sensory information". Pp. 252-269 in Information Theory (C. Cherry, Ed.) London: Butterworths (1961).
86. Verveen, A.A., and tenHoopen, M. "Nerve-model experiments on fluctuation in excitability". (to be published in Kybernetik)
87. Pecher, C. "La fluctuation d'excitabilité de la fibre nerveuse". Arch. Intern. Physiol., 49, 1939: 129-152.
88. Verveen, A.A. Fluctuation in Excitability. Amsterdam: Drukkerij Holland N.V. (1961).
89. Fatt, P. and Katz, B. "Spontaneous subthreshold activity at motor nerve endings". J. Physiol., 117, 1952: 109-128.
90. Verveen, A.A. "Axon diameter and fluctuation in excitability". Acta Morphologica Neerlandico-Scandinavica, V, 1963: 79-85.
91. Ibid.

92. Engström, H. "Electron micrographic studies of the receptor cells of the organ of corti". Pp. 48-64 in Neural Mechanisms of the Auditory and Vestibular Systems (G.L. Rasmussen and W. Windle, Eds.) Springfield: Charles C. Thomas, Publisher (1960).
93. Verveen, A.A., and tenHoopen, M., loc. cit.
94. Tasaki, I. "Conduction of the nerve impulse". P. 85 in Handbook of Physiology (J. Field, Ed.) Volume I--Neurophysiology, Section 1. Washington, D.C.: American Physiological Society (1959).
95. Rasmussen, G.L., loc. cit.
96. Galambos, R. "Suppression of auditory nerve activity by stimulation of efferent fibers to cochlea". J. Neurophysiol., 19, 1956: 424-437.
97. Fex, J. "Auditory activity in centrifugal and centripetal cochlear fibers in cat". Acta Physiologica Scandinavia, 55, Suppl. 189, 1962.
98. Fex, J. "Augmentation of cochlear microphonics by stimulation of efferent fibers to the cat". Acta Otolaryngol., 50, 1959: 540-541.
99. Galambos, R. "Studies of the auditory system with implanted electrodes". Pp. 137-151 in Neural Mechanisms of the Auditory and Vestibular Systems (G.L. Rasmussen and W. Windle, Eds.) Springfield: Charles C. Thomas, Publisher (1960).
100. Rice, S.O. "Mathematical analysis of random noise". Pp. 133-294 in Selected Papers on Noise and Stochastic Processes (N. Wax, Ed.) New York: Dover (1954).
101. McFadden, J.A. "The axis-crossing intervals of random functions". IRE Trans. Info. Theory, IT-2, 1956: 146-150. "The axis-crossing intervals of random functions II". IRE Trans. Info. Theory, IT-4, 1958: 14-24. "The fourth product moment of infinitely clipped noise". IRE Trans. Info. Theory, IT-4, 1958: 159-162. "The axis crossings of a stationary gaussian markov process". IRE Trans. Info. Theory, IT-7, 1961: 150-153.
102. Kac, M. and Slepian, D. "Large excursions of gaussian processes". Ann. Math. Stat., 30, 1959: 1215-1228.
103. Slepian, D. "The one-sided barrier problem for gaussian noise". Bell Syst. Tech. J., XLI, 1962: 463-501.

104. Clark, W.A. "The lincoln TX-2 computer development"; Frankovich, J.M., and Peterson, H.P. "A functional description of the lincoln TX-2 computer"; Forgie, J.W. "The lincoln TX-2 input-output system"; Best, R.L. "Memory units in the lincoln TX-2"; Olsen, K.H. "Transistor circuitry in the lincoln TX-2". Consecutive articles in Proc. Western Joint Computer Conf., February 26-28, 1957, Institute of Radio Engineers, pp. 143-171.
105. Verveen, A.A. Fluctuation in Excitability, loc. cit., pp. 60-64.
106. Verveen, A.A., and tenHoopen, M. loc. cit.
107. Feller, W. An Introduction to Probability Theory and Its Applications. New York: John Wiley & Sons, Inc. (1950) p. 278.
108. Frishkopf, L.S., loc. cit., p. 63.
109. Verveen, A.A., and tenHoopen, M., loc. cit.
110. Pecher, C., loc. cit.

Addendum

111. Zwislocki, J., and Feldman, A.S. "Post-mortem acoustic impedance of human ears". J. Acoust. Soc. Am., 35, 1963: 104-107.

ERRATA

- Page 26, lines 12 to 21: The discussion starting with, "The impedances of the cochlea..." and ending with "...round window displacements are equal." is irrelevant and should be ignored.
- Page 31, line 3: The last term in the equation should read
$$(z_{22} + z_0 - (z_{12}^2 / z_{11}))$$
- Page 51, line 20: Strike out the word "outer".
- Page 61, line 13: The parenthetical remark should read "(less than $1/(4f_0)$)".
- Page 61, line 21: The line should read, "that correspond to $1/(2f_0)$ ".
- Page 75, line 27: The line should read, "information in the VIIIth nerve,....".

BIOGRAPHICAL NOTE

Thomas Fischer Weiss

Born: October 17, 1934, Prague, Czechoslovakia
Naturalized citizen of U.S.A.-1951

Education

The City College of New York, Bachelor of Electrical
Engineering (Magna Cum Laude) June, 1956
Massachusetts Institute of Technology, Master of
Science, February, 1959

Professional Societies

Tau Beta Pi
Eta Kappa Nu
Sigma Xi
Institute of Mathematical Statistics
(formerly, Institute of Radio Engineers)

Teaching (M.I.T.)

Electronic Circuit Theory (6.02)
Feedback Theory Laboratory (6.213, 6.606)

Employment

Dynamic Analysis and Control Laboratory, M.I.T.
June, 1956-June, 1957, Research Assistant.
Worked on 1) the design of a transistorized,
digital-analog multiplier, and 2) analog
computer studies of an economic system
Douglas Aircraft Company, Santa Monica, California
June, 1957-September, 1957, Engineer
Worked on kinematics of the aircraft collision
problem
Lincoln Laboratory, M.I.T.
June 1961-September, 1961, Engineer
Worked on distribution of loop lengths in a
neural net
Research Laboratory of Electronics, M.I.T.
September, 1957-June 1961 and September, 1961-present
Research Assistant
Work is described in the Quarterly Progress
Reports of RLE: January 1958, July 1958,
January 1959, July 1959, April 1960, April 1963

Publications

1. B.G. Farley, L.S. Frishkopf, M.Z. Freeman, C. Molnar, and T.F. Weiss. A summary description of EEG data with the aid of a digital computer. Abstract No. 13 (p. 24) in Program and Abstracts of the Biophysical Society, 1958 Meeting, February 5,6,7, Cambridge, Massachusetts.
2. B.G. Farley, L.S. Frishkopf, M.Z. Freeman, C. Molnar, and T.F. Weiss. A summary description of EEG data with the aid of a digital computer. Abstract No. 13 (p. 5) in Abstracts of the 11th Annual Conference on Electrical Techniques in Medicine and Biology, Minneapolis, November 19-21, 1958.
3. T.T. Sandel and T.F. Weiss. Statistical characteristics of evoked cortical activity. Abstract No. 12 (p. 5) in Abstracts of the 11th Annual Conference on Electrical Techniques in Medicine and Biology, Minneapolis, November 19-21, 1958.
4. C.D. Geisler, C.E. Molnar, W.T. Peake, T.F. Weiss, and T.T. Sandel. Loudness judgments on clicks. J. Acoust. Soc. Am., 1959, 31: 128 (abstract).
5. T.F. Weiss. Some properties of the finite time sample autocorrelation of the electroencephalogram, M.S. Thesis, Department of Electrical Engineering, M.I.T., 1959.
6. T.T. Sandel, T. Weiss, and C.E. Molnar. Statistical analyses of evoked electrocortical activity. Abstract No. J7 in Program and Abstracts of the Biophysical Society, 1959 Meeting, Pittsburgh, Pennsylvania.
7. T.F. Weiss. Some statistics of the electroencephalogram, with emphasis upon autocorrelation. Abstract No. J8 in Program and Abstracts of the Biophysical Society, 1959 Meeting, Pittsburgh, Pennsylvania.
8. T.T. Sandel, C.E. Molnar, T.F. Weiss, J.S. Barlow, R.M. Brown, M.H. Goldstein, Jr., and W.A. Rosenblith. Quantitative methods in the analysis of neuroelectric activity. Medical Electronics (Proceedings of the 2nd International Conference in Medical Electronics, G.N. Symth, Ed.) Iliffe and Sons, Ltd; London, 1960, pp. 148-154.
9. T.F. Weiss and C.E. Molnar. Repetitive electrical activity of the cat's auditory cortex. Abstract No. O3, pp. 39-40, in Abstracts of the Fourth Annual Meeting of the Biophysical Society, February 24-26, 1960, Philadelphia, Pennsylvania.

10. C.E. Molnar, T.F. Weiss, and C.D. Geisler. Chapter 3, Two techniques for the processing of EEG data and M.H. Goldstein, Jr. and T.F. Weiss. Appendix B, Mathematical statistics. Pp. 36-61 and 88-98 in Processing Neuroelectric Data (W.A. Rosenblith, Ed.) The M.I.T. Press: Cambridge, Massachusetts (1962, 2nd Printing).
11. T.F. Weiss. A model for firing patterns of auditory nerve fibers. Abstract No. MF4 in Abstracts, Biophysical Society, Seventh Annual Meeting, February 18-20, 1963, New York City, N.Y.